Sofia Guerreiro dos Santos

Licenciada

Assessment of a novel Cu (II) complex as a potential anticancer agent

Dissertação para obtenção do Grau de Mestre em Genética Molecular e Biomedicina

Orientadora: Maria Alexandra Núncio de Carvalho Ramos Fernandes, Professora Doutora, FCT/UNL

Co-orientadora: Luísa Margarida Dias Ribeiro de Sousa Martins, Professora Doutora, Instituto Superior Engenharia de Lisboa

FACULDADE DE CIÊNCIAS E TECNOLOGIA
UNIVERSIDADE NOVA DE LISBOA

Setembro 2015

UNIVERSIDADE NOVA DE LISBOA
FACULDADE DE CIÊNCIAS E TECNOLOGIA
DEPARTAMENTO DE CIÊNCIAS DA VIDA

Sofia Guerreiro dos Santos

Licenciada

Assessment of a novel Cu (II) complex as a potential anticancer agent

Dissertação para obtenção do Grau de Mestre em Genética Molecular e Biomedicina pela Universidade Nova de Lisboa, Faculdade de Ciências e Tecnologia

Orientadora:

Maria Alexandra Núncio de Carvalho Ramos Fernandes, Professora Doutora, FCT/UNL

Co-orientadora:

Co-orientador: Luísa Margarida Dias Ribeiro de Sousa Martins, Professora Doutora, Instituto Superior Engenharia de Lisboa

Setembro 2015

My master studies have resulted in the following publication:

Coimbra J, Mota C, Santos S, Baptista PV, Fernandes AR (2015) Inorganic Compounds Going NANO. Ann Med Chem Res 1(2): 1010

Martins, Pedro; Jesus, João; Santos, Sofia; Raposo, Luis R.; Roma-Rodrigues, Catarina; Baptista, Pedro V.; Fernandes, Alexandra R. 2015. "Heterocyclic Anticancer Compounds: Recent Advances and the Paradigm Shift towards the Use of Nanomedicine's Tool Box." *Molecules* 20, no. 9: 16852-16891.

Assessment of a novel Cu (II) complex as a potential anticancer agent

Acknowledgments

Em primerio lugar gostaria de agradecer à minha orientadora, Professora Doutora Alexandra Fernandes, por todas as oportunidades que me proporcionou no decorrer do projecto, pela que confiança que depositou em mim e pela ajuda em todas as questões e dificuldades que tive durante o desenvolvimento da tese.

À minha co-orientadora, Professora Doutoura Luísa Fernandes, pelo fornecimento dos compostos, pela amabilidade e disponibilidade que demonstrou no decorrer da tese e que possibilitou a realização do trabalho.

Queria também agradecer ao Professor Doutor Pedro Viana Baptista pela disponibilidade que sempre demonstrou para me auxiliar em qualquer dúvida que surgisse. Queria agradecer também a oportunidade que me deu para realizar um dos objectivos da minha tese para o design e caracterização de uma nanoformulação contendo o composto.

Gostaria de agradecer à Professora Guadalupe Cabral e a todo o pessoal do CEDOC pela oportunidade de trabalhar com o citometro de fluxo e por toda a ajuda que forneceram durante o decorrer dos ensaios.

Ao Professor Pedro Costa, gostaria de agradecer a disponibilidade que sempre demonstrou e oportunidade de usar o microscopio de fluroescência para realizar os ensaios de Hoechst.

Ao Professor João Carlos Lima por disponibilizar o DLS para que conseguisse caracterizar a nanoformulação.

Não poderia deixar de agradecer à equipa de investigação *Human Genetics and Cancer therapeutics.* Primeiramente gostaria de agradecer à Dra. Catarina Rodrigues e ao Luís Raposo por toda a ajuda fornecida durante o decorrer dos ensaios e pela disponibilidade para tirar dúvidas. Gostaria também de agradecer à Joana Silva pelo fornecimento dos resultados dos ensaios de viabilidade celular da doxorubicina e por toda a ajuda e amabilidade com que me recebeu no laboratório. À minha querida Soraia Mendo, pela ajuda incondicional em todos os ensaios nomeadamente os ensaios das terapias combinadas e pelo fornecimento dos IC_{50} relativos de afatinib, cetuximab e lapatinib. Obrigada por me mostrares que as mulheres não se medem aos palmos. Ao Pedro Martins, ou à mãe, por tudo. Sem ti, tudo teria sido tão mais dificil. Obrigada pela ajuda incondicional, pelo apoio, por limpares as lágrimas, pelas garagalhadas, por estares sempre presente para ajudar, por teres feito muito mais do que te era pedido e pela amizade. Obrigada por me acreditares em mim e por me mostrares que a auto-confiança é meio caminho andado. Queria também agradecer às meninas, a Carolina "Motinha" Mota, a Joana "Dodots" Coimbra e a Francisca "Xica" Pereira, pelas lágrimas e sorissos partilhados. Porque apesar de tudo o que passamos, sei que me irei lembrar este ano com um sorriso. Porque rir foi uma certeza de todos os dias, mesmos naqueles dias

mais tristes. Ao meu querido Jonhy Jizuss, que me ensinou tanto e por quem eu tenho o maior respeito e apreço. Obrigada por me ensinares a por as coisas em perspectiva. À Débora Matinata um obrigada pelo apoio e pelas saídas. Obrigada por teres sido uma lufada de ar fresco! À Silvia Lino, que chegou tarde mas encheu o laboratório com uma maresia diferente. Que me fez sentir pequenina e me fez sonhar mais alto. À Rita Mendes que também chegou fora de horas mas que alegrou as últimas semanas. Obrigada pela tua boa disposição e bom carácter. Chegaste um ano mais tarde! Por fim gostaria de agradecer às meninas do projecto que alegraram tanto o laboratorio durante aquelas curtas semanas.

Gostaria também de agradecer a todo o grupo de Nanomedicine pela ajuda incondicional em qualquer dúvida que surgiu e pela boa diposição e companheirismo que demonstraram ao longo do ano: Larguinho, Sara, Raquel, Milton, Ana Sofia, Barbára, Rafaela, Marísa, Fábio e Rita Cabral.

Queria agradecer aos meus amigos que sentiram e muito a minha ausência durante este ano. Obrigada pela paciência e por estarem lá sempre, incondicionalmente, Ana Rita Valéria e João David. Os meus mais sinceros agradecimentos vão para vocês, que me dão força, hoje e sempre, mesmo estando longe.

Queria por fim agradecer à minha família pelo apoio incondicional e pelos almoços de domingo que serviram de escape às semanas longas . Obrigada Mãe e Pai pela paciência que tiveram comigo ao longo do ano e por me ensinarem a nunca desistir e ultrapassar os obstáculos.

A todos o mais profundo agradecimento da minha parte. Mais uma etapa alcançada e que acho que teria sido muito mais árdua sem a vossa ajuda.

"No great mind has ever existed without a touch of madness"

Aristotle

RESUMO

A quimioterapia é um dos tratamentos mais usados no combate ao cancro no entanto ainda tem desafios a ultrapassar tais como os efeitos adversos nos pacientes e a aquisiçao de resistência às drogas. Neste sentido, novos compostos com propriedades farmacocinéticas/farmacodinâmicas melhoradas têm sido sintetizados. Deste modo, o objectivo principal do projecto consistiu na caracterização do potencial antiproliferativo de um grupo de compostos metálicos. Adicionalmente a nanovectorização do composto mais promisor e a combinação com quimioterapeuticos comerciais consistiram nos objectivo secundários. Os ensaios de viabilidade celular demonstraram que o composto de cobre (II), K4, era o mais promisor obtendo um IC_{50} relativo de 6,10 µM e 19,09 µM para as linhas celulares HCT116 e A549 respectivamente. A exposição do composto a fibroblastos revelou um IC_{50} de 9,18 µM. Os ensaios com a Hoechst revelaram que o composto induzia a condensação da cromatina e fragmentação nuclear em HCT116. Estes reusltados foram corroborados pelos ensaios de citometria de fluxo com dupla marcação com Anexina V-FITC e iodeto de propídeo (morte celular inferior a 50 %). O composto K4 revelou interação com macromoleculas nomeadamente DNA (Kb = $2{,}17 \times 10^5$ M^{-1}), induzindo quebras na estrutura e retardamento e consequente atraso na fase S do ciclo celular. Ensaios adicionais revelaram interação com BSA mas inconclusivos relativamente à natureza de interação. Os ensaios de protéomica revelaram sobrexpressão de proteínas envolvidas na actividade metabólica e subexpressão de proteínas involvidas na apoptose, corroborando assim os resultados de Hoechst e de citometria de fluxo. A nanoformulação com K4 nao foi bem sucedida em parte devido à pouca solubilidade do composto em solventes aquosos. Os ensaios de terapias combinadas revelaram elevada citotoxicidade para as estratégias com afatinib e lapatinib. O perfil proteómico de K4 e lapatinib revelou sobreexpressão de proteínas envolvidas na actividade metabólica, apoptose e mecanismos compensatórios de replicação de DNA.

Palavras-chave: Cancro; Quimioterapia; Cancro colorectal; Compostos de cobre; terapias combinadas; Nanovectorização.

Abstract

Widely used in cancer treatment, chemotherapy still faces hindering challenges, ranging from severe induced toxicity to drug resistance acquisition. As means to overcome these setbacks, newly synthetized compounds have recently come into play with the basis of improved pharmacokinetic/pharmacodynamic properties. With this mind-set, this project aimed towards the antiproliferative potential characterization of a group of metallic compounds. Additionally the incorporation of the compounds within a nanoformulation and within new combination strategies with commercial chemotherapeutic drugs was also envisaged. Cell viability assays presented copper (II) compound (K4) as the most promising, presenting an IC_{50} of 6.10 μM and 19.09 μM for HCT116 and A549 cell line respectively. Exposure in fibroblasts revealed a 9.18 μM IC_{50}. Hoechst staining assays further revealed the compound's predisposition to induce chromatin condensation and nuclear fragmentation in HCT116 upon exposure to K4 which was later demonstrated by flow cytometry and annexin V-FITC/propidium iodide double staining analysis (under 50 % cell death induction). The compound further revealed the ability to interact with major macromolecules such as DNA (Kb = $2.17x10^5$ M^{-1}), inducing structural brakes and retardation, and further affecting cell cycle progression revealing delay in S-phase. Moreover BSA interactions were also visible however not conclusive. Proteome profiling revealed overexpression of proteins involved in metabolic activity and underexpression of proteins involved in apoptosis thus corroborating Hoechst and apoptosis flow cytometry data. K4 nanoformulation suffered from several hindrances and was ill succeeded in part due to K4's poor solubility in aqueous buffers. Other approaches were considered in this regard. Combined chemotherapy assays revealed high cytotoxicity for afatinib and lapatinib strategies. Lapatinib and K4 proteome profiling further revealed high apoptosis rates, high metabolic activity and activation of redundant proteins as part of compensatory mechanisms.

Key-words: Cancer; Chemotherapy; Colorectal cancer; Copper compounds; Combined therapy; Nanovectorization.

General Contents

Figure Index

Table Index

Abbreviation List

260/230 Ratio between 260 nm and 230 nm absorbance
260/280 Ratio between 260 nm and 280 nm absorbance
5-Fu 5-fluorouracil
Abs Absorbance
Apaf-1 Apoptosis protease activating factor-1
APS Ammonium Persulfate
ATP Adenosine-5'-triphosphate
AuNP Gold nanoparticles
AuNP@PEG PEGylated gold nanoparticles
AuNP@PEG@BSA PEGylated gold nanoparticles functionalized with BSA
AuNp@PEG@BSA@K4 PEGylated gold nanoparticles functionalized with BSA and K4 compound
BAX Encoding gene for pro-apoptotic protein Bax, of the protein family Bcl-2
Bax Bcl-2-associated X protein
BCL-2 Encoding gene for pro-apoptotic protein Bcl-2, of the protein family Bcl-2
Bcl-2 B-cell lymphoma protein 2
BRCA1 Breast cancer 1 susceptibility gene
BRCA2 Breast cancer 2 susceptibility gene
BSA Bovine serum albumin
Caspase Cysteine-aspartic protease
CDI Coefficient Drug Interaction
Cdk Cyclin-dependent kinases
Cetuxi Cetuximab
CHAPS (3-[(3-Cholamidopropyl)dimethylammonio]-1 propanesulfonate)
CT-DNA Calf Thymus-DNA
DISC Death inducing signaling complex
DLS Dynamic light scatter
DMEM Dulbecco's Modified Eagle Medium
DMSO Dimethyl Sulfoxide
DNA Desoxyribonucleic acid
DOX Doxorrubicin
DTNB 5,5'-dithiobis-(2-nitrobenzoic acid)
DTT Dithiothreitol
E2F E2 transcription factor
EGFR Epidermal growth factor receptor

EPR Enhanced permeability and retention

FADD Fas-associated death domain

FasL Fatty acid synthetase ligand

FBS Fetal Bovine Serum

FDA Food and Drug Administration

FITC Fluorescein Isothiocyanate

HCT116 Colorectal carcinoma cell line

HER Human epidermal growth factor receptor-2

HER2 Codifying gene for membrane receptor HER

IC50 50 % growth inhibition concentration

Kb Affinity binding constant

MPS Mononuclear phagocyte system

MTS 3-(4,5-dimetiltiazol-2-il)-5-(3-carboximetoxifenil)-2-(4-sulfofenil)-2H-tetrazólio

NPs Nanoparticles

PBS Phosphate Buffered Saline

PEG Polyethylene glycol

PI Propidium Iodide

PMS Phenazine Methosulphate

PMSF Phenylmethylsulfonyl fluride

Ptx Paclitaxel

pUC18 Plasmid DNA

Rb Retinoblastoma tumour suppressor protein

RT Room temperature

SDS Sodium dodecyl sulfate

SDS-PAGE Sodium dodecyl sulfate - Polyacrylamide gel electrophoresis

SMAC/DIABLO Second mitochondria-derived activator of caspase/Direct IAP-binding protein with low pI

SPR Surface Plasmon ressonance

TAE Tris base, acetic acid and EDTA buffer

TEMED Tetramethylethylenediamine

TEM Transmission electron microscopy

TNF Tumour necrosis factor

TP53 p53 protein encoding gene

Tris-HCl Tris-Hidroclorite

WHO World Health Organization

Units List

% (w/v) Weight/volume percentage
% (v/v) Volume/volume percentage
A; mA Amperes; miliamperes
AU Absorbance units
bp Base pairs
°C Celsius degrees
H; min; s Hours; minutes; seconds
kDa; Da KiloDalton; Dalton (10-3kg)
Kg; g; mg; µg; ng Quilogramas; grama (10-3kg); miligrama (10-6 kg); micrograma (10-9 kg); ng – nanograma (10-12 kg)
L; mL; µL Liter; mililiter(10-3 L); µL – microliter (10-6 L)
m; cm; mm; nm Meter; centimeter (10-2 m); milimeter (10-3 m); nanometer (10-9 m)
M; mM; µM Molar (mol/L); milimolar (10-3 M); micromolar (10-6 M)
mol; pmol Mole; picomole
rpm Rotations per minute
U Unit; mU – miliunit
V Volts
W Watts

Symbol List

[Compound] Complex concentration
[DNA] DNA concentration
ε Molar extinction coefficient
εa Apparent molar extinction coefficient
εb Molar extinction coefficient when bound to DNA
εf Molar extinction coefficient when unbound
λ Wavelength
b Optical path´

1. Introduction

1.1 A prelude to cancer: Causes, incidence and mortality

Cells are the building blocks of life and they are known as the structural, functional and biological units of all organisms. The human body has approximately 10^{14} cells and they act as a "society" constituting tissues, organs, systems and ultimately an organism. Each cell possess the ability to reproduce individually but in the event of an abnormality in a particular cell that jeopardizes the all set of cells, the first one is typically sacrificed for the greater good and in order to promote the overall system survivability. Cancer cells constitute an example where the mentioned processes above do not occur and eventually these cells break society rules of an organismic like structure, and divide uncontrollably leading to tumor formation and death of the organism (Weinberg 2013).

Ultimately, cancer arises from genetic and epigenetic modifications, however acknowledgment of lifestyle habits influence on tumor formation has been accepted by the scientific community. External causes may emerge from biological agents, such as infections from virus or bacteria; chemical agents, such as tobacco smoke components or water contaminants like arsenic; or physical agents like UV radiation. Additionally, ageing also plays an important factor in the process of tumor formation. Increased cancer incidence in older citizens has been intimately correlated with the accumulation of defects in DNA repair mechanisms rendering them less effective (Colditz et al. 2012). Ultimately despite the low mutation rate on DNA replication (as little as 1 in 10^9) (Loeb et al., 1974) the accumulation of genetic defects increases dramatically as a result of the impaired DNA repair mechanisms.

Risk factors are an important concept to grasp when considering cancer. *World Health Organization* claims that 30 % of cancers could be prevented if one modifies lifestyle habits. Reducing alcohol and tobacco consumption, an healthy diet and frequent exercise are the main recommendations to follow (WHO 2015b).

Hereditary factors consist of a minor fraction of cancer causes, composing about 5 to 10% of all cancer patients. The most common hereditary tumors are breast and ovarian, resulting from a mutation on *BRCA1* or *BRCA2* genes or even from hereditary non-polyposis colorectal cancer (Marchina et al. 2010).

According to World Health Organization (WHO) in 2012, 8.2 billions of people died of cancer, about 14.1 million new cancer cases were reported and it is estimated that the number of cases will rise 70 % in the next two decades. The deadliest cancers registered were lung cancer, with approximately 1.6 million deaths worldwide, liver cancer, with 745 thousands deaths and stomach cancer, with 723 thousand. Risk factors such as obesity, sedentary lifestyle and tobacco consumption were the main causes identified (WHO 2015b).

Cancer statistics, in Portugal in 2014, shown in Figures 1.1 and 1.2, reveal that prostate and breast cancers had the highest numbers in male and female patients respectively. Trachea, bronchus and lung were the most deadly cancers in males and breast cancer had the highest mortally ratio in women in the same year (WHO 2014).

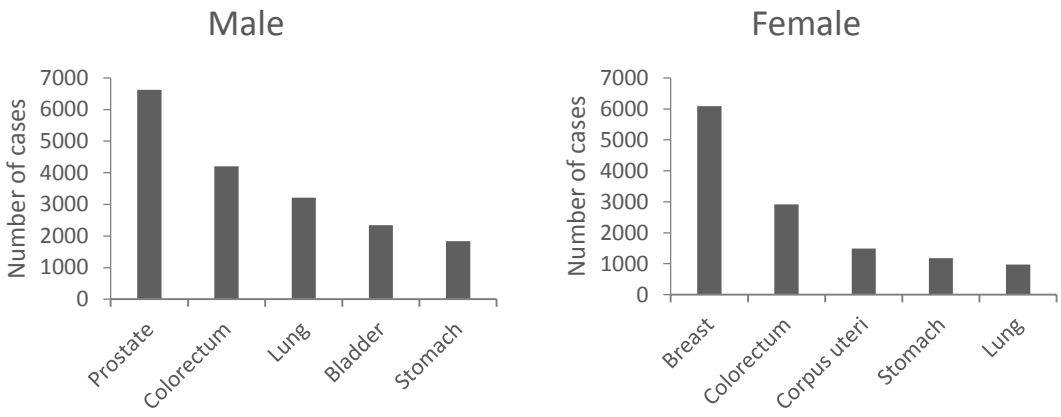

Figure 1.1 – Prime male and female cancer incidence in Portugal in 2014. Adapted from (WHO 2014)

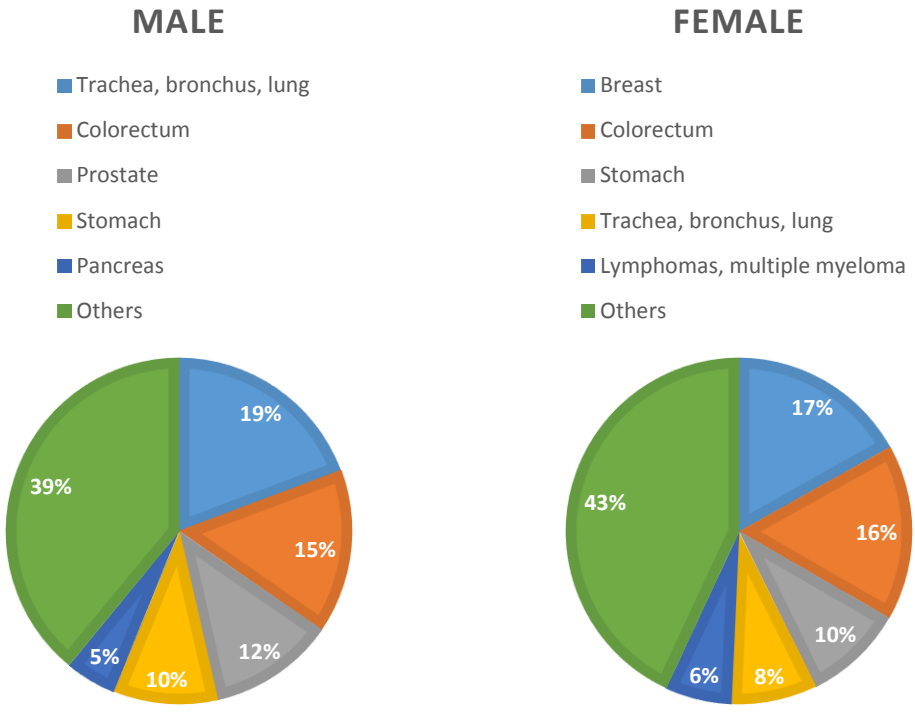

Figure 1.2 – Prime male and female mortality percentages in Portugal in 2014. Adapted from (WHO 2014)

1.1.1 Colorectal cancer

Colorectal cancer is one of the most threatening types of cancer worldwide. In 2012, was the third most common cancer in men with approximately 746 thousand new cases and 614 thousand new cases in women, being the second leading cause of cancer for this gender. Plus incidence rates are reportedly higher in developed countries than in developing ones (Ferlay et al. 2012). Nonetheless, contrasting mortality ratios indicate higher levels in developing countries than otherwise as shown in Figure 1.3. The highest incidence ratios have been reported in Australia and New Zealand and the lowest in Western Africa. On the other hand, mortality ratios have higher rates in Central and in Eastern Europe whereas Western Africa has the lowest mortality numbers (WHO 2015a).

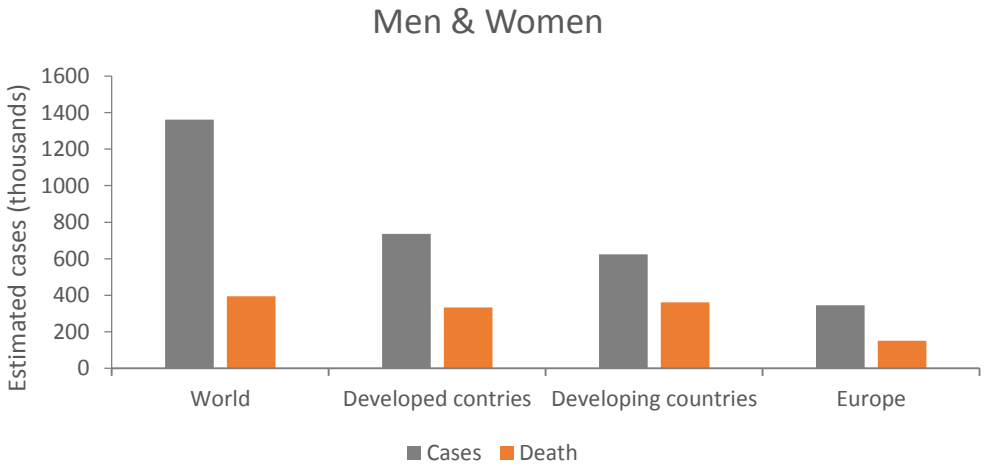

Figure 1.3 – Colorectal cancer estimated cases and deaths for men and women worldwide, in developed countries, in developing countries and in Europe in 2012. Adapted from (WHO 2015a)

World Health Organization revealed that in 2014 in Portugal, colorectal cancer was the second most common cancer for both men and women, with approximately 4000 and 3000 new cases, respectively. Mortality ratios have also pointed out colorectal cancer as the second leading cause of cancer related death for both genders (WHO 2014).

An important concept to grasp when considering colorectal cancer is the associated risk factors that may contribute towards the different stages of tumor development, which may be intricately related with age, lifestyle choices and heredity. Family history of adenomatous polyps, bowel disease or colorectal cancer is one paramount aspect of colorectal cancer incidence. Particularly individuals with personal history of adenomatous polyps present a higher risk of developing colorectal cancer than individuals with no personal

history. Additionally, a 5 to 10 years latency period is required to develop malignancy from polyps (Kushi et al. 2012). Nonetheless environmental risks are the major responsibles for worldwide colorectal cancer. Lifestyle choices such as smoking habits are often related to formation and growth of adenomatous polyps as DNA damage related from smoking habits is less prone to be repaired. Furthermore alcohol consumption concomitant to smoking habits not only triggers carcinogenesis as it quickens the process. Alcohol consumption at a younger age is hence linked to higher incidences of colorectal cancer. Particularly acetaldehyde, a reactive metabolite of alcohol can trigger carcinogenesis through DNA interaction. Correct lifestyle habits continues to have a major importance when referring incidence and mortality ratios of colorectal cancer thus the importance to follow strategies and advices proposed by WHO (Haggar et al. 2009).

1.2 Cancer Biology: What is cancer and how it is developed

1.2.1 Carcinogenesis: underlying biological mechanisms

As a multi-step process, cancer is a deeply complex disease that differs from patient to patient. Cancer cells undergo from considerable morphological, biochemical and genetic changes which allows to bypass immune system action and ultimately escape to a distant tissue in the organism. Such changes arise from genetic instability known as abundant genetic mutations in the genome (Huang 2013). Specific genes such tumor suppressor genes or oncogenes are usually mutated in cancer cells. Proto-oncogenes control cell growth hence their tight regulation in healthy cells. On the other hand, tumor suppressor genes, are typically activated in normal cells and when inactivated due to mutations they promote cell proliferation and ultimately tumor growth. Scientific community recognized genetic alterations, in particular mutations, as critical elements in the process of carcinogenesis, however recent discoveries suggest that epigenetic changes also play a critical role in tumor formation. Genetic and epigenetic modifications act sequentially, and together generate different pathways that a cell must undergo in order to become a cancer cell (Khare & Verma 2012).

Cancer cells possesses faulty regulatory mechanisms in opposite of what happens in healthy cells that keep a normal cell proliferation and tissue homeostasis maintenance. Carcinogenesis is a multi-step process where cells acquire genetic alterations and progressively become malignant. In 2000, Hanahan and Weinberg proposed six biochemical and morphological cell modifications that are associated with malignancy. Figure 1.4 outlines cancer hallmarks (Hanahan & Weinberg 2000). In 2011, the same authors proposed that cancer is not only a mass of uncontrollably cell proliferation but also a communicating system with neighbor healthy stromal cells that ultimately will improve malignancy. An increasing importance has been given to the tumor microenvironment in the carcinogenic process (Hanahan & Weinberg 2011).

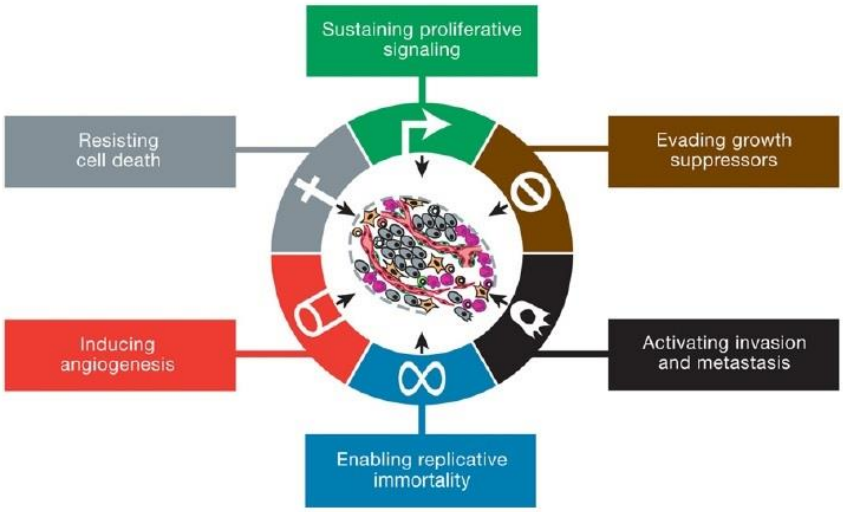

Figure 1.4 – Cancer hallmarks proposed by Hanahan and Weinberg. They comprise common features of cancer cells: sustaining proliferative signaling, evading growth suppressors, activating invasion and metastasis, enabling replicative immortality, inducing angiogenesis and resisting cell death (Hanahan & Weinberg 2011).

Sustaining proliferative signaling is one of the most important traits of cancer cells. Conducive to ensure tissue homeostasis, thigh mechanisms of proliferation and growth, regulate healthy cells whereas division mechanisms in cancer cells are dysregulated leading to a constant cell division. Extracellular growth signals binds to surface receptors with tyrosine kinase domains triggering a cascade of intracellular signaling of growth and proliferation. Cancer cells acquire this characteristic of continuous proliferation through several approaches: i) by producing growth factors ligands; ii) by sending a signal to the neighbor stromal cells to supply them with growth factors; iii) increasing levels of receptor proteins in the cell surface; iv) or by constitutive activating a downstream pathway signaling of those receptors (Hanahan & Weinberg 2011).

In addition of triggering proliferating signals, cells must also gain the ability of evading growth suppressors. Retinoblastoma (Rb) and p53 are the main proteins that regulate cell fate such as apoptosis, proliferation or a senescence state. For instance Rb protein decides if a cell divides or not depending on specific intracellular/extracellular stimuli. Cells with mutated Rb are not able to regulate cell division and divide uncontrollably. On the other hand p53 acts a stress sensor of intracellular environment. Damaged DNA or low abundance of nucleotides, glucose or growth signals are the main triggers of p53 thus inducing cell cycle arrest and delaying cell growth until allowance of optimal intracellular conditions. p53 can also trigger apoptosis if the intracellular signals indicate irreparable damage (Hanahan & Weinberg 2011).

Normal cell injury allows them to trigger programmed cell death. Another acquired characteristic of cancer cells is the ability to evade cell death. Overexpression of oncogenes or hyperproliferation signals leads cells

to overcome apoptotic signals. In cancer cells, a common trait is the loss of activity of TP53, a tumor suppressor gene that will no longer trigger apoptosis. Cancer cells also prompts anti-apoptotic proteins overexpression and survival signaling (Hanahan & Weinberg 2011).

Normal healthy cells have a finite number of cell divisions however cancer cells have the ability of enabling replicate immortality. After some cell division an healthy cell passes through a senescence state, where it no longer proliferates, followed by an event called crisis in which a great part of the cells in the population dies. Carcinogenic mechanism can overcome senescence and crisis phases. The scientific community evidence telomerase as the main responsible for cell life expectancy. Telomere length dictates the life expectancy of a cell and in healthy ones they tend to shorten with time. In cancer cells telomerase levels are much higher than in healthy cells thus preventing telomeres to shorten and prevent senescence and crisis/apoptosis events (Hanahan & Weinberg 2011).

Angiogenesis is a normal process in the human body to form vessels near cells in order to require nutrient and oxygen and expel metabolic waste and carbon dioxide. It occurs mainly in fetal development or in injury. However, cancer cells have the ability to induce angiogenesis thus potentiating cancer cells activity. The most well-known angiogenic regulators are the vascular endothelial growth factor-A (VEGF-A) that acts as angiogenic inducer and thrombospondin-1 (TSP-1) that acts as an angiogenic inhibitor. For instances, VEGF-A can be stimulated by a hypoxia environment or proliferating signals. Morphological characteristics such as leaky vessels, massive vessel branching, large vessels and abnormal cell proliferation are common in angiogenic processes. Additionally, a recent and important concept is that angiogenesis mechanisms are frequent triggered in the early development of invasive cancers (Hanahan & Weinberg 2011).

As the last referred cancer hallmark, cells acquire invasion and metastatic features. E-cadherin, an essential protein to cell-to-cell adhesion, it is lost during malignancy final steps. Other cell-to-cell or cell-to-extracellular matrix proteins are typically mutated in aggressive carcinomas. N-cadherin, is another case of a mutated protein present in aggressive carcinomas which is normally activated in embryonic development for neuron migration. Invasion-metastasis process can be defined as a multi-step morphological modifier that occurs in cancer cells. In the first place local neoplasic cells invade the circulatory system. Sequentially, extravasion of cancer cells into the parenchyma of distant tissues forms micrometastasis. A final step of colonization occurs where small nodules turn into macroscopic tumors (Brooks et al. 2010)(Hanahan & Weinberg 2011).

1.2.2 Cell cycle regulation

The cell cycle comprehends four distinct phases: G1 (gap 1), S (synthesis), G2 (gap 2) and M (mitosis), all of them highly regulated in order to assure a correct cell division. During these events a variety of errors

can occur, namely DNA replication abnormalities. These eventually prompt cell cycle interruption by specific molecular mechanisms activation leading cells to a senescence state or unable to activate repair mechanisms to prevent programmed cell death. Occasionally, a cell cycle deregulation may lead to inefficient or insufficient repair mechanisms. Mutations on key genes like oncogenes or tumor suppressor genes such as TP53, will overcome cell cycle thigh regulation and attend to an uncontrollably cell multiplication and ultimately tumor formation (Lim & Kaldis 2013)

Cell cycle phases may be divided into two major groups: interphase that comprises G1, S and G2 phases which are responsible for cell growth and DNA replication; followed by mitosis (M phase) that comprises prophase, metaphase, anaphase and telophase which is shorter and responsible for nuclear and cell division. G1 phase, also known as growth phase is responsible for the increase of the biosynthetic activity rate and biosynthetic machinery, namely increased numbers of organelles, proteins and size. S phase is a crucial stage in interphase being responsible for the correct replication of DNA. At the end of this phase all chromosomes have an identical copy of itself. In G2 phase, cells continue to grow and ensure that "everything is ready" to enter in mitotic phase and divide. Apart from all described phases, cells may enter in G0 phase (followed by G1). It is a resting phase where cells do not grow nor multiply. Most non-proliferating cells are in G0, a quiescent phase (Kar et al. 2009).

Cell cycle major events of regulation are known as checkpoints. For commitment to progress in the cycle, cells must meet the criteria and conditions. Despite the variety of checkpoints, the dominant ones described in the literature are: i) G1/S restriction point; ii) G2/M transition checkpoint and; iii) metaphase to anaphase transition. These are regulated by cyclin dependent kinases (CDK) and cyclins were CDK, is a family of serine/threonine kinases proteins that are activated during each cell cycle phase and initiate a downstream signal to phosphorylate a set of specific proteins. CDK levels are maintained constant throughout the cell cycle in opposite of what happens with cyclin levels (Novák et al. 2009). Figure 1.5 synthetizes cell cycle phases as well as the regulating cyclins and CDK types of each phase.

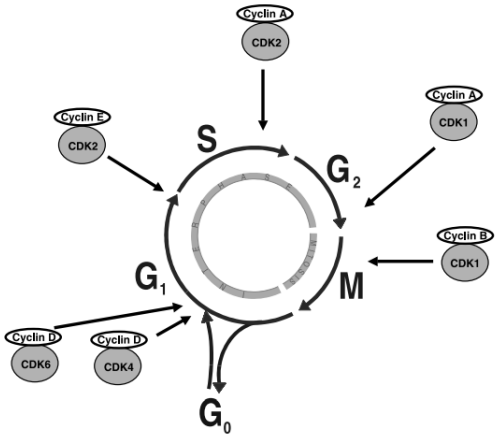

Figure 1.5 – Cell cycle phases and the respectively activated CDK/cyclin complexes in each phase. In late G1 phase CDK4/cyclin D and CDK6/cyclin D complexes are involved in regulation. G1/S transition is implicated CDK2/cyclin E complex. Late S phase regulator is CDK2/cyclin A complex. In G2/M transition, CDK1/cyclin A complex regulates the process. Mitosis progression is regulated by CDK1/cyclin B complex. Adapted from (Vermeulen et al. 2003)

G1 phase regulation assess if a cell passes to the S phase and ultimately to a new cell division or if the cell enters in a senescent phase, called G0. G1/G0 transition is characterized by retinoblastoma (Rb) protein and E2F transcription factors complex formation (occurring in early G1 phase). However if the cell is committed to enter in the S phase, CDK4 and CDK6, activated by increasing levels of cyclin D phosphorylates E2F, preventing Rb/E2F complex formation. A downstream signaling promotes the increase of other cyclins levels, namely cyclin E, that subsequently activates CDK2 promoting an S phase transition. DNA damage, promoted for instances by a ionizing radiation that induces DNA double-stranded brakes, triggers phosphorylation and activation of ATM (Ataxia telangiectasia mutated), a serine/threonine protein kinase that consequently phosphorylates a range of substrates involved in DNA repair, cell cycle arrest or programmed cell death. ATM inactivates MDM2 protein recurring to phosphorylation. MDM2, an ubiquitin ligase, targets p53 for degradation, allowing a p53 accumulation in the cell nucleus. By promoting transcription of genes like p21, a known inhibitor of all CDK/cyclin complexes, p53 promotes DNA repair and cell cycle arrest and can potentially trigger mechanisms of programmed cell death. Additionally, ATM activates Chk1 and Chk2 proteins that trigger p53 and Cdc25 phosphorylation. Cdc25, is known as the G1/S phosphatase and it is responsible to activate CDK2/cyclin E. As a phosphorylated protein, it cannot activate CDK-cyclin complex thus promoting cell cycle arrest (Bertoli et al. 2013).

To undergo from G2 phase to mitotic phase, cell mechanisms must confirm a fully and correct DNA replication. A damaged DNA triggers ATR (Ataxia Telangiectasia and Rad3 related) activation and subsequently Chk1 and Chk2 activation. This signaling pathway promotes Cdc25 (activator of CDK-cyclin complexes) phosphorylation. Progression in the mitotic phase is regulated by Cdk1-cyclin B complex which can no longer be activated due to the phosphorylated Cdc25 (Niida & Nakanishi 2006).

The spindle checkpoint between metaphase and anaphase controls if all chromatids are attached to the mitotic spindle by kinetochores. Cells with free kinetochores do not complete mitosis. CDK1-cyclin B promotes early mitosis events such as spindle assemble and nuclear membrane degradation. This complex also promotes Cdc20-APC activation (cell-division cycle protein 20-anaphase promoting complex), which breaks down cohesin, a protein involved in holding sister chromatins together. By promoting chromatids separation, anaphase and subsequently mitosis, are achieved. With free kinetochores, Mad2 protein (mitotic arrest deficient 2) is activated and binds to Cdc20. Unable to form Cdc20-APC complex, cell cycle mechanisms breaks down mitotic cyclins and promotes cell cycle arrest (Stumpf et al. 2013).

1.2.3 Cell death mechanisms

Trillions of cells constitute the human body and everyday intrinsic mechanisms control cell death. Since egg formation, cells suffer normal processes of death which balances the total number of cells in the organism. For instances, fingers on human embryos are formed by cell death of interdigital web (Elmore 2007a).

Referring to 1974, S. Brenner established *C. elegans* as a pioneering an experimental model organism that linked genetic analysis to cell division (Brenner 1974). Sequently Horvitz and coworker, which had continued Brenner's work, by discovering the main genes present in programmed cell death (Ellis & Horvitz 1986). Ever since the pioneering work in *C. elegans*, new mechanisms of cell death have been identified and new forms of classifying such mechanisms have been proposed.

In terms of classification, Nomenclature Committee on Cell Death (NCCD), improved directives to classify cell death (Kroemer et al. 2009). In 2015, new recommendations of NCCD have been published, discriminating cell death through biochemical parameters, in opposite of previous morphological parameters, and referring as either: i) accidental cell death (ACD) or; ii) regulated cell death (RCD) (Galluzzi et al. 2014).

Accidental cell death is indicated when cells are exposed to extreme stimuli such physical, chemical or mechanical, leading to a rapid loss of cell integrity. Alternatively, regulated cell death term is applied when the external or intrinsic stimuli triggers regulated machinery in cells leading to a controlled cell death. Programmed cell death, which includes caspase dependent apoptosis, is a subtype of RCD and involves mechanisms that preserves tissue homeostasis or occur as part of a developmental procedure (Galluzzi et al. 2014).

In literature are reported a wide diversity of regulated cell death modes such as necroptosis, autophagic cell death, pyroptosis, mitotic catastrophy, caspase-dependent apoptosis among others (L Galluzzi, Vitale, et al. 2012). Nonetheless, the scope of this thesis is mainly focused on caspase-dependent apoptosis and its intrinsic and extrinsic pathways thus for further consideration on ACD, RCD or on caspase-independent apoptosis refer to:(Galluzzi et al. 2014); (Sinha et al. 2013); (Vanden Berghe et al. 2014).

1.2.3.1 Caspase-dependent Apoptosis

Keer et al proposed in 1972, the first definition of apoptosis recurring to cells morphological features by electron microscopy. The spectrum of morphological characteristics that a cell passes through, comprises chromatin condensation, nuclear and cell shrinkage. A later event occurs, blebbing, the process by which the plasma membrane involves solid cellular material, typically occurs during the final stages of the apoptosis mechanisms, and it is the process by which apoptotic bodies are created. These structures,

containing nuclear material and organelles, are rapidly phagocytized by surrounding macrophages or parenchymal cells in a non-inflammatory process (Wickman et al. 2013).

Apoptosis is a highly regulated mechanism involving energy-dependent molecular events. The scientific community establishes the two most well-known apoptotic pathways as the intrinsic or mitochondrial pathway and the extrinsic or death receptor pathway (Ouyang et al. 2012). Ultimately, the two pathways converge on pro-caspases activation that subsequently activates other pro-caspases thus amplifying apoptotic signal – a caspase dependent apoptotic process. Caspases are known by their proteolytic activity and are efficient protein cleavers at their aspartic acid residues. Once caspase activation takes place, it seems to be an irreversible commitment towards programmed cell death (Snigdha et al. 2012).

An intrinsic apoptotic pathway is initiated by a non-receptor mediated stimuli (p53 activation due to irreparable DNA damage, temperature, high concentrations of Ca^{2+}, hypoxia, nutrient shortages among others) that triggers intracellular signaling (Bensinger & Christofk 2012). Consequently the stimuli causes changes in mitochondria namely, membrane pore opening and loss of the mitochondrial transmembrane potential thus forming mitochondrial outer membrane permeabilization (MOMP). Several pro-apoptotic proteins are released from mitochondria such as cytochrome c, Smac/DIABLO, and the serine protease HtrA2/Omiand. Cytochrome c binds to apoptotic protease activating factor 1 (APAF-1) as well as pro-caspase 9 to form the apoptossome. The protein complex activates pro-caspase 3 into caspase 3 that ultimately cleaves proteins (Lorenzo Galluzzi et al. 2012). Blebbing and apoptotic body formation occurs, and cells are later phagocytized by the primary immune system. Regulation of these events arise from B-cell CLL/lymphoma 2 (BCL2)-associated X protein (BAX) and BCL2-antagonist/killer 1 (BAK1) complex formation. BAX-BAK1 complex formation are under the control of BH3-only proteins (from BCL-2 protein family) (Aitken et al. 2011). The thin balance between pro-apoptotic and anti-apoptotic BCL-2 protein family regulates if a cell goes under apoptosis or not by altering mitochondria membrane permeability. About 25 genes of BCL-2 family were described as pro-apoptotic proteins such as Bcl-10, Bax, Bak, Bid and Bad or anti-apoptotic proteins such as Bcl-2, Bcl-x, Bcl-XL, Bcl-XS, Bcl-w and BAG (Kang & Reynolds 2009).

Extrinsic apoptotic pathway involves transmembrane death receptors and extrinsic pro-apoptotic ligands that transduce apoptotic signals and ultimately trigger cell death. Transmembrane death receptors are mainly members of the tumor necrosis factor (TNF) receptor gene superfamily that share a cysteine rich extracellular domain called “the death domain”, responsible to transmit death signal from membrane surface onto intracellular signaling. The best characterized ligands and respectively receptors are Fas Ligand/Fas Receptor and TNF-α/TNFR1. An initial receptor trimerization with ligands occurs and a cytoplasmic adapter protein is recruited. For instances, Fas ligand bind to Fas receptor and recruits FADD adapter protein. FADD protein binds to pro-caspase 8 formatting death-inducing signaling complex (DISC) and subsequently, activating caspase 8 – apoptotic signaling is triggered (Lavrik & Krammer 2012). As an example of regulation of extrinsic apoptotic pathway, cellular FLICE-like inhibitory protein (c-FLIP), a protein that binds to FADD

and/or to pro-caspase 8, interferes with DISC formation and consequently inhibiting apoptotic signaling (Bagnoli et al. 2010).

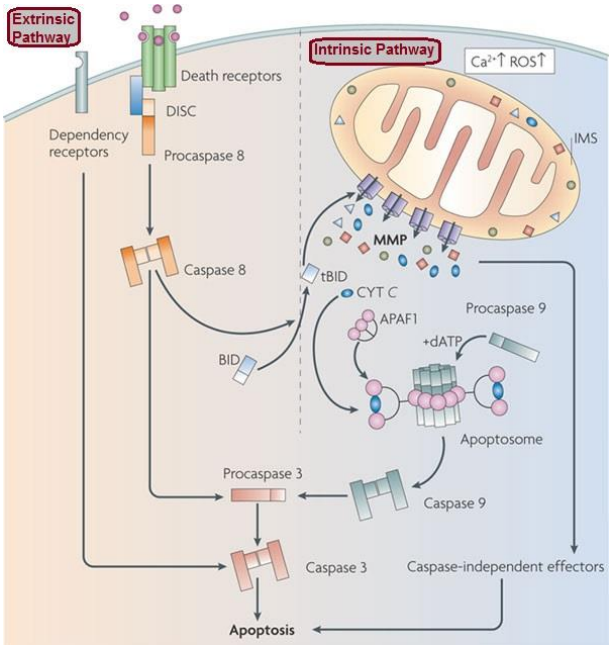

Figure 1.6 – Extrinsic (left) and intrinsic (right) pathways of caspase-dependent apoptosis. All pathways converge to caspase 3 activation, triggering protein cleavage. Adapted from (Galluzzi et al. 2009).

1.3 Cancer therapy: a variety of choices

As a highly complex disease, cancer therapy has a variety of choices and combinations. In general, all therapies emerge to be more specific, deadly and with less side effects for patients. Choosing the right therapy is also an insightful procedure that depends on the type of cancer, stage, molecular and physiological characteristics of cancer, location in the organism, patient socioeconomic environment and health conditions (Watanabe et al. 2012). The past few years, technological revolution has emerged to improve imaging, diagnosis and treatment approaches for cancer patients as in magnetic resonance, mutation maps and positron emission tomography (PET) scans (Seddon & Workman 2003).

Common therapies comprise surgery, chemotherapy and radiotherapy and can be used alone or in combination with each other simultaneously. Surgery is the typical first line therapy for early staged cancers. It is normally used as a coadjutant for other therapies such chemo- or radiotherapy. Based on cancer nature and stage, surgery is an insightful and thigh approach that takes into account the benefits over the disadvantages for the patient. Besides tumor removal, surrounding tissue is simultaneously removed as a preventive measure. Radiotherapy is frequently used in combination with surgery where an ionizing radiation, namely x-ray, is used to control or kill cancer cells. It is applied specially in localized solid tumors (Watanabe et al. 2012).

Other current therapies are being exploited with manifested benefits. Immunotherapy, hyperthermia, nanoparticle targeted therapy (Cabral & Baptista 2014), and photodynamic therapy are some examples of cancer therapy however the scope of this thesis will be mainly about chemotherapy discussed in the following chapter. For more information about the mentioned therapies refer to: (Alderton & Bordon 2012); (Soares et al. 2012); (Brannon-Peppas & Blanchette 2012); (Sanchez-Barcelo & Mediavilla 2014).

1.3.1 Chemotherapy

Chemotherapy is one the most employed therapies in cancer patients where are administrated systemic drugs to kill cancer cells or to treat symptoms as palliative care. It is a therapy applied in medicine over than 50 years and kills rapid proliferating cells or inhibits proliferation by selectivity of DNA or metabolic intervenient targeting. Chemotherapeutic drugs are ideally made with propose of being specific to cancer cells avoiding damaging healthy ones. Uncompromised cells with rapid proliferation ratios such as bone marrow cells are frequently killed by these drugs leading to secondary effects on patients (Bouwman & Jonkers 2012). Another disadvantage of chemotherapy is the acquired drug resistance during this procedure that will be addressed in the next chapters. Chemotherapeutic drugs can be grouped in several classes. Alkylating agents are a group of drugs that damages directly DNA molecules. Are examples cisplatin and oxaloplatin. Antimetabolites are a group of agents such as 5-fluorouracil, that interfere with DNA replication, affecting mainly cell cycle S-phase. They are analogous molecules of cells metabolites hence the irreversible interaction with DNA and impossibility of DNA replication. Antracyclines are an example of antitumor antibiotics which interferes with enzymes involved in DNA replication (e.g. doxorubicin). Topoisomerase inhibitors are a class of drugs that block the action of topoisomerases I or II, which are responsible for DNA unwinding just before replication. Doxorubicin is also included in this group. Mitotic inhibitors such as paclitaxel are often derived from natural products and act by blocking enzymes involved in protein synthesis essential to mitosis development. Corticosteroids are natural hormones of the human organism or hormone-like such as Prednisone or Dexamethasone. Other chemotherapeutic drugs such as hydroxiurea or L-asparaginase are a class of drugs that, by having different mechanism of action, do not fit in any of the previous classes (Tukenova et al. 2010). For this project, a combination therapy approach was performed using the Copper (II) compound and some FDA-approved chemotherapeutic drugs which will be addressed.

A common commercial chemotherapeutic drug is 5-fluorouracil (5-Fu), a uracil analogous used in cancer therapy namely in colorectal cancer. Approved by FDA, is a drug employed in combination with other chemotherapeutic drugs such as leucovorin, irinotecan or oxaloplatin. It inhibits thymidylate synthase and it is also a DNA or RNA intercalator. 5-Fu enters in the cell by facilitated transport such as uracil and is immediately converted into fluorodeoxyuridine monophosphate (FdUMP), fluorodeoxyuridine triphosphate (FdUTP) and fluorouridine triphosphate (FUTP) that ultimately disrupts RNA synthesis and inhibits

thymidylate synthase (TS). TS metabolizes deoxyuridine monophosphate (dUMP) into deoxythymidine monophosphate (dTMP) with folate as electron donor. FdUMP, the 5-fu metabolite, binds to the active site of TS forming a stable ternary complex with folate thus inhibiting dUMP binding and dTMP formation (Longley et al. 2003).

Afatinib is a heterocyclic compound used as first line treatment of non-small cell lung cancer (NSCLC) with positive mutation in epidermal growth factor receptor (EGFR). Acts as an inhibitor of tyrosine kinase such as Her-2 and EGFR (all from Herb2 protein family). As the first Herb2 family blocker being approved by FDA, inhibits signal transduction and consequently growth and proliferation signals. This protein family is often mutated in cancers (also including breast and colorectal cancers) thus plays a critical role in prevention of growth and proliferation of cancer cells(Janjigian et al. 2014). Cetuximab is a chimeric monoclonal antibody that was approved by FDA for several cancer types such as K-RAS wild type colorectal cancer or head and neck cancer. It bounds to extracellular domain of EGFR and consequently blocks cascade signaling of proliferation and growth (Lenz 2007). Dasatinib is a tyrosine kinase inhibitor of BCR-ABL and SRC family (but not from erbB kynases) and the mechanism of action passes through binding to these molecular targets. Dasatinib is indicated for treating chronic myeloid leukemia (CML) and Philadelphia chromosome-positive acute lymphoblast leukemia (Aguilera & Tsimberidou 2009). Doxorubicin is an antracycline firstly extracted from *Streptomyces peucetius* var. *caesius* in the 1970's. It is indicated for treating breast, gastric, ovarian, non-Hodgkin's and Hodgkin's lymphoma, thyroid, sarcoma, and lung cancers. Mechanism of action passes through blocking topoisomerase II, responsible for DNA replicative procedure. The stabilized protein no longer unwinds DNA molecule and replication stops (Thorn, Caroline; Oshiro, Connie; Marsh, Sharon; Hernandez-Boussard, Tina; McLeod, Howard; Klein, Teri; Altman 2012). Lapatinib is a dual tyrosine kinase inhibitor by binding to EGFR and HER2. It enters onto the cell and binds to the intracellular domain of tyrosine kinases thus blocking cascade signaling of cell growth and division. It is indicated for metastatic breast cancer with HER-2 positive mutation (Paul et al. 2008). Paclitaxel is a natural product first isolated in 1967 from *Taxus brevifolia*. Later discoveries assess that paclitaxel was also produced by a fungal endophyte in a synthetic medium. Paclitaxel is a microtubule stabilizer protecting them from disassembling in cell cycle causing a halt in anaphase. This drug is indicated for breast, lung, ovarian and liver cancers (Lever 2012)

1.3.1.1 Metallic complexes in cancer

Medicinal inorganic chemistry is a growing field where compounds containing metallic elements are employed in several human diseases as treatment. They benefit from organic compounds by possessing several coordination numbers, geometries, redox states and the intrinsic characteristics of the metal itself (Alessio 2011). Cisplatin was the first FDA-approved metallic compound to be applied in cancer therapy and was indicated for treating testicular and ovarian cancers. Nowadays it is being applied in additional cancers

such as bladder, cervical, malignant mesothelioma and non-small cell lung cancers. Despite encouraging results, the use of cisplatin endows several adverse characteristics such as secondary effects in patients and acquired drug resistance by cancer cells (Martins et al. 2014). This prompted chemists to synthetize new compounds with different metals such as gold, copper, ruthenium and new ligands, selected for improving compounds pharmacological and pharmacodynamics properties (Martins et al. 2014).

Based on the concept that endogenous metals are less toxic for the organism, copper-based compounds have shown promising results in cancer therapy. Copper is an essential element in the organism, important in several biochemical reactions and, as a metal, is highly reactive with biomolecules, hence the tight intracellular regulation. Some dysregulation on those mechanisms are often linked to illness such as Wilson's disease, Alzheimer's, aceruloplasminemia and cancer. Some case reports show that increased copper and ceruloplasmin levels in human tissues are related with cancer progression. Copper leads to reactive oxygen species (ROS) production in cells and is associated with metabolic changes in cancer cells. The altered metabolism and different response in cancer cells lead to a boom in copper-compound synthesis to treat cancer. Compounds synthetized are mainly copper (I) and (II), and as anticancer drugs exhibited several classes of mechanisms including: DNA interaction by intercalation, groove binding, oxidative or hydrolytic cleavage; topoisomerase inhibition and; proteasome inhibition (Mendo et al. 2015)(Iakovidis et al. 2011).

The copper compound used in this project is a copper (II) 1,3,5-triazapentadienato complex (Kopylovich et al. 2010) (named hereafter K4) and is shown in Figure 1.7. Cyclic ligands with nitrogen elements, in copper complexes, have shown mechanisms of DNA binding in cancer therapy, revealing cytotoxic effects at a nanomolar scale (O'Connor et al. 2012)(Jaividhya et al. 2012).

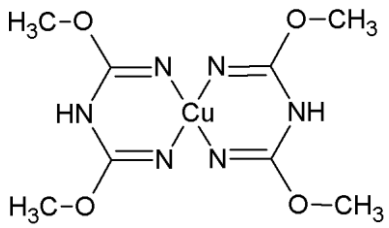

Figure 1.7 – Chemical structure of copper (II) 2,4-metoxy 1,3,5-triazapentadienato, referred as K4 and used in this project.

1.3.1.2 Combined therapies

Chemotherapeutic approach in cancer therapy has shown in last decade to be a major solution with a wide range of promising results. However, as mentioned above, cancer cells often acquire resistance to drugs.

The mechanisms that a cancer cell passes to become resistant to a drug includes loss of membrane receptor or transporter, mutation of molecular targets of the drugs, limiting uptake and increase efflux rates (Holohan et al. 2013). Additionally, a tumor possesses several genetically different mutated cells. Genetic and epigenetic changes occur in each cell differing them from the neighbor. These factors lead to an inefficient treatment for cancer patients.

Combined therapy is a type of treatment that includes more than one drug or therapy for a disease. Through the use of two or more different types of drugs, the acquired drug resistance or tumor heterogeneity can be overcome. Ideally it is used drugs with different mechanisms of action in order to avoid drug resistance mechanisms by cells. Combination approach has been employed clinically and has emerge to be specific for each cancer type (Pinto et al. 2010).

1.3.2 Nanomedicine

Nanomedicine is defined as the application of nanotechnology to medicine. Nanoparticles (NPs) appliance in cancer treatment show paramount efficacy in targeting tumors as well as imaging and therapy. The employment of nano-sized particles (1-100 nm) has its benefits such high surface/volume ratios, versatile particles sizes and versatile structures, thus revolutionizing cancer diagnosis and treatment (Coimbra et al. 2015)

Concepts such as i) enhanced retention and permeability (EPR) effect, ii) mononuclear phagocyte system (MPS) and iii) optimal intrinsic features are important concepts to grasp concerning nanocarriers benefits. Considering a rapid cell proliferation, tumor vasculature is abnormal with leaky walls and lymphatic vessels collapse in solid tumors. A porous tumor vasculature and an impaired lymphatic system are the ideal feature for nanoparticles to accumulate in tumors sites – EPR effect - thus achieving passive targeting of NPs. Mononuclear phagocyte system is part of the immune system and is responsible for macromolecules clearance. Nanoparticles may, however, interact with MPS conducting to their elimination from circulatory system which consequently lowers NPs effects. One strategy to avoid MPS clearance is to attach macromolecules onto NPs surface such as polyethylene glycol (PEG) in other to enhance their biodistribution. Particularly, bifunctional PEG, a polyether molecule with a thiol group at an end and a carboxyl group at the other end serves a double purpose nanovectorization approach. It is simultaneously used to extend compounds biodistribution and increase nanoparticle stability. Furthermore it reduces clearance and toxicity in the organism (Conde, Baptista, et al. 2012). Nanoparticles have intrinsic features that make them ideal for cancer therapy. For instances, NPs under 100 nm are exceptional tumor targets although exhibited lower internalization rates. However NPs smaller than 20 nm have high internalization rates but lower retention effects. Charge and shape are also important features defining uptake, macrophage clearance and biodistribuiton success (Bao et al. 2014)(Wang et al. 2012). Among the wide

variety of NPs they can be grouped into polymer-based or lipid-based nanoparticles, dendrimers, ceramic nanoparticles, metal nanoparticles and carbon nanotubes (Coimbra et al. 2015). We distinguish a subgroup of metal nanoparticles: Gold nanoparticles that possess unique optical features that makes them suitable for systems of drug delivery and diagnosis. Surface plasma resonance (SPR), an intrinsic characteristic of gold nanoparticles, results from high absorption and light scattering (Cabral & Baptista 2014).

Nanotechnology improves drugs pharmacokinetics and pharmacodynamics. Grafting an anticancer drug to a gold nanoparticle can improve their biodistribution, physical-chemical properties as the targeting effect. Nanovectorization of compounds is suitable approach for adding the benefits of chemotherapeutic drugs with the benefits of the nanocarriers – a smart and improved choice for cancer therapy.

1.4 Aims and goals

The first goal for this project was the assessment of the antiproliferative potential of a selection of metallic compounds in lung adenocarcinoma and colorectal cancer cell lines. From the wide number of compounds initially tested, only a copper (II) compound (K4) was selected for further biological studies in colorectal carcinoma cell line. In order to establish K4 mechanism of action and molecular targets in colorectal carcinoma cell line, mechanism of death, cell cycle analysis, proteome analysis and *in vitro* interaction between K4 and nucleic acids (DNA) or proteins (BSA) were performed. Another goal of this project was the design and characterize a novel nanovectorization system for delivering the copper (II) compound to cancer cells and to compare the cytotoxic effect of this system with the free compound. The final goal of this project was to established new therapeutic combinatory approaches using K4 compound and commercial anticancer drugs such as 5-fluorouracil, afatinib, cetuximab, dasatinib, doxorubicin, lapatinib and paclitaxel, for targeting colorectal cancer.

2. Materials and Methods

2.1 Metallic complexes and other FDA approved drugs studied

Metallic compounds studied were synthetized in Center of Chemistry of Instituto Superior Técnico and provided by Drª. Luísa Martins. The plethora of metallic complexes, containing iron, manganese, cobalt and copper centers were either dissolved in distilled water (dH_2O) or dimethyl sulfoxide (DMSO) (Table 2.1). Compounds were stored at room temperature (≈25ºC) in the absence of light along with the remaining compound powder. Table 2.1 summarizes metallic complexes general features.

Table 2.1 - Code name, chemical formula and molecular weight of every compound studied as the respective solvent they were dissolved with.

Code name	Chemical formula	Molecular weight ($gmol^{-1}$)	Solvent
K0	$C_{10}H_{10}Cl_2FeN_6$	340.98	dH_2O
K1	$C_{12}H_6Cl_{18}FeN_9$	1126.50	DMSO
K2	$C_{12}H_6Cl_{18}MnN_9$	1047.50	DMSO
K3	$C_{12}H_6Cl_{18}CoN_9$	1049.50	DMSO
K4	$C_8H_{14}O_4CuN_6$	829.40	DMSO

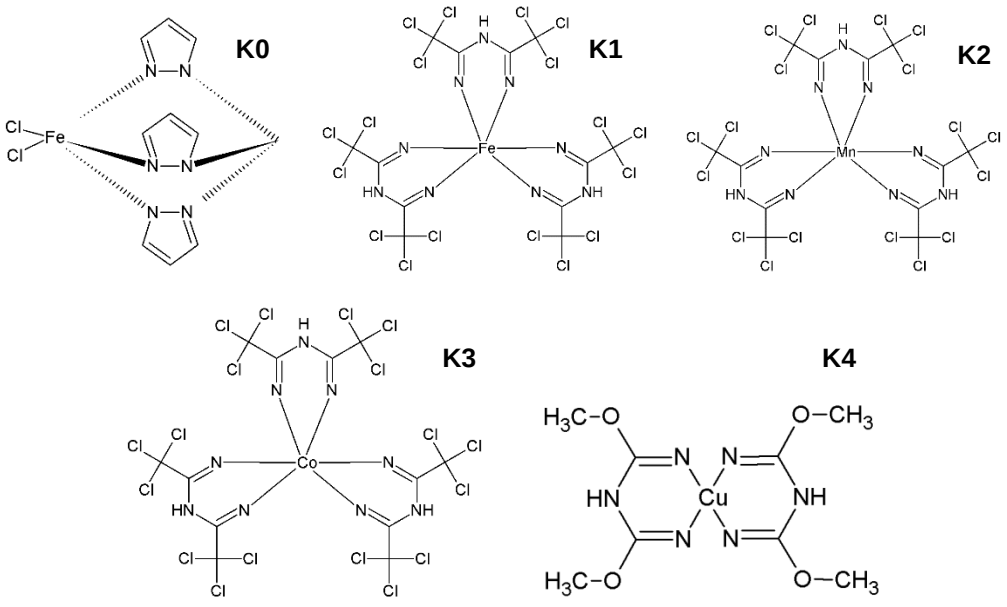

Figure 2.1 – Molecular structure of metallic compounds studied in the development of this project. Compounds K0, K1, K2, K3 and K4.

Other commercial drugs used clinically in cancer treatment were also employed during the development of this project in order to establish new potential anticancer strategies. Respectively the features of doxorubicin, afatinib, lapatinib, 5-fluorouracil, paclitaxel, dasatinib and cetuximab are compiled in section 2.10.1.

2.2 Human Cell lines: tissue types, maintenance and quality control

Throughout the development of this project, two types of adherent human cancer lines, A549 (lung adenocarcinoma) and HCT116 (colorectal carcinoma), were used in order to evaluate antiproliferative effect of the compounds described in section 2.1. A primary culture of fibroblasts was also used for assessing compound K4 cytotoxicity in healthy cells. All cell types were obtained from ATCC®. Table 2.2 summarizes cell lines used and general characteristics such as source, morphology and growth medium.

Table 2.2 - Cell lines used during the project development and its generic characteristics such as source, morphology and growth medium. DMEM - Dulbecco's Modified Eagle Medium (Invitrogen, New York, EUA); FBS - Fetal Bovine Serum (Invitrogen, New York, EUA). Pen/Strep - antibiotic/antimicotic (Penicilin-Streptomicin (Pen–Strep) + Antimicotic); Invitrogen, New York, EUA). NEA – Non-essential amino acids 100x (Sigma, St. Louis Missouri, EUA). *- healthy primary culture. (Source: ATCC: The Global Bioresource Center, 2015)

Cell lines	Source	Morphology	Growth medium % (v/v)
A549	Non-small cell lung adenocarcinoma	Epithelial	DMEM FBS 10 % Pen/Strep 1 %
HCT116	Colorectal carcinoma	Ephitelial	DMEM FBS 10 % Pen/Strep 1 %
***Fibroblasts**	Foreskin	Sindle-shaped/ bipolar and refractile	DMEM FBS 10 % Pen/Strep 1 % NEA 1x

As an animal cell culture standard procedure, all cell types used were cultivated in 75 cm^2 BD vented cell culture flasks (BD Biosciences, New Jersey, EUA) in DMEM (Invitrogen, New York, EUA) supplemented with 10 % (v/v) FBS (Invitrogen) and 1 % (v/v) of Pen–Strep + Antimicotic; Invitrogen, New York, EUA). Additionally, healthy fibroblasts were cultured in DMEM supplemented with 10 % (v/v) FBS, 1 % (v/v) of Pen–Strep + Antimicotic and non-essential amino acids 100x (NEA, Sigma, St. Louis Missouri, USA). All cell types were maintained in an incubator with controlled atmosphere (5 % (v/v) CO_2 and 99 % (v/v) humidity) at 37 ºC (SANYO CO_2 Incubator, Electric Biomedical Co., Osaka, Japan).

Concerning the already mentioned monolayer cell cultures, regular subculturing was required to maintain an exponential growth. Upon reaching 80% cell confluence (Olympus CXX41inverted microscope, Tokyo, Japan), cells are ready to be subcultured to avoid lack of nutrients in the growth medium and loss of growth due to contact inhibition. Initially, medium was discarded and replaced by 2 mL of TrypLE™ Express, a trypsin analogous which helps cells to detach culture flaks, (Invitrogen, New York, EUA). After 5 minutes at 37ºC, 5% (v/v) CO_2 and 99% (v/v) humidity, TrypLE™ Express action was blocked by the addition of 2 mL of fresh medium (Table 2.2). Cell suspension was transferred to 15 mL BD Falcons (BD Biosciences) and centrifuged for 5 minutes under 233 g at 15ºC (Sigma 3-16K 10280, Tuttlingen, Germany). Supernatant containing trypsin analogous, old medium and cellular debris was discarded and the remaining pellet was resuspended in 2mL fresh growth medium. The appropriate volume of the cell suspension was added to 10 mL of fresh growth medium depending on the requirements for further assays, and maintained in a new 75 cm^2 cell culture flask, incubated at 37ºC in a controlled atmosphere of 5% (v/v) CO_2 and 99% (v/v) humidity.

Due to cell culture susceptibility to foreign contaminations a periodically quality control assessment was performed. Prone to alter DNA, RNA and protein expression, Mycoplasma is recognized by the scientific community as highly common cell culture contamination. Characterized, among other features, by its lack of cell wall and by the ability to internalize animal cells it is often found to be resistant to common antibiotics present in growth medium such as penicillin and streptomycin. Furthermore by being imperceptible to the naked eye, a regular polymerase chain reaction (PCR) method is recommended to guarantee a free contamination cell culture (Drexler & Uphoff 2002). The procedure for Mycoplasma detection is described in Appendix A.

2.3 Cytotoxic potential evaluation

2.3.1 Cell viability essays

Cell viability assays were performed for every compound mentioned in section 2.1 in A549, HCT116 and fibroblasts, using CellTiter 96® AQueous Non-Radioactive Cell Proliferation Assay (Promega, Madison, USA), a colorimetric method employed to determine viable cells.

Cells were harvested and centrifuged as mentioned in section 2.2. After the addition of 2 mL of fresh growth medium, cell density assessment was required in order to obtain 0.75 cell/mL in each well of a flat bottomed 96-well plates (VWR, Radnor, Pennsylvania, USA). Applying trypan blue exclusion method, cell count was performed using a hemocytometer (Hirschmann, Eberstadt, Germany) loaded with a solution of cell suspension 1:10 and trypan blue solution 1:5 (Sigma, St. Louis, USA) diluted in fresh growth medium. Cells were observed using an Olympus CXX41inverted microscope, Tokyo, Japan. Trypan blue is a dye selective to cells with loss of membrane permeability thus is used to exclude unviable cells from count. Final assessment of cell density (in cells/mL) is given by equation (1):

$$\frac{Total\ cell\ count\ from\ 4\ quadrants}{4} \times 10\ (\text{Dilution factor}) \times 10^4(chamber\ volume) \qquad (\mathbf{1})$$

After a 24h cell seeding at 37ºC in a 5% CO_2 (v/v) and 99% (v/v) humidity atmosphere, a range of concentrations of each compound diluted in fresh medium, were added to the cells with a subsequently incubation period of 48h. A solution of *[3-(4,5-dimethylthiazol-2-yl)-5-(3-carboxymethoxyphenyl)-2-(4-sulfophenyl)-2H-tetrazolium*, MTS (inner salt) and *phenazine methosulfate*, PMS (electron coupling agent) diluted in fresh medium in a proportion of 100:19:1 was added. After an incubation period of approximately 45 minutes under the conditions described above, absorbance measurement at 490 nm of each well was determined with Tecan Infinite F200 Microplate Reader (Tecan, Männedorf, Switzerland).

The theoretical basis for the application of this assay is based on the MTS reduction by mitochondrial dehydrogenases, only found in metabolic active cells, into a water soluble compound namely formazan which absorbs at approximately at 490 nm. The amount of formazan produced is hence directly proportional to the number of viable cells (Promega 2012).

Obtained data was normalized relative to control samples in order to obtain cell viability for each compound concentration with Equation (2):

$$Cell\ viability(\%) = \frac{Sample\ absorbance\ (490\ nm)}{Control\ absorbance\ (490\ nm)} \times 100 \qquad (\mathbf{2})$$

The relative IC_{50} values for each compound was also calculated using GraphPad software (Graph Pad Software Inc., San Diego, CA, USA). Absolute IC_{50} corresponds to a compound concentration that causes 50% of cell metabolic inhibition. Notwithstanding, relative IC_{50}, concept used in this project, corresponds to the halfway point from maximum viability *plateau* and minimum viability *plateau* from an inhibition curve, not always corresponding to a 50% cell viability (Neubig et al. 2003).

In order to select the most promising compound an initial screening was made by testing a range of concentrations of all metallic complexes in A549 (lung adenocarcinoma) and HCT116 (colorectal carcinoma) cell lines. From this initial screen, K4 compound containing a copper center was selected to continue further studies and HCT116 cell line owing to its most promising results.

2.4 Apoptotic potential evaluation

2.4.1 Hoechst 33258 Staining

An initial apoptotic potential evaluation was assessed by the use of Hoechst 33258 dye (Phenol, 4-[5-(4-methyl-1-piperazinyl)[2,5'-bi-1H-benzimidazol]-2'-yl]-, trihydrochloride 23491-45-4). Hoechst 33258, a cell permeable dye that presents high affinity for A-T rich regions in the minor groove of DNA allowing its visualization in a fluorescence microscopy (excitation and emission wavelengths of 352 and 461 nm) (Invitrogen 2005). It is a powerful tool to detect apoptosis hallmarks such aberrant nuclei morphology, chromatin condensation and apoptotic bodies (Elmore 2007b).

HCT116 cells were cultivated in 35 mm^2 plates with lamellae (VWR, Radnor, Pennsylvania, USA), previously washed with 70% (v/v) ethanol and phosphate buffered saline 1x (PBS), at a cell density of $1x10^5$ cells/mL. After a 24 h incubation at 37 ºC, 5 % (v/v) CO_2 and 99 % (v/v) humidity, culture medium was removed and replaced by K4 compound at his IC_{50} concentration diluted in fresh medium. Following a 48h incubation at 37 ºC, 5 % (v/v) CO_2 and 99 % (v/v) humidity, the medium was removed once more and cells were rinsed three times with PBS 1x. Afterwards, cells were fixed in the lamellae with cold paraformaldehyde 4% (v/v) (PFA), in the absence of light, at room temperature for 10 minutes. Cells were again washed three times with PBS 1x to remove all PFA. In the following step, cells were incubated with a Hoechst solution of 0.8µL Hoechst 33258 from Sigma-Aldrich (5 mg/ml) and 400µl of PBS 1x in the absence of light, at room temperature, for 15 minutes, followed by a 3 times wash with PBS 1x. Separately slides were prepared with 5 µl of a solution of glycerol diluted with PBS in 1:3 ratio. Then, very carefully, each lamellae was detached from the plate, inverted and observed and photographed with an Olympus BX51 fluorescent microscope with an attached Olympus DP50 (Olympus) camera. Photographs were acquired with Infarview software.

2.4.2 Annexin V-FITC and Propidium iodide staining

Annexin V-FITC (Fluorescein Isothiocyanate) and propidium iodide double staining is a common procedure to discriminate viable, early apoptotic, late apoptotic and necrotic cells in a sample by exploiting morphological and molecular hallmarks of apoptosis. One of the early apoptosis events is characterized by the translocation of phosphatidylserine (PS) from inner membrane leaflet to outer membrane leaflet. Annexin V, a Ca^{2+} dependent phospholipid-binding protein possess high affinity to PS and so by capitalizing on this protein interaction it is possible to assess early apoptosis in cells with exposed PS through Annexin V-FITC. On the other hand, propidium iodide, with a high affinity to nucleic acids, only internalizes cells with compromised cell membrane, thus allowing to assess late apoptosis and necrosis. The combination of this two dyes is an efficient method to quantify viable, apoptotic or necrotic cells in a sample (Invitrogen 2010) .

HCT116 cells were initially seeded with a cell density of $1x10^5$ cells/mL in 35 mm culture dishes over 24 h at 37 ºC, 99 % (v/v) humidity and 5 % (v/v) CO_2. After seeding, cells were exposed for a 48 h incubation

period to: 1) a solution of compound K4 (at its IC_{50} concentration), 2) a solution of K4 compound (at 1.5 fold the IC_{50} concentration) and 3) a solution of 0.1 % (v/v) DMSO (control group). Upon completion of the 48 h incubation period, cells were centrifuged at 233 g for 5 minutes at room temperature, trypsinized (section 2.2), and the cell pellet resuspended in PBS 1x. The wash procedure was repeated three times. 100 µL of annexin binding buffer 1x (Invitrogen, CA, USA) were added to cell suspension. Afterwards 5 µL of annexin V-FITC and 2 µL of propidium iodide were added to cell samples followed by 15 min incubation at room temperature in the absence of light. 400 µL of annexin binding buffer 1x and 500 µL of PBS 1x were added to the 100 µL cellular suspension. Following the staining procedure, cells were analyzed by flow cytometry on an Attune® Acoustic Focusing Flow Cytometer (Life Technologies, California), with the acquisition of at least 10000 events per each sample.

2.5 Cell Cycle Progression analysis

2.5.1 Propidium iodide staining

The effects of compound K4 exposure on cell cycle progression was performed using a standard propidium iodide staining procedure followed by flow cytometry analysis. Propidium iodide is a fluorescent intercalating agent that as high affinity to nucleic acids (excitation maximum of 535 nm and emission maximum of 617 nm)(Krishan 1975).

HCT116 cells were seeded and incubated for 8 h at 37 ºC, 99 % (v/v) humidity and 5 % (v/v) CO2 with a cell density of $1x10^5$ cells/mL. Cell cycle synchronization was achieved by a double block with thymidine, a common S-phase blocker used to arrest and synchronize cells in the early S-phase (Bostock et al. 1971). After 8 h incubation, the first block was performed by adding 2 mM thymidine (Sigma, St. Louis, USA) followed by a 14 h incubation. Afterwards, the old medium was removed and replaced with fresh medium without thymidine for a 10 h incubation period at 37 ºC, 99 % (v/v) humidity and 5 % (v/v) CO_2. The second blockage was performed by adding 2 mM thymidine followed by a 14 h incubation period. Concluded the thymidine block procedure, K4 compound was added to HCT116 cells in the respective IC_{50} concentration and as a control group a solution of 0.1% DMSO was added in parallel. Cells were exposed to compound and DMSO for 3, 6 and 9 h. After each time point, cells were trypsinized with TrypLE™ Express and centrifuged for 5 minutes at 415 g at 4 ºC (Sigma 3-16K 10280, Tuttlingen, Germany). Supernatant was removed and the pellet was resuspended in PBS 1x. An additional centrifugation was performed in the previous mentioned conditions. Subsequently, supernatant was discarded and the pellet was resuspended in PBS 1x and ethanol 80 % (v/v) in a proportion of 1:1. Ethanol solution was added cautiously and with constant vortex agitation. Cells were stored at 4 ºC for at least 12 h. After incubation, cells were centrifuged for 5 min at 415 g at 4 ºC. Supernatant was removed and the pellet resuspended in a propidium iodide solution (50 µg/mL propidium iodide, 0.1 % sodium citrate, 0.02 ng/mL RNAse, 0.20 % NP-40 pH=7, diluted

in distilled water) for 30 min. The analysis was performed on Attune® Acoustic Focusing Flow Cytometer (Applied Biosystems). Data collected was treated in Microsof excel 2010 software.

2.6 DNA interaction analysis

2.6.1 UV-Vis spectroscopic assays

Some anticancer compounds mechanism of action comprises interaction with DNA. Cisplatin mechanism of action for instance is known to affect DNA's overall architectural structure in a crosslinking fashion that ultimately triggers apoptosis (Hurley 2002). The ability of compound K4 to interact with DNA was assessed.

As a preliminary assay the compound stability assessment in aqueous buffer over time was performed in order to obtain a stability curve. An 80 µM K4 solution diluted in 5 mM Tris-HCl (Merck), 50 mM NaCl (Panreac), pH 7.0 buffer was incubated at 37 ºC for a time period of 15, 30, 60, 180 and 360 min. Spectra was obtained using Evolution 300 UV-Vis spectrophotometer (Thermo Scientific). Data analysis revealed that 30 min incubation was the optimum time point to perform further assays since at this time point the compound maintained its characteristic absorption peak.

For DNA interaction assays it was used Calf Thymus-DNA (CT-DNA, Invitrogen) which concentration was determined using NanoDrop by reading its absorbance at 260 nm and considering DNA molar extinction 6600 $M^{-1}cm^{-1}$ (Saha et al. 2010). Applying Lambert Beer's law it is possible to calculate CT-DNA concentration:

$$\boldsymbol{A = \varepsilon \times b \times C} \quad (\mathbf{3})$$

Where A is 260 nm absorbance, ε is molar extinction coefficient of DNA described above, b is the optical path in cm and C is CT-DNA concentration in M (Huang et al. 2013).

Absorption titrations were performed with fixed amount of K4 compound (80 µM) and increasing concentrations of CT-DNA (0-160 µM). Samples were prepared in 5 mM Tris-HCl (Merck), 50 mM NaCl (Panreac), pH 7 buffer and incubated for 30 minutes at 37ºC. Control group was performed in relation to a solution of CT-DNA with DMSO in the same proportion used for compound K4. Spectra was obtained using Evolution 300 UV-Vis spectrophotometer (Thermo Scientific). Data was analyzed in Microsoft Excel 2010 software and it was possible to calculate binding constant of K4 to CT-DNA using the following equation:

$$\frac{[\boldsymbol{DNA}]}{(\boldsymbol{\varepsilon a - \varepsilon f})} = \frac{[\boldsymbol{DNA}]}{(\boldsymbol{\varepsilon b - \varepsilon f})} + \frac{\mathbf{1}}{\boldsymbol{Kb}(\boldsymbol{\varepsilon b - \varepsilon f})} \quad (\mathbf{4})$$

Where [DNA] is CT-DNA concentration in M, εa, εf and εb are the apparent, free and bound complex extinction coefficients and Kb is the binding constant of K4 to CT-DNA in M^{-1}(Huang et al. 2013).Kb was calculated by a linear regression of [DNA]/(εa-εf) over [DNA] (equation 4). Respective slope and intercept values of the linear regression were divided to obtain Kb value. (Subhan et al. 2012).

2.6.2. pDNA cleavage assays

K4 interaction with DNA was performed by pDNA (pUC18 plasmid (Fermentas, Maryland, EUA) cleavage assays. Samples were prepared with a constant concentration of pUC18 (10 ng/µL) and a range of K4 concentrations (0 to 160 µM) diluted in 5 mM Tris-HCl 50 mM NaCl pH 7.0 buffer incubated for 30 min at 37ºC. Control solution contained DMSO in the same proportion used for K4 compound. After incubation, samples were loaded with 4 µL of 6x loading dye (Fermentas, Maryland, EUA) and an electrophoresis was performed with 0.7 % (w/v) agarose gel stained with 2 % (v/v) GelRed (10 000x; Biotarget, Portugal) under 70 Volts for 2 h. Molecular weight marker used was λ/HindIII (Fermentas, Maryland, EUA). The obtained gels were visualized and acquired with Molecular Imager® Gel Doc™ XR, System with Image Lab™ Software (BioRad, Berkley, California) and GelDoc software. Data was analyzed using FIJI is just ImageJ (FIJI) software.

2.7 BSA interaction analysis

As means to assess K4 ability to bind to proteins, bovine serum albumin (BSA) was chosen as the gold standard protein model for interaction studies. The compound K4 ability to interact with proteins could be indicative of intrinsic molecular targets and increased systemic biodistribution.

2.7.1 UV-Vis spectroscopy assays

K4 stability curve was assessed using 10 mM pH 7 phosphate buffer 0.15 M NaCl buffer in the same conditions mentioned in section 2.6.1. A 30 min incubation period at 37 ºC was chosen to perform K4 and BSA interaction studies in similarity with K4 DNA interaction assays.

For K4 and BSA interaction assays, several solutions were prepared containing a constant BSA concentration (Sigma, St. Louis, USA) (15 µM), and a range of K4 concentrations namely 10, 20, 40 and 80 µM, diluted in 10 mM pH 7 phosphate buffer/0.15 M NaCl buffer. Control solutions contained only K4 compound in the same proportions used in previous solutions (10, 20, 40 and 80 µM). After a 30 min incubation at 37 ºC, UV-Vis spectrum of each solution was obtained (from 230 nm to 500 nm) as mentioned

in section 2.6.1. Results were analyzed using Microsoft Excel 2010 software by subtracting control group spectra from samples spectra.

2.7.2 Spectrofluorimetric assays

To further assess K4 interaction, spectrofluorimetric assays with BSA, were performed. For this purpose several solutions were prepared containing a fixed BSA concentration (2 µM) and increasing K4 concentrations (5, 10, 20, 40, 80 and 160 µM). Samples were prepared in 10 mM pH 7 phosphate buffer/0.15 M NaCl buffer. Control solutions contained only K4 compound in the same concentration used in previous solutions (5, 10, 20, 40 and 160 µM). After a 30 min incubation at 37 ºC, fluorescence measurements (between 300 and 500 nm) were performed at room temperature (RT) using a Spex FL-1057 Tau 3 spectrofluorometer (Horiba, Kyoto, Japan). Results obtained were analyzed using Microsoft Excel 2010 software and the following equations.

$$\frac{F_0}{F} = 1 + K_{SV}[K4] \quad (5)$$

Where F and F_0 are fluorescence maximum intensity of BSA with and without quencher (K4) respectively, Ksv is the Stern-Volmer constant and [K4] is the quencher concentration. A Stern-Volmer plot (F_0/F vs [K4]) was obtained (Gelamo et al. 2002). Data obtained from fluorescence measurements was also analyzed using the following equation:

$$log\left(\frac{F_0 - F}{F}\right) = log\, K + n\, log[K4] \quad (6)$$

Where K is the binding constant and n is the number of BSA binding sites to K4. Log (F_0-F/F) was plotted against log[K4] to obtain K and n values from slope and intercept numbers (Chakraborty & Basu 2009). However, K and n values were not possible to obtain due to negative results of log(F_0-F/F).

2.8 Proteome profiling: Two-Dimensional Gel Electrophoresis

2.8.1 Cell line compound exposure

HCT116 cells were cultured in 75 cm^2 BD vented cell culture flasks as mentioned in section 2.2. After a 24 h seeding, the depleted growth medium was discarded and replaced by K4 IC_{50} concentration or 0.1% (v/v) DMSO as control group, all diluted in fresh medium. Cells were incubated for 48 h, harvested and centrifuged as mentioned in section 2.2. Two additional centrifugations at 500 g for 5 min were performed, discarding the supernatant and ressuspending the pellet with PBS 1x. Trypan blue exclusion method and

cell counting was performed as mentioned in section 2.2 however cells were diluted in PBS 1x and not in fresh medium.

2.8.2 Sample preparation: Protein extraction and purification

Cells diluted in PBS 1x were centrifuged for another 5 min at 500 g discarding the supernatant. A final spin was performed to ensure the complete removal of the supernatant in excess. Lysis buffer containing NaCl-Tris-EDTA buffer (150 mM NaCl; 50 mM Tris, pH=8; 5 mM EDTA), phosphatase inhibitors 1x (PhosStop, Roche), protease inhibitors 1x (complete ULTRA Tablets, Mini, EASYpack, Roche, Basel, Switzerland), 0.1 % (w/v) dithiothreitol (DTT) (AMRESCO, USA), 1 mM of phenylmethylsulfonyl fluoride (PMSF) (Sigma), 2 % (w/v) Nonidet P-40 (Thermo Scientific, Massachusetts, EUA) was added to HCT116 cells (100 µL per $4x10^6$ cells/mL). After a 2h incubation period at RT cell suspension was ultrasonicated as mentioned in Table 2.3 and stored at -80 ºC.

Table 2.3 – Ultra sonication protocol used for total protein extraction. After each cycle, cells were maintained on ice for 30 seconds to overcome protein loss and overheating.

Cycles	Pulses	Output (%)
5	5	70 %
15	10	80 %
20	20	90 %

Total protein precipitation and purification was performed using 2D Clean-Up Kit (GE, Healthcare, Little Chalfont, United Kingdom) according to the manufacturer's protocol (Healthcare 2009) with exception for wash additive and wash buffer step, where cell lysates were incubated overnight at -20 ºC. Moreover an additional wash step was also performed, where 25 µL of dH_2O were added to disperse pellet. Wash buffer and wash additive were added in the same proportions according to the manufacturer's protocol.

After centrifugation, 100 µL of re-hydration buffer (7 M urea (BDH Prolabo, VWR International), 2 M Tiourea (Merck, Frankfurt, Germany), 2 % (w/v) (3-[(3-Cholamidopropyl)dimethylammonio]-1 propanesulfonate) (CHAPS) (GE Healthcare), phosphatase inhibitors 1x, protease inhibitors 1x, bromophenol blue (Merck), 1 µL 10 % (w/v) DTT and 1µL of 100 mM PMSF)) were added to protein extract, and allowed to react overnight at RT. After a 15 min centrifugation under 13000 g, supernatants were recovered.

For total protein quantification, Pierce Protein Assay kit (Thermo Scientific, MA, USA) was used. Initially, a calibration curve was established with several standard bovine serum albumin (BSA) solutions from 0 to 1000 µg/mL (Thermo Scientific, MA, USA). On the other hand, protein extracts were diluted in 1:10

proportion in dH_2O. Sequentially, it was added 150 µL Pierce reagent followed by 5 min incubation at RT. Absorbance's were measured at 660 nm in a microplate reader (Thermo 2000).

2.8.3 Isoeletric focusing

For isoelectric focusing, 200 µg of protein extract resuspended in 125 µL of re-hydration buffer supplemented with 0.5 % (v/v) destreak (GE, Heathcare) and 0.5 % (v/v) Immobilized PH Gradient (IPG) was loaded onto a 7 cm strip holder (GE Heathcare). A 7 cm long Immobiline DryStrip pH 3-10 NL (GE Healthcare) was overlaid onto sample with special care in order to avoid bubble formation between the sample and the DryStrip. Additionally, 750 µL of DryStrip Cover fluid (GE, Healthcare) were added and strip holder was closed. Isoelectric focusing (IEF) method was performed in Ettan IPGphor3 IEF System (GE Healthcare) (Healthcare 2006), according to protocol mentioned in table 2.4:

Table 2.4 – Isoelectric focusing protocol in Ettan IPGphor3 IEF System (GE Healthcare).

Steps	Volt-Hours	Voltage (V)	Temperature (ºC)	Procedure
1	0.5	30	20	Step-n-hold
2	50	100	20	Step-n-hold
3	250	500	20	Gradient
4	500	1000	20	Gradient
5	5000	5000	20	Step-n-hold

2.8.4 2D Gel Electrophoresis – SDS-PAGE

After first-dimension, IPG Strips were submerged into two equilibrium solutions in order to assure the protein's primary structural conformation. Initially, strips were loaded onto an equilibrium solution (70 mM Tris-HCl pH 8.8, 6M Urea, 30 % (v/v) glycerol and 2 % (w/v) SDS, GE Healthcare) supplemented with 1 % (w/v) DTT for 15 min at RT. Afterwards, strips were loaded onto a new equilibrium solution supplemented with 2.5 % (w/v) iodoacetamide (GE, Healthcare) for 15 min with constant stirring.

For second-dimension, a 12.5 % (v/v) polyacrylamide gel was prepared - 4 mL of a 30 % (w/v) acrylamide/bis-acrylamide mix, 3.5 mL of deionized water, 2.5 mL of Tris-HCl buffer (Merck) 1.5 M pH 8.8, 75 µL of a 10 % (v/v) ammonium persulfate (APS) (Biorad, California, USA) and 10 µL of tetramethylethylenediamine (TEMED) (Sigma). After gel polymerization (about 1 h), IPG Strips were placed on top of polyacrylamide gel and sealed with a 0.5 % (v/v) agarose solution diluted in running buffer (3.79 g/L Tris, 18 g/L glycine, 1.25 g/L SDS, and bromophenol blue traces). Molecular weight protein marker used

was HyperPage I (Bioline, London, UK). SDS-PAGE Mini-PROTEAN® 3 System was used to perform electrophoresis run – an initial 30 V run to assure all protein transfer to polyacrylamide gel followed by a 150 V run. The system was shut down prior to the exiting of bromophenol blue from the gel.

2.8.5 Imaging

After second-dimension, polyacrylamide gel was stained through 3 PhasTGelTM Blue R tablets (Coomassie R350) (GE Healthcare) diluted in 1 L, 10 % (v/v) acetic acid. Afterwards a 30 min incubation at 50 ºC followed by another 30 min incubation at room temperature with constant stirring was performed and gels were rinsed with mili-Q water (18.2 MΩ.cm at 25 °C) until protein spots were clearly observable. Gel images were acquired using Magic Scan software in Tiff and Lab Scan format, and protein spot analysis was performed using Melanie 7.0 software (GeneBio, Genebra, Switzerland). Protein spots of control gel and sample gel were compared to evaluate possible abundance levels variation. An intensity ratio between homologous spots of the two gels was carried out. Abundance levels inferior to ≤ 0.7 (protein subexpression) and superior to ≥ 1.5 (protein overexpression) were considered significant.

2.9 Nanovectorization approach

2.9.1 Gold nanoparticles synthesis and characterization

Gold nanoparticles synthesis was performed using the citrate reduction method, described by Turkevich and coworkers (Turkevich et al. 1951), that is based on the principle that sodium citrate acts as reducing and a capping agent of tetracloroauric acid (Larguinho & Baptista 2012).

Prior to synthesis, fresh *aqua regia* (nitric acid and chloride acid in a proportion of 1:3, all from Sigma, St. Louis, USA) was used to wash and remove any potential interfering particles from all the required glass material. Glass material was maintained in *aqua regia* overnight, after which it was thoroughly washed with mili-Q water to assure the removal of any *aqua regia* residues. Synthesis protocol was initiated by the addition of 1 mM of tetracloroauric acid (Sigma, St. Louis, USA) to 250 mL of miliQ water into a 500 mL round-bottom flask. Synthesis solution was maintained in constant stirring at 200ºC and upon reaching reflux, 38.8 mM of sodium citrate (Sigma, St. Louis, USA) were added followed by an incubation in the same conditions previously mentioned for a further 20 min. Lastly, the heat was turn off and the solution was left cooling at room temperature (RT) until storage in the absence of light.

Upon conclusion of the synthesis protocol, gold nanoparticles were characterized through the application of specific techniques, such as transmission electron microscopy (TEM), dynamic light scattering (DLS) and UV/Vis spectroscopy. TEM and DLS allowed to infer about the overall diameter of the nanoparticles' core

and their hydrodynamic diameter, respectively. UV/Vis spectroscopy was used in tandem in order to assess the nanoparticles solution concentration and overall homogeneity.

TEM analysis was performed as a contracted service in Instituto de Ciência e Engenharia de Materiais e Superfícies at Instituto Superior Técnico (ICEMS/IST). Samples were prepared by the transfer of 10 µL of AuNP solution onto carbon copper grids and subsequent wash (2x) with milli-Q water and promptly air dried. DLS technique was performed using a Nanoparticle Analyzer SZ-100 (Horiba Scientific, Japan) at 25 ºC, with a scattering angle of 90 º. A 2 mM solution of colloidal gold was diluted in mili-Q water and a total of 3 measurements were performed for each sample. UV-Vis spectroscopy characterization was achieved by using an UV-Vis spectrophotometer (UVmini-1240, Shimadzu, Germany). With a final volume of 100 µL, samples were loaded onto quartz absorption cells (105.202-QS, Hellma, Germany).

2.9.2 Polyethylene glycol functionalized gold nanoparticles: synthesis and characterization

Functionalization protocol was carried out by gold nanoparticle incubation with 0.028 % SDS, and bifunctional polyethylene glycol (PEG, Iris BIOTECH, MW 458.57 Da) for a period of 16 h under agitation at room temperature. More specifically to obtain a 50 mL final solution of AuNP@PEG, 0.028 % SDS are added to 10 mM naked AuNPs in the presence of 0.035 mg/mL of PEG. The solution was agitated for 16 h at room temperature in the absence of light. After the incubation period, the solution volume was distributed by 2 mL tubes and centrifuged at 14 000 g for 30 minutes at 4 ºC (Sigma 3-16K 10280, Tuttlingen, Germany). The process was repeated 3 times always removing and storing supernatants and replacing them with mili-Q water, with exception for the last centrifugation were supernatant was not replaced in order to obtain a concentrated solution of AuNP@PEG. All concentrated solutions were added in a single tube and storage at 4 ºC, protected from light.

In order to assess PEG functionalization efficiency, an Ellmans test was performed using Ellmans reagent, 5,5'-dithio-bis-(2-nitrobenzoic acid) – DTNB. It allows to quantify the remaining amount of thiol groups in the supernatant solution and hence estimate the amount of functionalized PEG. DTNB reacts with thiol groups originating TNB^- thus ionizing to TNB^{2-} in water. TNB^{2-} is a molecule that in solution exhibits yellowish color susceptible to be quantified by UV-Vis spectroscopy at 412 nm(Sigma-Aldrich 2014).

Initially, stored supernatants were centrifuged for 30 min under 14000 g at 4 ºC to remove excess of particles in solution. Sequentially it was performed a linear standard curve with a range of PEG concentrations solutions from 0 to 0.5 mg/ml diluted in mili-Q water. In a 96 well plate (VWR, Radnor, USA) 200 µL of each PEG solution were added, plus 100 µL 0.5 M pH 7 phosphate buffer – 288.55 mM Na_2HPO_4 (Sigma, MW 141.96 Da) and 211.45 mM NaH_2PO_4 (Sigma, MW 119.98 Da) – and 7 µL of a solution of 2 mg/mL 5,5'-

dithiobis-(2-nitrobenzoic acid) (DTNB, Sigma, MW 396.35 Da). In the same 96 well plate 200 µL of supernatant from AuNP@PEG functionalization were added, along with 100 µL 0.5 M pH 7 phosphate buffer and 7 µL of a solution of 2 mg/mL DTNB. After 10 min incubation period at room temperature, absorbances were measured resorting to a Tecan Infinite F200 Microplate Reader (Tecan, Männedorf, Switzerland). Using Lamber-Beer's law and calibration curve it was possible to correlate aborbances of PEG solutions and supernatants PEG concentrations. Data was analyzed using Microsoft Excel 2010 software.

Characterization of AuNP@PEG was achieved by DLS to calculate hydrodynamic diameter and UV-Vis spectroscopy to determine the nanoparticle's solution concentration.

2.9.3 Bovine serum albumin functionalized gold nanoparticles: synthesis and characterization

Bovine serum albumin (BSA) functionalization was performed through EDC/NHS coupling reaction. By combining the action of 1-Ethyl-3-(3-dimethylaminopropyl) carbodiimide (EDC), that acts as a reaction catalyzer and N-hydroxysulfosuccinimide (sulfo-NHS), that acts as a stabilizer of active intermediates through formation of ester functional groups with carboxylates (Guirgis et al. 2012), the method allows the covalent binding of biomolecules containing amino groups with free carboxyl groups..

For AuNP@PEG functionalization with BSA, a master mix containing 1.25 mg/mL sulfo-NHS (Sigma, MW 217.13 Da), 0.312 mg/mL EDC (Sigma, MW 191.70 Da), 2.5 mM pH 6 MES buffer (2-(N-morpholino)ethanesulfonic acid) (Sigma, MW 195.24 Da) and 21 nM of AuNP@PEG (previous synthetized) was mixed for 30 minutes at RT. Subsequently, the master mix solution was centrifuged (Sigma 3-16K 10280, Tuttlingen, Germany) for 30 minutes at 14000 g at 4 ºC, after which the supernatant was removed and substituted with 2.5 mM pH 6 MES buffer. The obtained solution was aliquoted and a solution of BSA was added to a final concentration of 0.01 mg/mL. After 16 h incubation at RT and constant stirring, the solution was centrifuged for 30 minutes at 14000 g at 4 ºC. A total of three centrifugations were performed, while storing the supernatants and replacing them with identical volume of 2.5 mM pH 6 MES buffer, with exception for the final centrifugation**.**

To characterize BSA functionalization, Bradford protein assay was applied. As a colorimetric method it determines the protein amount in a sample. It is based on the principle that *Comassie Brilliant Blue*, a protein staining dye, turns from red to blue when bound to proteins under acidic conditions. Sample absorbance was assessed at 595 nm, the maximum absorbance of bound *Comassie*. Thus, there is a direct proportionality of 595 nm absorbance and the amount of protein present in a solution (Scientific 2012).

Stored supernatants of AuNP@PEG@BSA functionalization were quantified by Bradford protein assay resorting to a previously performed linear standard curve with a range of BSA concentrations from 0 to 9

µg/mL diluted in mili-Q water. In 96 well plates (VWR, Radnor, Pennsylvania, USA) was added 150 µL of BSA solutions and 150 µL of Comassie Brilliant Blue (*Coomasie Protein Assay Kit*, Thermo Scientific). In the same 96 well plate it was added 150 µL of BSA functionalization supernatants and 150 µL of Comassie Brilliant Blue. After 10 minutes of incubation at room temperature, absorbance of each plate was measured at 595 nm using Tecan Infinite F200 Microplate Reader (Tecan, Männedorf, Switzerland). Using Lamber-Beer's law and calibration curve it was possible to correlate BSA solution's absorbance with the remaining BSA molecules in the supernatant that have not been attached to the nanoparticle's surface. Data was analyzed using Microsoft Excel 2010 software.

Characterization of AuNP@PEG@BSA was simultaneously achieved by dynamic light scattering (DLS) to calculate hydrodynamic diameter and UV-Vis spectroscopy to determine the nanoparticle's solution concentration.

2.9.4 Metallic compound functionalized gold nanoparticles: synthesis and characterization

Functionalization of AUNP@PEG@BSA with K4 compound comprehended the last step in the conclusion of the nanoformulation. For this purpose a master mix containing 6 nM of AuNP@PEG@BSA, 50 µM of K4 compound and mili-Q water to a final volume of 1 mL was incubated for 1 h at 4 ºC. Afterwards, the solution was centrifuged for 30 min at 14000 g at 4 ºC and the supernatant was removed for subsequent characterization by UV-Vis spectroscopy allowed to determine the amount of non-functionalized K4 in the supernatant, using Lambert Beer's law. Concentrated nanoparticles were stored at 4 ºC in the absence of light as well as the supernatant.

Characterization of AuNP@PEG@BSA@K4 was simultaneously achieved by dynamic light scattering (DLS) to calculate hydrodynamic diameter and UV-Vis spectroscopy to determine the nanoparticle's solution concentration.

2.9.5 Cell viability assays of the nanovectorized compound

To assess the effect of vectorization of compound K4 compared to the free compound in HCT116 cells, cell viability assay was performed as described in section 2.3.1. After 24 h seeding, cells were incubated with AuNP@PEG@BSA@K4 particles in the required concentration to obtain IC_{50} value of K4 free compound. Control groups implemented in this method were AuNP@PEG, AuNP@PEG@BSA (particle concentration equal to AuNP@PEG@K4) and 0.1 % (v/v) DMSO solution. Following a 48 incubation CellTiter 96®

AQueous Non-Radioactive Cell Proliferation Assay (Promega, Madison, USA) standard procedure was performed and the, absorbance was measured as mentioned in section 2.3.1.

2.10 Combined therapy strategies

2.10.1 Commercial chemotherapeutic drugs used

Main features of commercial chemotherapeutic drugs used in the course of this project are described in table 2.5 and compounds structure are represented in figure 2.2. Drugs such 5-fluoracil, dasatinib and lapatinib were aliquoted and stored at -80 ºC, afatinib and paclitaxel were stored at -20 ºC and cetuximab and doxorubicin were stored at 4 ºC.

Table 2.5 – Main features of commercial chemotherapeutic drugs used in the course of this project described as drug denomination, molecular weight, manufacturing company and mechanism of action.

Drug Denomination	Molecular weight ($gmol^{-1}$)	Solvent	Manufacturing company	Molecular targets
5-Fluorouracil	130.08	DMSO	Sellekchem	Thymidylate synthase inhibitor (Longley et al. 2003)
Afatinib	485.94	DMSO	Sellekchem	Irreversibly EGFR/HER2 inhibitor (including EGFR) (Solca et al. 2012)
Cetuximab	145781.60	DMSO	Merck Serono	EGFR inhibitor (Bardelli & Siena 2010)
Dasatinib	488.01	DMSO	Sellekchem	BCR/Abl, Src and c-Kit tyrosine kinases inhibitors (not EGFR or Her2) (Huang et al. 2007)
Doxorubicin hydrochoride	579.98	DMSO	Sigma-Aldrich	DNA intercalator (Denny 1989)
Lapatinib	581.06	DMSO	Sellekchem	EGFR and ErbB2 inhibitor (Konecny et al. 2006)
Paclitaxel	853.90	DMSO	Cytoskeleton	Microtubule depolymerization inhibitor (Perez et al. 2012)

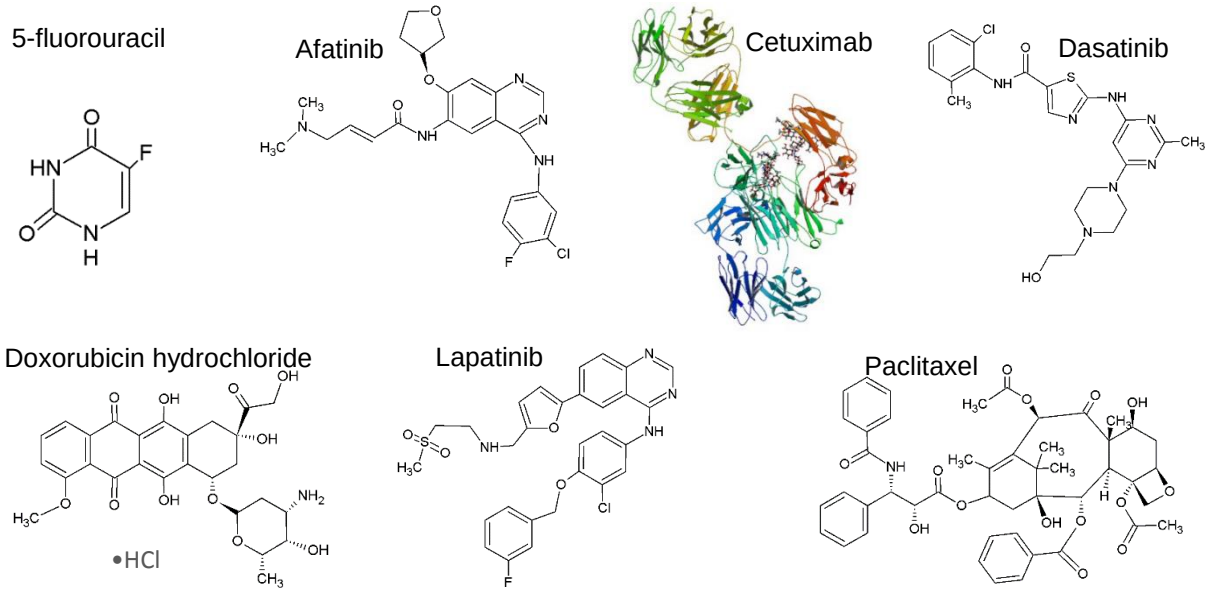

Figure 2.2 – Chemical structure of commercial chemotherapeutic drugs used in the course of this project: 5-fluorouracil, afatinib, dasatinib, doxorubicin hydrochloride, lapatinib and paclitaxel. Protein structure of cetuximab (DrugBanK 2015).

2.10.2 Cytotoxic potential evaluation

2.10.2.1 Cell viability assays

Cells were seeded and harvested as mentioned in section 2.3.1. However, instead of incubating HCT116 cells with K4 IC_{50} concentration for 48 h, the following combined strategies were applied:

$$(\boldsymbol{I})\ \boldsymbol{A + B\ 48h}$$

$$(\boldsymbol{II})\ \boldsymbol{A\ 24h \rightarrow B24h}$$

$$(\boldsymbol{III})\ \boldsymbol{B\ 24h \rightarrow A\ 24h}$$

Where A is K4 compound at IC_{50} concentration and B is a commercial drug at IC_{50} concentration for HCT116 cell line. Strategy I combines the two drugs simultaneously for a 48h incubation period at 37ºC in a 5% CO_2 (v/v) and 99% (v/v) humidity. In strategy II, K4 compound is firstly added to cells during 24 h and then commercial drug is added for 24 h. In strategy III, commercial drug is firstly added to cells for a 24h incubation period, followed by K4 addition for another 24 h incubation period. Control groups used were a 0.1 % (v/v) DMSO solution and compounds A and B at their IC_{50} concentrations. The following procedure was carried out as mentioned in section 2.3.1. Data obtained was analyzed by Microsoft Excel 2010 software using the following equation:

$$\boldsymbol{CDI = \frac{AB}{A \times B}} \qquad (\boldsymbol{6})$$

Where CDI is coefficient drug interaction, AB is the cell viability ratio of combinatory strategy, A is the cell viability ratio of single agent A and B is the cell viability ratio of single agent B. Coefficient drug interaction (CDI) is a tool to analyze interaction between drugs allowing to distinguish synergistic, additive and antagonistic effects (Zhou et al. 2012). For CDI values < 1, drugs have a synergistic effect, for CDI = 1, drugs have an additive effect and for CDI values > 1, drugs have an antagonistic effect.

2.10.3 Apoptotic potential evaluation

2.10.3.1 Hoechst 33258 staining

For apoptotic evaluation of combinatory strategies, procedure described in section 2.4.1 was followed with exception of samples preparation conditions. The most promising combinatory strategies from cell viability assays (section 2.10.2) were chosen and applied in Hoechst 33258 staining:

$$(\boldsymbol{I})\ \boldsymbol{A + B\ 48h}$$

$$(\boldsymbol{II})\ \boldsymbol{A\ 24h \rightarrow B24h}$$

$$(\boldsymbol{III})\ \boldsymbol{B\ 24h \rightarrow A\ 24h}$$

Where A is K4 compound at IC_{50} concentration and B is a commercial drug at IC_{50} concentration for HCT116 cell line. Strategy I combines the two drugs simultaneously for a 48 h incubation period at 37 ºC in a 5 % CO_2 (v/v) and 99 % (v/v) humidity. In strategy II, K4 compound is firstly added to cells during 24 h and then commercial drug is added for 24 h. In strategy III, commercial drug is firstly added to cells for a 24 h incubation period, followed by K4 addition for another 24 h incubation period. Control groups used were a 0.1 % (v/v) DMSO solution and compounds A and B at their IC_{50} concentrations. The following procedure was carried out as mentioned in section 2.4.1.

2.10.4 Proteome profiling: Two-Dimensional Electrophoresis

A final analysis of drug combination, proteome profiling studies, was performed using the most promising combinatory strategy.

$$(\boldsymbol{III})\ \boldsymbol{B\ 24h \rightarrow A\ 24h}$$

For strategy III, commercial drug is firstly added to cells for a 24h incubation period, followed by K4 addition for another 24 h incubation period. Control groups used were a 0.1 % (v/v) DMSO solution and compounds A and B at their IC_{50} concentrations. Overall procedure was carried out as mentioned in section 2.8 with exception of *Cell line compound exposure* where it was applied the mentioned combinatory strategy.

3. Results and Discussion

3.1 Cytotoxic potential evaluation

3.1.1 Cell viability assays

Growth inhibition assays were performed in order to evaluate the cytotoxic potential of compounds mentioned in section 2.1. A paramount pharmacological parameter such as relative IC_{50} was determined using GraphPad software which allowed to evaluate the compound with higher cytotoxic potential. An initial screening of all compounds exposed to A549 and HCT116 cell lines enabled to determine the most promising and cytotoxic compound. From the plethora of all compounds, K4 revealed the lowest IC_{50} concentrations for both cancer cell lines. Appendix B shows K0, K1, K2 and K3 compound's growth inhibition curves in A549 and HCT116 cell lines. The copper (II) compound, K4, reveal the lowest IC_{50}, and so the remaining investigation proceeded with this compound.

K4 compound exhibited a 48 h relative IC_{50} for A549 cell line (lung adenocarcinoma) of 19.09 μM while for HCT116 (colorectal cancer) the value was approximately 3 times lower – 6.10 μM (see Figure 3.1 and 3.2). K4 compound presents an IC_{50} in the range of 10^{-6} to 10^{-5} M and the highest cytotoxic potential was evidenced for HCT116 cell line, among both cell lines. Comparatively, a common chemotherapeutic agent, containing a metallic element, such as cisplatin, presents a relative IC_{50} of 15.3 μM for HCT116 (Silva 2012), a value about 2.5 times higher than K4's Cu (II) compound thus proving higher cytotoxic potential. An IC_{50} of 37.8 μM for A549 cell line is reported for cisplatin (Http://www.cancerrxgene.org/translation/Drug/1005 2015), a value 2 times higher than K4 compound IC_{50}, thus showing the chemotherapeutic potential for A549 cell line. Nonetheless these results alone have little meaning, especially considering a clinical translation, without taking into consideration the effect of the tested compound on healthy cells, as the later will deeply influence the compound's application range as well as the spectrum of possible side effects in future patients.

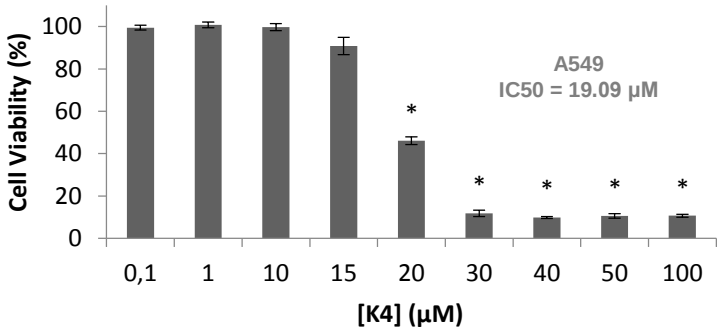

Figure 3.1 - Cell viability assays of K4 compound on A549 (lung adenocarcinoma). Cells were exposed during 48h to K4 and to a solution of 0.1% DMSO (control). In the upper right corner is displayed cell line and respective relative IC_{50} calculated. The results are represented as MEAN±SEM from at least three independent assays. *- statistical significance with $p<0.05$ compared to control group.

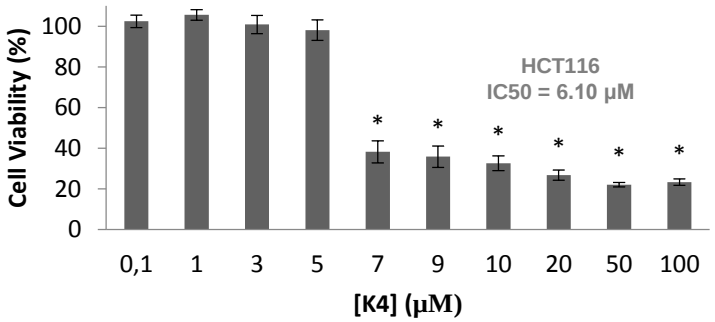

Figure 3.2 - Cell viability assays of K4 compound on HCT116 (colorectal cancer). Cells were exposed during 48h to K4 and to a solution of 0.1% DMSO (control). In the upper right corner is displayed cell line and respective relative IC_{50} calculated. The results are represented as MEAN±SEM from at least three independent assays. *- statistical significance with $p<0.05$ compared to control group.

In these sense growth inhibition assays on fibroblasts were performed in order to evaluate cytotoxicity potential in healthy cells (see Figure 3.3). Relative IC_{50} was calculated with GraphPad software revealing a value of 9.18 µM. A value of 1.5 times higher compared with HCT116 cell line thus showing that 6.10 µM K4 manly affect colorectal cancer cells without inducing, to a certain degree, severe toxicity into healthy cells, namely fibroblasts. Furthermore, Cu (II) compound evidenced higher cytotoxicity for A549 cell lines than for fibroblasts, about 2 times higher. K4 compound revealed a higher relative IC_{50} for A549 when comparing with fibroblasts and HCT116 cell line evidencing perhaps different mechanisms of action and different cell line susceptibilities. By showing lowest cytotoxic potential among the cancer cell lines in study, further studies into the discovery of K4 mechanism of action in A549 were not pursued.

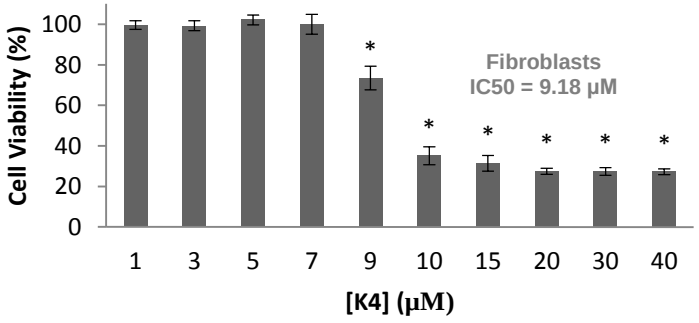

Figure 3.3 - Cell viability assays of K4 compound on fibroblasts (healthy neonatal foreskin cells). Cells were exposed during 48h to K4 and to a solution of 0.1% DMSO (control). In the upper right corner is displayed cell line and respective relative IC_{50} calculated. The results are represented as MEAN±SEM from at least three independent assays. *- statistical significance with $p<0.05$ compared to control group.

Table 3.1 – Relative IC_{50} values of K4 and cisplatin on lung adenocarcinoma (A549), colorectal cancer (HCT116) and on human fibroblasts. Values were obtained from at least three independent assays. [a] (Silva 2012) [b] (Http://www.cancerrxgene.org/translation/Drug/1005 2015).

Cell line	K4 relative IC_{50} (μM) 48h	Cisplatin relative IC_{50} (μM) 48h
A549 (lung)	19.09	$37.8_{[a]}$
HCT116 (colorectal)	6.10	$15.3_{[b]}$
Fibroblasts (healthy tissue)	9.18	-

K4 compound reveals a higher cytotoxic potential for HCT116 cell line when comparing to fibroblasts. A fold variation of about 1.5 reveals that Cu (II) compound has a higher cytotoxic potential in cancer cells of colorectal adenocarcinoma than for fibroblasts given an indication of low toxicity towards healthy cells. Nonetheless, considering the fold variation presented the clinical applicability range would be rather limited, leading to the consideration of a targeted therapy with K4 compound in order to avoid toxicity in healthy cells once the difference of IC_{50} for HCT116 cell line and fibroblasts is low. Vectorization of K4 compound into nanocarriers could be a solution for colorectal cancer treatment. Additionally it also presents a higher cytotoxicity than cisplatin for HCT116, a common and employed chemotherapeutic drug with a metallic center. K4 shows potential as an anticancer drug with increased interest for further studies to unravel the underlying mechanisms of action.

These results were performed *in vitro* and that must be taken into account when transposing to *in vivo* assays. Pharmacokinetics and pharmacodynamics properties of K4 compounds within the organism may be intricately different from the *in vitro* environment.

3.2 Apoptotic potential evaluation

3.2.1 Hoechst 33258 staining

A preliminary assay of apoptotic potential was performed using Hoechst 33258 dye. As a permeable cell membrane dye it allows to visualize morphologic modifications such as chromatin condensation, nuclear fragmentation and the presence of apoptotic bodies, that as mentioned in section 1.2.3.1 and 2.4.1 comprehend hallmarks of apoptosis.

HCT116 cells were exposed for 48 h to K4 compound in the concentration of IC_{50} and 1.5 fold IC_{50}, with a control solution of 0.1 % DMSO. Hoechst images are shown in Figure 3.4. Cells exposed to 6.10 μM K4 exhibit several hallmarks of apoptosis such as aberrant nuclear morphology and the presence of apoptotic bodies. Control cells not exposed to K4 show a uniform distribution of fluorescence indicative of homogenous chromatin and cell viability. A decrease in cell density was visible in the IC_{50} preparation when

compared to control group. Cells exposed to a higher concentration of K4 (9.15 μM) shown less cellular density in the preparations than with 6.1 μM. Apoptotic hallmarks were also visible in all preparations with different levels of magnitude. Figure 3.5 evidences apoptosis percentage in every condition tested. Only the presence of apoptotic bodies were considered for the quantification of apoptosis in Figure 3.5. Cells incubated with IC_{50} concentration exhibited 1.5 % apoptosis, a 15 fold increase when comparing to control group. In the same way cells exposed to 9.15 μM of K4 compound exhibited 10.5 % of apoptosis, a 105 fold increase when comparing to control group. These results demonstrate that K4 compound can induce apoptosis in HCT116 cell line. The results here presented appear to indicate that K4 mechanism of action induces processes of programed cell death such as apoptosis however the molecular targets involved are to be deciphered

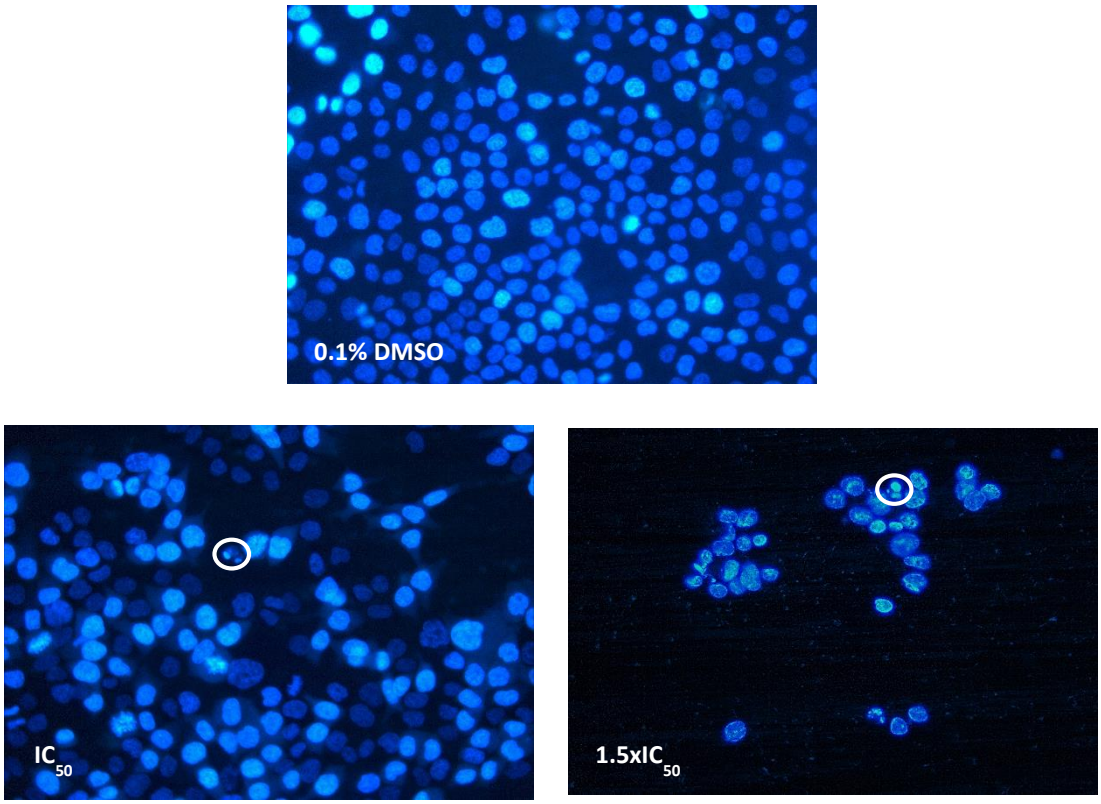

Figure 3.4 - Hoechst 33258 staining of HCT116 cell line exposed to 6.1 μM K4 (IC_{50}) and 9.15 μM K4 ($1.5xIC_{50}$) over 48h. A 0.1% DMSO solution was used as a control group. White circle indicates nuclear fragmentation and apoptotic bodies' presence.

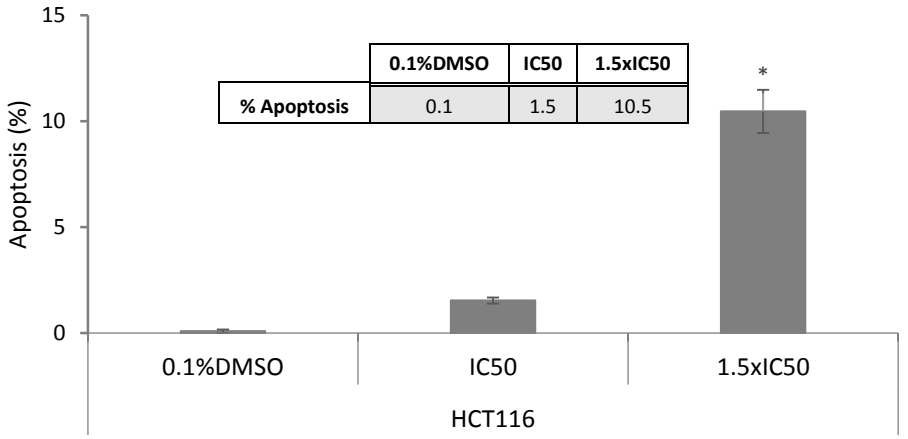

	0.1%DMSO	IC50	1.5xIC50
% Apoptosis	0.1	1.5	10.5

Figure 3.5 – Percentage of apoptosis in HCT116 cells exposed to K4 at its IC_{50} concentration and 1.5 fold IC_{50} concentration. Control group used was a 0.1 % DMSO solution. Only cells with apoptotic bodies were consider as being in apoptosis. Data represented are from at least 3 independent assays. On the top there is a table indicating apoptosis percentage of each preparation. Data are represented as means ± SEM. *- one way ANOVA test with $p<0.05$. Results were normalized in relation to control group of cells treated with 0.1%DMSO.

3.2.2 Annexin V-FITC and propidium iodide staining

Following a preliminary assay of apoptotic potential by Hoechst staining, a quantitative assay of K4's apoptosis induction percentage was performed through a double staining method with Annexin V-FITC and propidium iodide (PI). This assay allows to distinguish viable cells with a $FITC^-/PI^-$ ratio, from early apoptotic cells ($FITC^+/PI^-$) from late apoptotic cells with a $FITC^+/PI^+$ ratio and necrotic cells ($FITC^-/PI^+$).

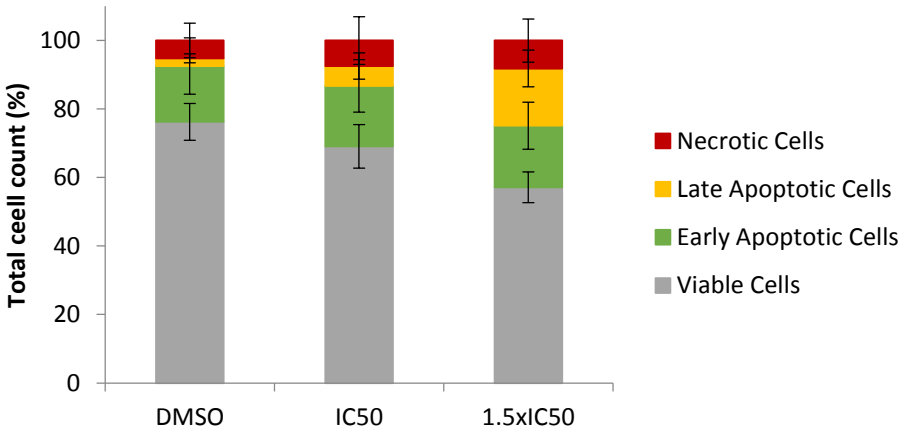

Figure 3.6 - Percentage of viable, early and late apoptotic and necrotic cells in HCT116 upon exposure to 0.1% DMSO (control group), K4 at IC_{50} concentration and K4 at 1.5 fold the IC_{50} concentration over 48h incubation period. Cells were analyzed by flow cytometry after double staining with Annexin V-FITC and propidium iodide and the data presented is the result of three independent experiments.

Table 3.2 - Percentage of viable, early and late apoptotic and necrotic cells in HCT116 upon exposure to 0.1% DMSO (control group), K4 at IC_{50} concentration and K4 at 1.5 fold the IC_{50} concentration over 48h incubation period. Values were obtained based on Figure 3.6 results. Data is represented as MEAN±SEM and is from three independent assays.

	0.1 % DMSO	IC_{50}	1.5 fold IC_{50}
Viable Cells	76.3 (±5.4)	69.1 (± 6.3)	57.1 (±4.5)
Early apoptotic cells	16.3 (±8.2)	17.6 (±7.7)	18,0 (±6.9)
Late apoptotic cells	2.2 (±1.3)	5.8 (± 3.8)	16.7 (±5.4)
Necrotic cells	5.2 (±5.1)	7.5 (± 6.9)	8.2 (±6.3)

Results are shown in Figure 3.6 and Table 3.2. Cells exposed to K4 IC_{50} concentration during 48 h exhibited an increase of non-viable cells, about 30.9 %, when comparing to the control group, which exhibited a value of 23.8 %. Considering cell viability assays, it was expected a higher apoptotic percentage in cells exposed to IC_{50} concentration of K4. Viable cells decreased from 76.3 to 69.1 % with the concomitant increase of early apoptotic cells, late apoptotic cells and necrotic cells. Cells exposed to 1.5 fold IC_{50} concentration of K4 revealed a decrease of viable cells, to 57.2 %, with a visible increase of late apoptotic cells when comparing to cells exposed to IC_{50} concentration. Late apoptosis increases about 11% however early apoptosis and necrosis increases about 1% when comparing IC_{50} and 1.5 fold IC_{50} conditions. HCT116 cells exposed to K4 reveal a significate increase for late apoptotic events wherein there are no significant changes in early apoptotic and necrotic cells.

Annexin V-FITC and propidium iodide staining assay corroborates results from Hoechst staining indicating a trend of increased apoptosis for increasing K4 concentrations. The percentage of apoptotic cells in a sample, which includes early and late stages, represents about 23 % of the total cell population, when considering exposure to IC_{50} concentration. As mentioned above, K4 compound leads cells to an apoptotic pathway. However, under 50 % of total cell count goes under apoptosis suggesting a cytostatic mechanism. Drugs could exhibit two types of mechanism of action: cytotoxic or cytostatic. A cytotoxic mechanism of action is correlated with cell damage effects such as apoptosis, necrosis or cell lysis. On the other hand, cytostatic mechanism of action is related to cell growth/proliferation inhibition effects (Kustermann et al. 2013). Further studies will be addressed to identify and understand molecular targets of K4 compound. As mentioned above, K4 compound leads cells to an apoptotic pathway however is necessary to identify and understand molecular targets and mechanism of action with further studies.

3.3 Cell cycle progression analysis

3.3.1 Propidium iodide staining

Given the literature reports on the effect of other Cu (II) compounds on hindering cell cycle progression HCT116 cells were exposed to a double thymidine blockage for a complete synchronization in G1/S cell cycle phase in order to assess the full spectrum of alteration upon exposure to K4. Sequentially cells were exposed to K4 in order to detect any cell cycle abnormality such as cell cycle delay or arrest due to K4 compound presence.

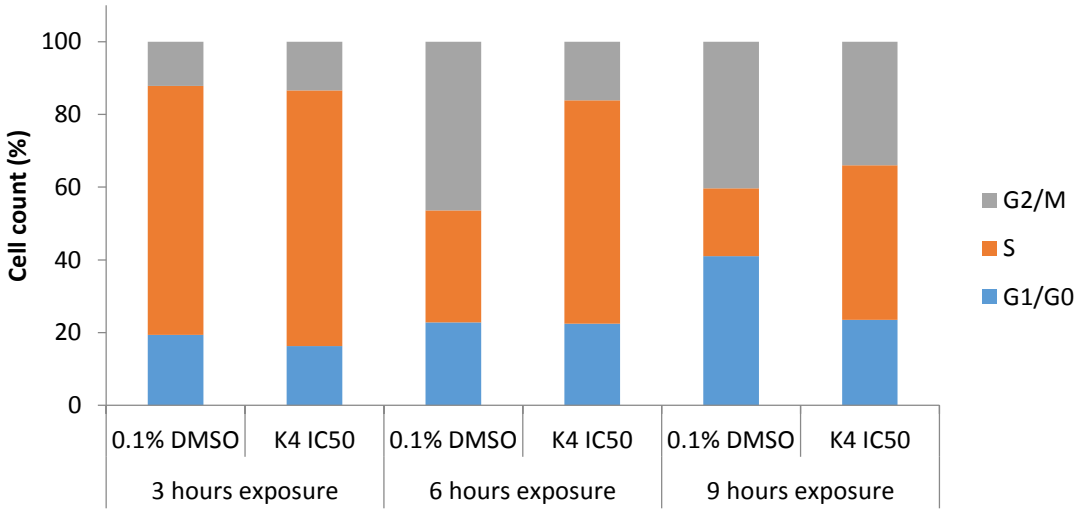

Figure 3.7 - Percentage of HCT116 cells in each phase of the cell cycle – G2/M, S and G1/G0 phases. Cells were exposed to a 0.1% (v/v) DMSO solution (control) or K4 compound (IC_{50}) for 3, 6 and 9 h and analyzed by flow cytometry. Analyzed data correspond of to two independent assays.

Table 3.3 - Percentage of HCT116 cells in each phase of the cell cycle – G2/M, S and G1/G0 phases. Cells were exposed to a 0.1% (v/v) DMSO solution (control) or K4 compound (IC_{50}) for 3, 6 and 9 h and analyzed by flow cytometry. Analyzed data is represent as means ± SEM of two independent assays.

Cell cycle phase	3 hours exposure		6 hours exposure		9 hours exposure	
	DMSO	K4	DMSO	K4	DMSO	K4
G1/G0	19.4 (±1.3)	16.4 (±2.4)	22.9 (±1.9)	22.5 (±6.1)	41,0 (±2.7)	23,5 (±3.8)
S	68.5 (±3.2)	70.3 (±0.1)	30.8 (±1.6)	61.4 (±0.03)	18,7 (±3.4)	42,5 (±17.3)
G2/M	12.1 (±4.5)	13.3 (±2.5)	46.3 (±3.5)	16,1 (±6.1)	40,3 (±6.1)	34,0 (±21.1)

Results shown in Figure 3.7 and Table 3.3 reveal that after a 3h incubation in the presence of K4 at its IC_{50} concentration, the majority of HCT116 cells (approximately 70.3 %) were in S phase. When comparing to the control group, 0.1 % (v/v) DMSO, the majority of cells were also in S phase. This trend may be reminiscent from the double blockage performed with thymidine. Only a small percentage of cells are in G1/G0 phase, respectively 19.4 % and 16.4 % for control group and K4 samples. Concomitant, a small percentage of total cell count are in G2/M phase corresponding to 12.2 % and 13.4 % for 0.1 % (v/v) DMSO and K4 samples respectively. After a 6 hour exposure to K4 compound, the majority of HCT116 cells remained in S phase (61.4 %) whereas in the control group cells progressed into G2/M phase (46.4 %). Analyzing the control group, it is visible that about 38 % of S phase cells progressed into the G2/M phase of the cell cycle (from 3 to 6 hour) emphasizing the progression of the cell cycle in the control group . Analyzing a 9 h exposure to K4 compound in HCT116 cells, about 20 % of S phase cells progressed in the cell cycle to G2/M phase (from 6 to 9 h). When comparing to control group after 9h, the majority of cells are in G2/M phase and G1/G0 phase. These results provide evidence of a potential delay in the S phase of the cell cycle due to the exposure of K4 compound (IC_{50}).

Cell cycle's S-phase is responsible for a full and correct DNA replication. A paramount regulator of the S-phase is CDK2-cyclin A complex, which might constitute a possible target of K4' mechanism of action given the previously mentioned results (Coronado et al. 2013). In this sense K4 compound may be interfering with the activation of this complex, triggering an S-phase delay. Additionally, an intra S-phase checkpoint regulates if the cell progresses into the G2/M phase by assuring that DNA replication fork or DNA itself are not damaged (Hu et al. 2012). These evidences may explain K4 mechanism of action which the literature corroborates in the sense that many anticancer drugs have a similar mechanisms of action, through the delay in the cell cycle's S-phase (Wu et al. 2013; Luo et al. 2012). Ultimately, if DNA repair mechanisms alt the cell cycles progression at the intra S-phase checkpoint, cells eventually enter into a senescence state or into the apoptotic pathway. Proteomic studies could reveal to be fruitful in the understanding of the molecular targets that influence the delay in S-phase of HCT116 cells treated with K4. Additionally DNA interaction studies could be equally important to assess if the compound interacts with this macromolecule as well as the nature of the interaction.

3.4 DNA interaction analysis

3.4.1 UV-Vis spectroscopic assays

Interaction with DNA macromolecule is an important feature of any anticancer drugs. Taking as an example, cisplatin, it possess as a prime mechanism of action DNA interacting properties (L Galluzzi, Senovilla, et al. 2012). Concerning this assay, CT-DNA interaction studies with K4 compound were performed in order to assess the presence or absence of a complex-DNA interaction and the nature and strength of interaction.

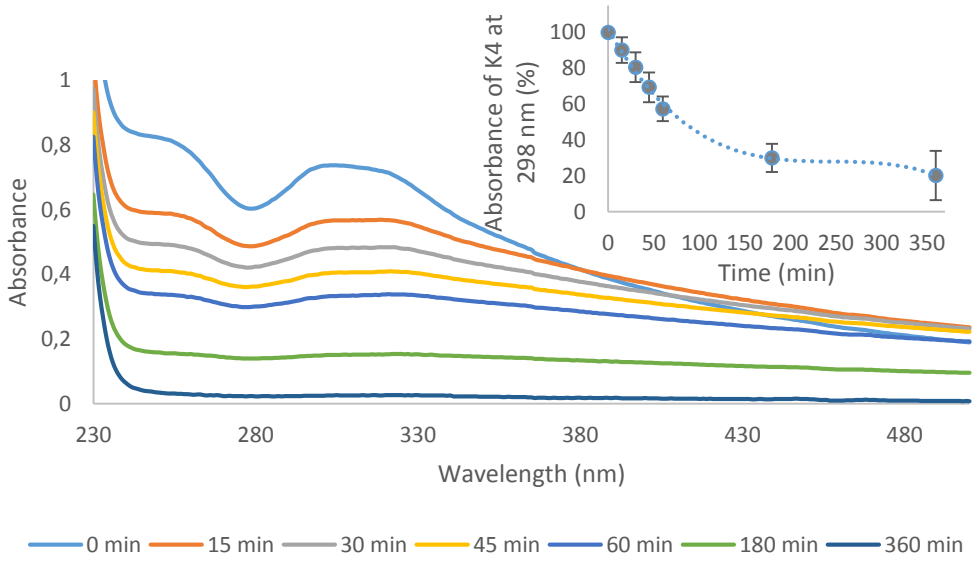

Figure 3.8 - Evaluation of K4 stability in 0.2M Tris-HCl pH 7.0 with 50mM NaCl buffer over time. 80 µM K4 compound were incubated at 37ºC during 15, 30, 45, 60, 180 and 360 minutes. In the upper right corner is the K4 absorbance at 298 nm over 15, 30, 45, 60, 180 and 360 minutes.

Table 3.4 – K4 Absorbance at 298 nm (in percentage) over 15, 30, 45, 60, 180 and 360 minutes. The author selected the 298 nm peak with no incubation as 100% of absorbance. Data was obtained based on Figure 3.8 from three independent assays.

Time (min)	K4 Absorbance at 298 nm (%)
0	100
15	90
30	81
45	69
60	57
180	30
360	20

Initially it was performed a compound stability assay to assess the optimal incubation time-point. Maximum peak at 260 nm was not chosen as a comparison method due to its proximity to DNA maximum absorbance at 260 nm (Agarwal et al. 2013). Figure 3.8 and table 3.4 reveal the loss of K4 stability by the decrease in the characteristic peak absorbance at 298 nm throughout the time of incubation. Admitting that 100 % is the absorbance at 298 nm with no period of incubation it is evidenced that with a 180 min incubation period less than 50 % of the K4 characteristic peak at 298 nm is maintained. Thus, it was chosen a 30 min period of

incubation of K4 compound at 37 ºC diluted in 0.2 M Tris-HCl pH 7.0 with 50mM NaCl buffer by exhibiting about 80 % of its characteristic peak.

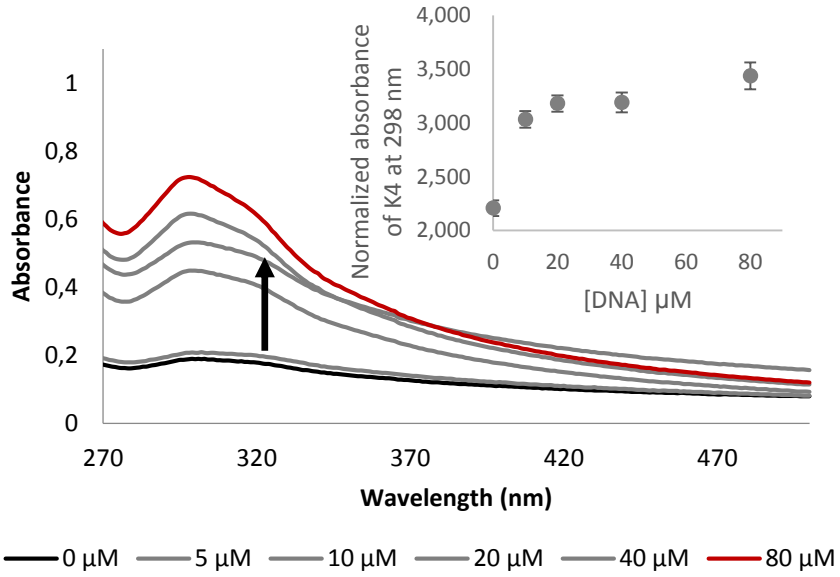

Figure 3.9 – Absorbance spectra of K4 with 5, 10, 20, 40 and 80 µM of CT-DNA. Solutions were incubated 30 minutes at 37ºC in 0.2M Tris-HCl buffer with 50 mM NaCl pH=7.0. The black arrow represents the CT-DNA concentrations increment. In the upper right corner it is the absorbance spectrum of K4 at 298 nm normalized with absorbance at 500 nm. Data are represented as MEAN±SEM and are from three independent assays.

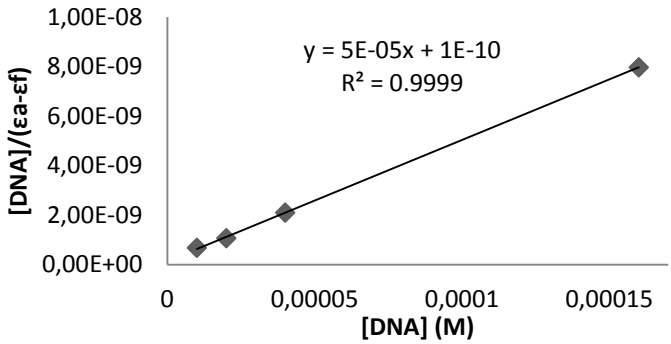

Figure 3.10 - Linear regression used to calculate binding affinity constant (Kb) of K4 with CT-DNA.

Table 3.5 - Molar extinction coefficient (ε) and binding affinity constant (Kb) values of K4 obtained over three independent assays. Binding affinity constant of doxorubicin is also described (Luís 2011). Data is represented as means ± SEM.

	ε ($M^{-1}cm^{-1}$)	**Kb ($x10^5$ M^{-1})**
K4	8866.7 ± 1146.5	2.17 ± 1.42
Doxorubicin	-	3,48 ± 0,04

Interaction of metallic compounds with DNA may be performed by covalent binding or non-covalent binding which include intercalation, groove binding and external electrostatic bonding (Sirajuddin et al. 2013). Compounds are stabilized when bound to DNA through the interaction between aromatic rings of the complex and the nucleotide bases. An absorption spectrum with an intense hypochromic or a bathochromic effect could indicate an interaction through intercalation of metallic compound and the DNA molecule. The absence of these effects could indicate an interaction through the DNA grooves by relatively weak bonds (Sirajuddin et al. 2013).

Figure 3.9 reveals that K4 has the ability to bind to DNA with an observable hyperchromic effect of DNA in the presence of a fixed K4 concentration. According to literature, K4 compound may be interacting with DNA grooves due to the established hyperchromic effect. No hypo or bathochromic shifts were verified thus showing that no intercalation with DNA must be occurring. To evaluate Cu (II) interaction strength with DNA, K_b was calculated; revealing a value of $2.17x10^5$ M^{-1} (see Table 3.5). Doxorubicin as a common DNA intercalator chemotherapeutic drug has a binding constant in the same order of magnitude as shown for K4 compound (see table 3.5). K4 interacts with DNA grooves in a strong fashion, revealing a binding constant in the same order of magnitude of a common and strong DNA intercalator, doxorubicin.

Previous assays such as cell cycle progression and Hoechst staining are in line with the results obtained in the DNA interaction assays that suggested K4 interaction with DNA macromolecule. Cu (II) compound interaction with DNA may be compromising DNA replication and consequently cell cycle S-phase that as shown in section 3.3 suffers a delay when cells are exposed to K4. Cu (II) compound mechanism of action, if able to enter the nucleus, may be explained through the interaction of K4 with DNA grooves, leading to a struggle in a correct DNA replication and consequently delaying S-phase cell cycle. When DNA repair mechanisms are not able to overcome damages, the cell enters in a senescence state or into the apoptotic pathway.

3.4.2 pDNA cleavage assays

According to previous *in vitro* assays, there is an interaction between K4 and DNA grooves. To a better understanding of K4 mode of interaction with DNA, pDNA cleavage assays were. Concerning a low stability in 0.2M Tris-HCl pH 7.0 with 50mM NaCl buffer, a 30 minute period of incubation at 37ºC was chosen in similarity with previous assays. After a 30 min incubation period of K4 with pUC18, an agarose gel electrophoresis was performed as shown in Figure 3.11. The results reveal loss of intensity of supercoiled isoform bands as K4 and DMSO's concentrations gradually increase. The observable effect was not directly related to the increase of the circular or linear isoform intensities, either in the presence or absence of K4. This loss of intensity was however not due to the formation of a possible pDNA-K4 complex and its retention within the electrophoresis wells or in the upper regions of the gel (due to the increase in the overall molecular weight of the complex). Noteworthy, the linear isoform was completely absent from the gel (with exception

for the linearization control), being only visible its circular isoform counterpart. This suggests that K4 has the ability to induce nicks in double-stranded DNA. Figure 3.12 assesses differences between circular intensities and supercoiled intensities of K4 samples normalized with DMSO. Circular isoform intensities were proven to be gradually higher for increasing K4 concentrations, however only a slight change is verified relative to the control group. Results suggest that K4 interaction with pUC18 is only observable for compound concentrations equal or above 40 µM. As a complementary assay a 24 h incubation period was equally performed under the same conditions mentioned, on the basis that, previous reports by the research group stated a 24 h incubation period has the optimum period to observe alterations on the DNA molecule upon exposure to drug compounds.

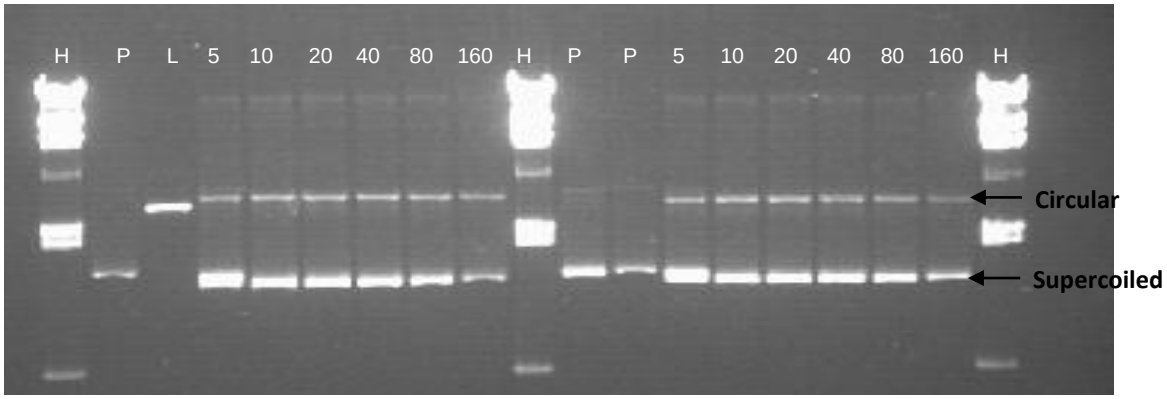

Figure 3.11 – pUC18 cleavage assay with increasing K4 (or DMSO) concentrations, respectively left and right. 10 µM pUC18 were incubated with K4 increasing concentrations (in µM) over 30 minutes (in 0.2M Tris-HCl pH 7.0 50mM NaCl buffer). Agarose gel electrophoresis 0.7% 2h at 70V. H- λ/HindIII ladder; P- pUC18; L- Linear pUC18; 5 to 160- increasing concentrations of K4 (gel on the left) or DMSO (gel on the right); Supercoiled- Supercoiled isoform; Circular – Circular isoform.

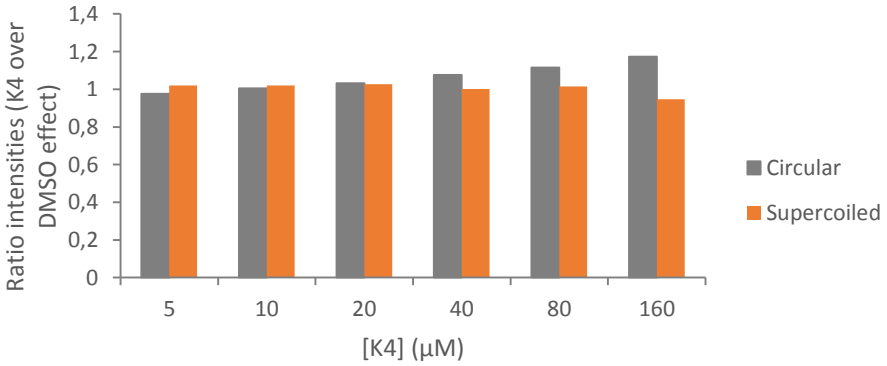

Figure 3.12 – Ratio intensities of circular isoform and supercoiled isoform. Samples with an incubation period of 30 minutes. It is shown K4 effect over DMSO with increasing concentrations (based on Figure 3.11).

Figure 3.13 exhibits an agarose electrophoresis gel with a 24 h incubation period, revealing a gradually decrease in DNA electrophoretic mobility of circular isoform for samples treated with K4 compound. An

interaction between pUC18 and Cu (II) compound could result in the formation of a complex with the DNA molecule, consequently increasing the overall molecular weight and so evidencing an electrophoretic retardation in comparison to the remaining bands. Notwithstanding linear isoforms (except for linearization control) were absent in the gel, being only visible supercoiled and circular isoforms. These results corroborate previous assays of CT-DNA interaction which suggested a groove binding of K4 compound to DNA. Intensity ratio on Figure 3.14 shows that for increasing K4 concentrations, the circular isoform increase as well. Comparing the 30 min and 24 h incubation agarose gels, it is possible to assess that the increasing intensity of the circular isoform is due to the gradual increase of K4 concentration. Both conditions evidenced similar cleavage of DNA molecule. However considering the 24 h incubation period an electrophoretic retardation of pUC18 is observable for increasing K4 concentrations, which corroborates UV-Vis spectroscopy assays that evidenced DNA groove binding of K4 compound.

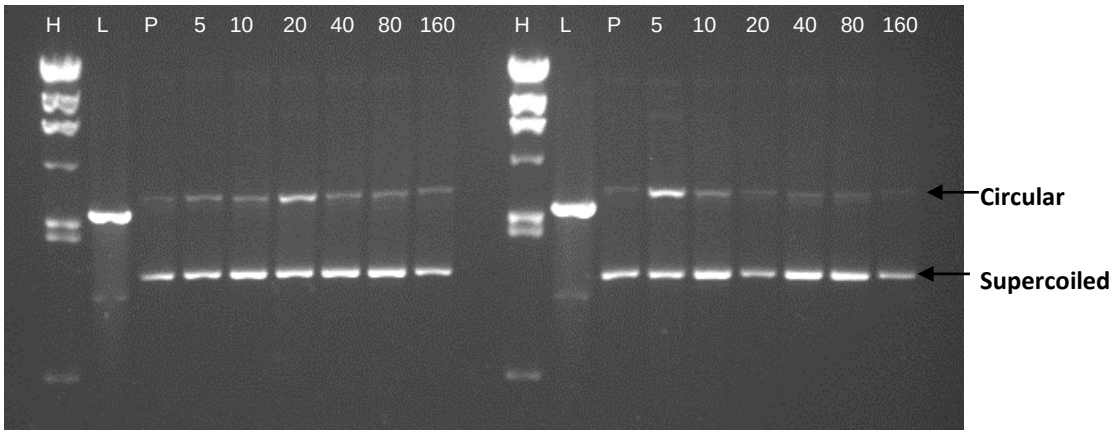

Figure 3.13 – pUC18 cleavage assay with increasing K4 (or DMSO) concentrations, respectively left and right. 10 µM pUC18 were incubated with K4 increasing concentrations (in µM) over 24 hours (in 0.2M Tris-HCl pH 7.0 50mM NaCl buffer). Agarose gel electrophoresis 0.7% 2h at 70V. H- λ/HindIII; P- pUC18; L- Linear pUC18; 5 to 160- increasing concentrations of K4 (gel on the left) or DMSO (gel on the right); Supercoiled- Supercoiled isoform; Circular – Circular isoform.

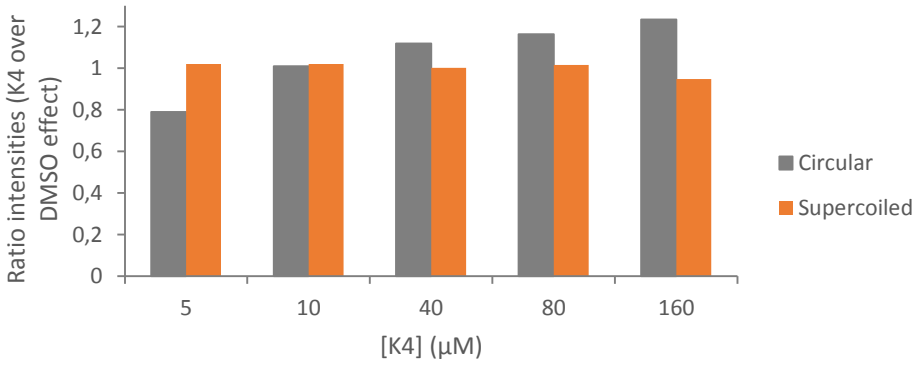

Figure 3.14 – Ratio intensities of circular isoform and supercoiled isoform. Samples with an incubation period of 24 hours. It is shown K4 effect over DMSO with increasing concentrations (based on Figure 3.13).

3.5 BSA interaction assays

3.5.1 UV-Vis spectroscopic assays

As the most abundant protein in bovine plasma, BSA has a high capacity to bind small molecules in circulation, including chemotherapeutic drugs. Given the fact that it can influence drug concentration in the blood, as an important pharmacokinetics study, BSA interaction studies were performed to evaluate K4's potential of interaction with this macromolecule (Ghosh, Jana, & Guchhait, 2012).

.

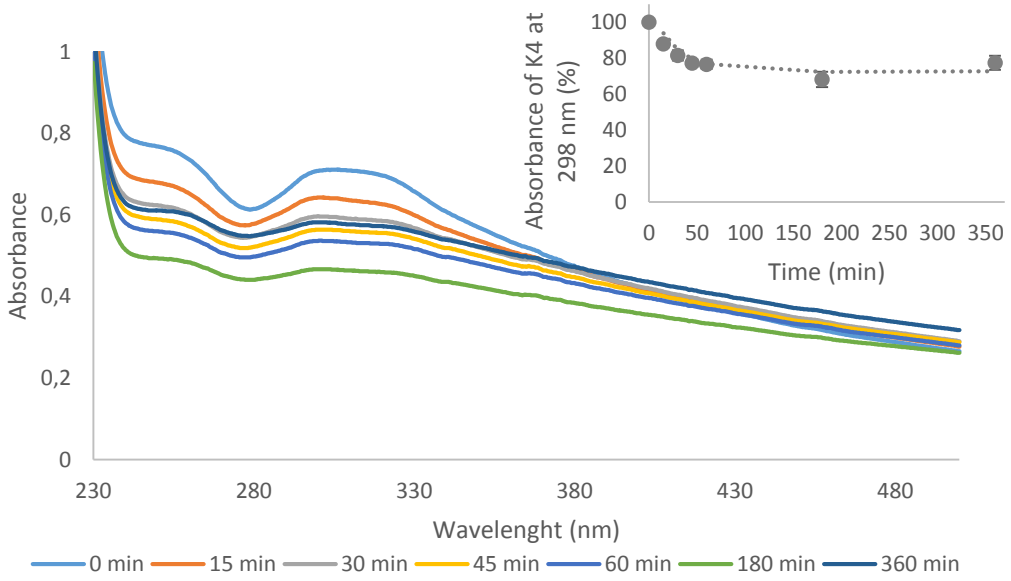

Figure 3.15 - Evaluation of K4 stability in 10 mM phosphate buffer pH 7.0 /0.15 M NaCl over time. 80 µM K4 compound were incubated at 37ºC during 15, 30, 45, 60, 180 and 360 minutes. In the upper right corner is the K4 absorbance at 298 nm over 15, 30, 45, 60, 180 and 360 minutes.

Table 3.6 - K4 Absorbance at 298 nm (in percentage) over 15, 30, 45, 60, 180 and 360 minutes. The author admitted that 298 nm peak with no incubation corresponds to 100%. Data was obtained based on Figure 3.15 from three independent assays.

Time (min)	K4 absorbance at 298 nm (%)
0	100
15	88
30	82
45	77
60	77
180	68
360	77

An initial stability assay of K4 compound in 10 mM phosphate buffer pH 7.0 /0.15 M NaCl was performed in order to assess the optimal incubation period. As in section 3.4.1 only 298 nm absorption peak was take into account and so in this assay it will be reflected the same analysis. Absorption spectra shown in Figure 3.15 exhibited a loss of K4 characteristic peak throughout the incubation period. Considering K4 maximum absorption peak at 298 nm with no incubation as 100 %, the loss of K4's absorbance characteristic peak over time is displayed on Table 3.6. The lowest absorption value is observed after a 180 min incubation period where K4 maintains about 70 % of its characteristic absorption peak. Stability assays in 0.2 M Tris-HCl pH 7.0 with 50 mM NaCl buffer (see section 3.4.1) reveal the lowest percentage value of 20 %. Results of both assays demonstrate K4's low stability in aqueous buffers, however, the latter is found to be far superior in phosphate buffer than in Tris-HCl buffer. Similarly results suggest that in cellular media, K4 also loses stability. This observation leads us to infer about how this loss of stability affects K4's overall internalization rates as well as the therapeutic mechanism of action, given the fact that when in solution the compound's structure might be altered. Nevertheless, a 30 minute period incubation of K4 with phosphate buffer was selected in order to maintain reaction conditions between assays.

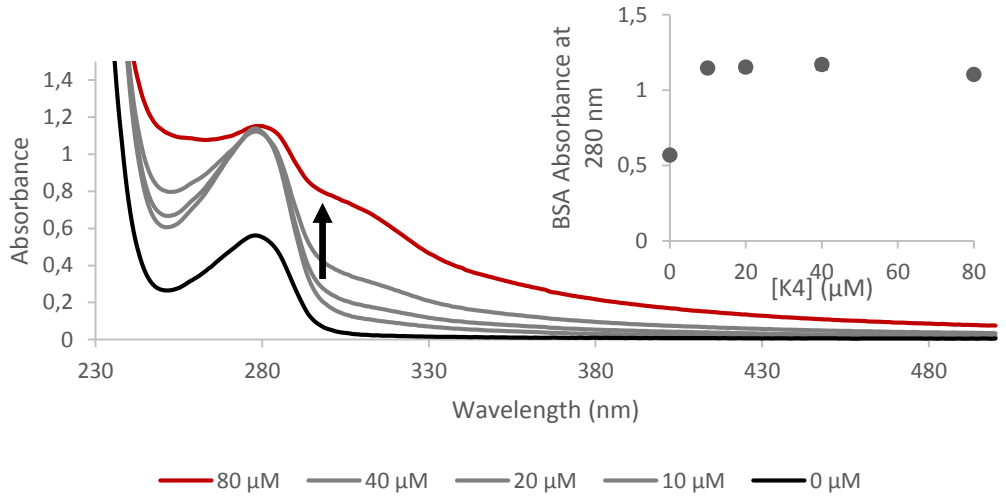

Figure 3.16 - Absorbance spectra of BSA with 10, 20, 40 and 80 µM of K4. Solutions were incubated 30 minutes at 37ºC in 10 mM phosphate buffer pH 7.0 /0.15 M NaCl. The black arrow represents the K4 concentrations increment. In the upper right corner it is the absorbance spectrum of BSA at 280 nm with increasing K4 concentrations. Data are represented as means ±SEM and are from three independent assays.

Absorption spectra of Figure 3.16 reveals a maximum absorbance at 280 nm corresponding to tryptophan and tyrosine residues of BSA. An hyperchromic effect is verified when BSA is exposed to several K4 concentrations thus suggesting that Copper (II) compound binds to BSA. No hypso or batochromic effects were observed in spectra results which indicates that no conformational changes occur when K4 binds to BSA (Sanatkar et al. 2014). Despite substantial increase of maximum peak from BSA to BSA with 10 µM of K4, the same raise was not verified when adding more K4 concentrations. Cu (II) compound seems to

interact with BSA macromolecule however it is an event not dependent of compound's concentration. A possible saturation of the BSA binding sites could be occurring thus revealing no absorption increase in the spectra. Further spectrofluorometric studies will confirm the possible interaction of K4 and BSA.

3.5.2 Spectrofluorometric assays

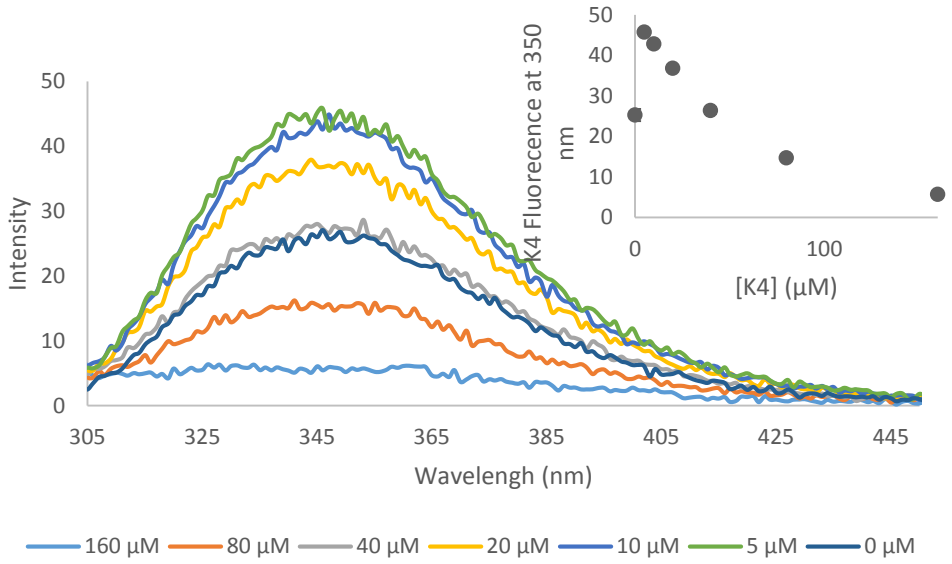

Figure 3.17 – Steady-state fluorescence data of BSA with increasing K4 concentrations in 10 mM pH 7 phosphate buffer/0.15 M NaCl. Solutions were incubated 30 min at 37ºC. In the upper right corner is shown spectrum of K4 maximum fluorescence at 350 nm with increasing K4 concentrations. Data is represented as means ± SEM.

Spectrofluorometric assays were performed conducive to a better evaluation of K4 interaction properties with BSA. Figure 3.17 exhibits steady-state fluorescence of BSA with K4 compound. A quenching effect is observed for increasing compound concentrations thus suggesting that Cu (II) compound binds to BSA molecule, corroborating the previous UV-Vis spectroscopy assay. Reported quenching mechanisms could be appointed as dynamic quenching or static quenching. Static quenching occurs when a ground-state complex is formed among the fluorophore and the quencher, thus exhibiting modifications in absorption spectra and steady-state fluorescence analysis. On the other hand, dynamic quenching is when the interaction of quencher and fluorophore occurs due to collisional encounters reporting modifications only in the steady-state fluorescence spectra (Sanatkar et al., 2014). Spectrofluorometric assays and UV-Vis spectroscopy assays exhibited quenching effect and hyperchromic effect respectively, thus suggesting that a mechanism of static quenching is occurring. However, in the absence of quencher, BSA as a maximum

intensity fluorescence lower than the majority of samples of BSA in the presence of quencher (except for 80 and 160 µM). A conformational change in BSA upon K4 binding could expose tryptophan or tyrosine residues thus increasing fluorescence intensity when adding quencher to BSA. However, no red or blue shift were observed in steady-state fluorescence as well as in UV-Vis absorption spectra, thus suggesting that no conformational change is occurring (Sanatkar et al., 2014). Another suggested hypothesis is that K4 compound could have fluorescence thus increasing intensities when bound to BSA.

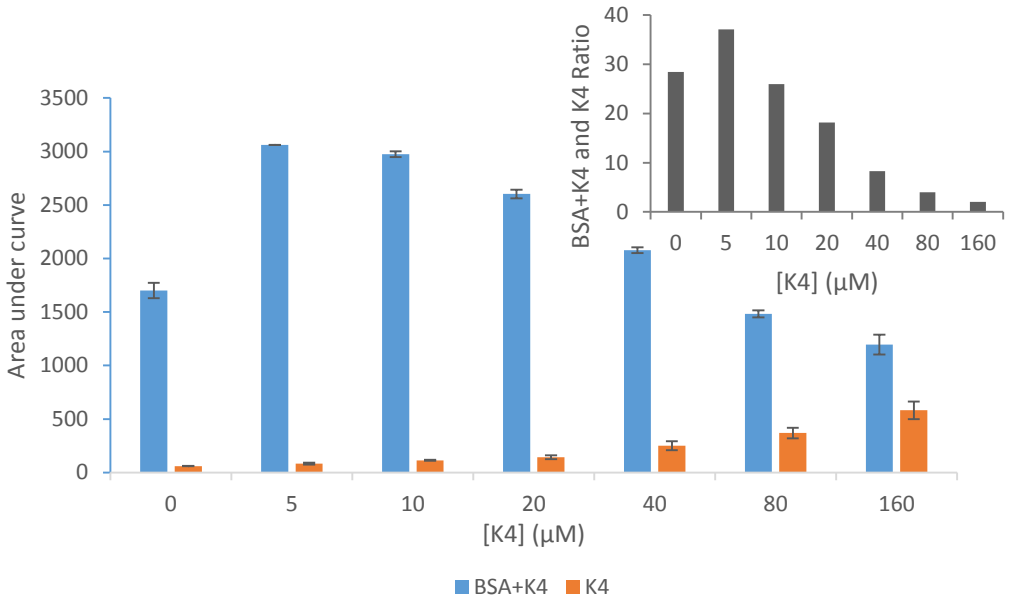

Figure 3.18 – Area under the curve of fluorescence spectra of K4 solutions with or without BSA macromolecule. In the upper right corner is the ratio of area under the curve of BSA+K4 samples and K4 samples. Samples were incubated at 37ºC over 30 min. Results are represented as means ± SEM from at least three independent assays.

Fluorescence intensities ratio between BSA+K4 and K4 (Figure 3.18) exhibits that for increasing quencher concentrations, fluorescence intensity decreases. It also evidences that BSA in presence of quencher, exhibits higher fluorescence than in the absence of quencher, for concentrations inferior to 80 µM. The results suggest that K4 intensities do not influence on BSA+K4 fluorescence. In this sense, inconclusive data shown no apparent explanation for the mechanism of interaction between BSA and K4.

A Stern-Volmer plot, in Figure 3.19, was used to calculate copper (II) compound's Stern-Volmer constant (Ksv). Considering the higher values of fluorescence for BSA in the presence of the quencher, Ksv value obtained was negative from 5 to 20 µM of K4 compound. Regardless it is visible an increase of this constant which indicates that K4 has a large extended quenching effect. The assessment of the total number of coordination sites of K4 to the BSA molecule was hindered by the sudden fluorescence increase upon K4 exposure. As a result the determination of the number of coordination sites was inconclusive due to the negative values of Ksv. Further assays are required to fully understand the interaction between K4 and the BSA molecule.

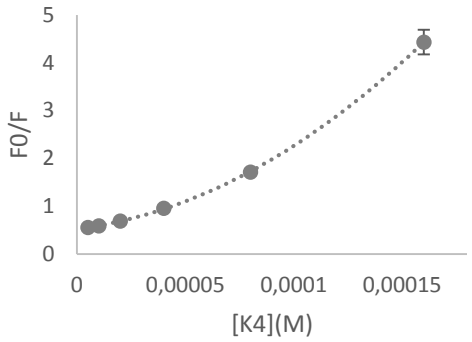

[K4] (μM)	Ksv (M^{-1})
5	-96802.6
10	-43532.9
20	-17262.2
40	-1690.35
80	8511.116
160	19820.72

Figure 3.19 – Stern-Volmer plot of quenching of BSA by K4 compound. [BSA] = 2 μM; K4 compound concentrations ranges from 5 to 160 μM. On the right, a table shows Ksv values in M^{-1} for each concentration of the quencher.

Final conclusions for these assays report a K4 binding ability with BSA macromolecule. It is known that no conformational changes occur upon binding as a result of no visible red or blue shifts on UV-Vis absorption spectra or on the steady-state fluorescence spectra. Regarding the high fluorescence intensity of BSA in the presence of quencher, the majority of Ksv values were negative which impossibilities the calculous of the number of binding sites of BSA to Cu (II) compound.

3.6 Proteome profiling: Two-Dimensional Electrophoresis

In order to better understand the molecular mechanism underlying the biological activity of the Cu (II) compound, a proteome profiling study was performed resorting to HCT116 cell line. Cells were exposed to K4 relative IC_{50} using as control a 0.1 % (v/v) DMSO solution. Resulting 2D electrophoresis gels were analyzed using Melanie 7.0 software. Spots with fold variation under 0.7 (underexpression) or over 1.5 (overexpression) were considered as significantly different. Obtained gels were compared with reference gel (Appendix C) to determine the 15 under- and overexpressed identified proteins. Maldi-MS analysis was not achieve due to time limitations however a latter spots characterization and confirmation will be performed.

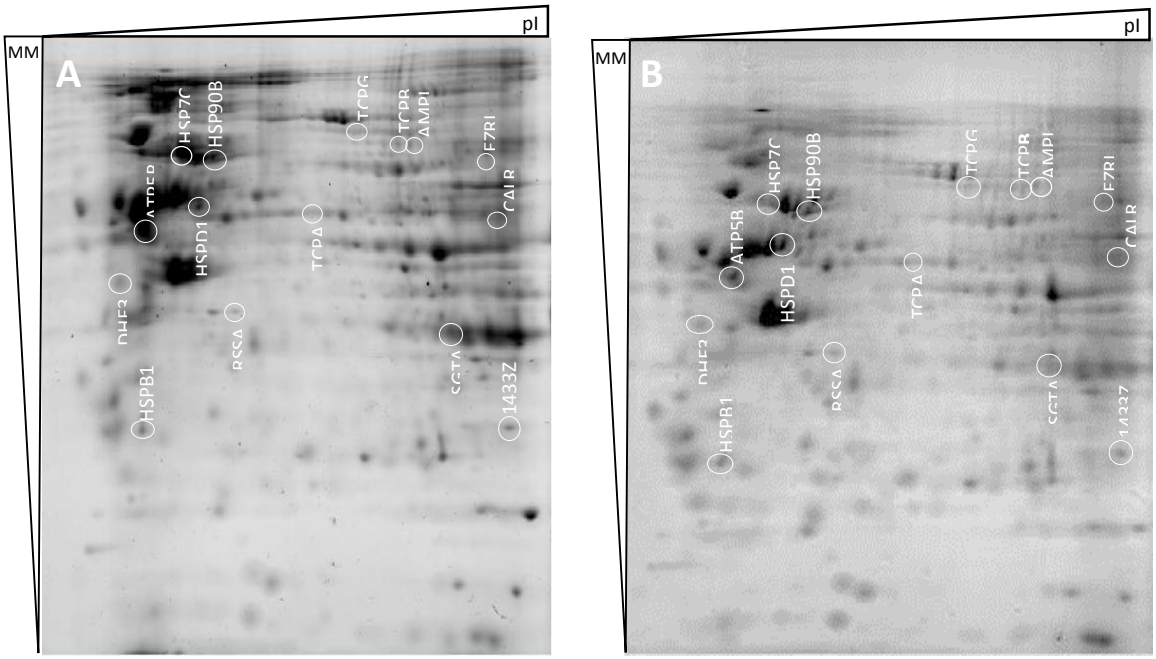

Figure 3.20 - 2D-Electrophoressis gel of HCT116 cells exposed for 48 h to (A) 6.10 µM of K4 compound and (B) 0.1 % (v/v) DMSO. 200 µg of protein extract were loaded and obtained gels were stained with Comassie Blue. Spots with a significant variance of abundancy (fold variation under 0.7 or over 1.5) were marked in circles and tagged with abbreviation name.

Table 3.7 - Proteins identified in 2D gels being underexpressed (green) and overexpressed (red). Proteins are presented as their abbreviation, name, molecular weight in Da, isoelectric point and fold variation (obtained from comparison to control group). Data represented is from two independent assays. Fold variation under 0.7 was consider as underexpression and fold variation over 1.5 was considered as overexpression.

Abbreviation	Protein name	MW (Da)	pI	Fold Variation	Protein Function
1433Z_Human	14-3-3 protein zeta/delta	27745.0	4.73	**1.76**	Signal transduction
AMPL_human	Cytosol aminopeptidase	56565.7	7.91	**1.90**	Protein binding/folding
ATP5B_Human	ATP synthase subunit beta, mitochondrial	56560.0	5.10	**1.56**	Metabolic activity

CALR_Human	Calreticulin	48111,8	4.29	**0.33**	Chaperone/ Stress response
DHE3_Human	Glutamate dehydrogenase 1, mitochondrial	61359.2	7.66	**2.20**	Metabolic activity
EZRI_Human	Ezrin	68527.0	5.87	**0.57**	Cytoskeleton mobility
HSP7C_Human	Heat shock cognate 71 kDa protein	71126.3	5.20	**1.61**	Transcription/ translational machinery
HSP90B_Human	Heat shock protein HSP 90-beta	83606.5	4.77	**1.97**	Chaperone/ Stress response
HSPB1_Human	Heat shock protein beta-1	22768.5	5.98	**0.63**	Chaperone/ Stress response
HSPD1_Human	Heat shock 60 kDa protein 1	61016.4	5.70	**0.52**	Cytoskeleton mobility
IFSA1_Human	Eukaryotic translation initiation factor 5A-1	17060.4	4.90	**0.49**	Transcription/ translational machinery
RSSA_Human	40S ribosomal protein SA	32968.2	4.59	**1.58**	Protein binding/folding
SGTA_Human	Small glutamine-rich tetratricopeptide repeat-containing protein alpha	34291.3	4.59	**1.80**	Chaperone/ Stress response
TCPA_Human	T-complex protein 1 subunit alpha	60856.9	5.71	**2.00**	Chaperone/ Stress response
TCPB_Human	T-complex protein 1 subunit beta	57452.1	6.01	**1.57**	Chaperone/ Stress response

In response to different extrinsic cellular stresses, such as chemotherapeutic drugs or metallic complexes, cells tend to increase their metabolism, namely ATP synthesis, protein synthesis and signaling cascade activation (O'Brien et al. 2013). Analyzing Table 3.7, several identified proteins indicate an increased metabolic activity based on their biological roles. The elicited effect is in part due to K4 exposure to HCT116 cells. One of the most overexpressed proteins, DHE3, the mitochondrial glutamate dehydrogenase 1, presents a fold variation of approximately 2.20. DHE3 is an enzyme responsible for glutamine anaplerosis with following production of α-ketoglutarate in the mitochondria. It is an essential enzyme for intermediate catalysis in citric acid cycle (Singh & Costello 2012). It is well known that cancer cells have metabolic

modifications in comparison with healthy cells, in response to proliferation and growth signals. In this regard, cancer cells prefer glycolysis as an ATP production method instead of oxidative phosphorylation, since it is a faster process to obtain ATP – Warburg effect (Jiang et al. 2012). DHE3 overexpression could describe the metabolic activity increase, as a response of metabolic stress caused by K4 compound (possible organelle reparation or increasing efflux pumps synthesis). Cytosol aminopeptidase, AMPL, is another protein with a high fold variation value (1.9) upon HCT1116 exposure to K4 compound. It is typically involved in the normal process of intracellular protein turnover and also catalyzes the release of N-terminal from several peptides. Normally overexpressed in cancer cells namely in colorectal cancer, it can be used as a tumor marker prognosis (Perez et al. 2015). Overexpression of this protein when exposed to K4 compound could be related to a metabolic stress response of HCT116 cells resulting from increased protein synthesis and additional biologic cascade initiation, as means of a countermeasure against the mechanisms of action of K4. ATP synthase subunit beta mitochondrial, ATP5B, is a protein involved in ATP synthesis catalysis from mitochondria (Singh & Costello 2012). HCT116 exposure to K4 compound elicits an overexpression of this protein within the cell. Metabolic activity in cancer cells is much higher than in healthy cells. In response to stimuli, such as K4 compound, cells metabolism increases. In this sense, overexpression of ATP synthase could be originated from cell response to stress (K4 compound) conducive to provide ATP for all metabolic activities, as for example to provide energy towards drug efflux pumps to remove K4 from the cytosol and hence counter it's action. HSP7C is a protein that acts a transcriptional activation repressor and it plays an important role in spliceosome assembly and is thus required for pre-mRNA splicing (Gloghini et al. 2014). Cells exposed to K4 compound exhibit overexpression of this protein thus suggesting increases in spliceosome assembly and protein synthesis – extrinsic stress due to K4 compound provides an increase in metabolic cell activity. HSP90B is a chaperone involved in regulation and maintenance of target proteins involved in cell cycle regulation and signal transduction. It has an ATPase activity that is responsible for protein activation (Jego et al. 2013). In HCT116 cells exposed to K4, the overexpression observable could be explained due to the increased metabolic activity of cells and consequently the substantial cell needs of ATP. 40S ribosomal protein SA is a protein mainly involved in 40S ribosomal subunit assembly and stability (Bolze et al. 2013). Exhibiting an overexpression pattern in cells exposed to K4 compound, it indicates that an increased protein synthesis and assembly constitutes a cell response to extrinsic stress. Small glutamine-rich tetratricopeptide repeat-containing protein alpha, SGTA, is a co-chaperone involved in ATPase activity regulation of HSC70 and HSP70, which are proteins namely involved in protein folding (Philp et al. 2013). SGTA overexpression could explain the increased protein synthesis and assembly and consequently the increase of metabolic activity in response to K4 compound. TCPA is a chaperone protein that also is involved in protein folding in an ATP-dependent hydrolysis (Finka & Goloubinoff 2013). It shows overexpression in cells treated with K4 compound. Increase metabolic activity of cells when exposed to drugs could explain overexpression of TCPA protein. An increased metabolic activity is implicated with increased protein synthesis and new cascade activation.

Previous assays of apoptotic evaluation, in section 3.2.1, reveal a small percentage of cells entering into the apoptotic pathway, less than 50 %. Some identified proteins in proteome analysis might provide an explanation for this results. Calreticulin, is a calcium-binding chaperone present in endoplasmatic reticulum. CALR also regulates protein folding in cells. When translocated to cell surface, promoted by Ca^{2+} accumulation, it acts an apoptosis marker, requesting macrophages to opsonize those cells (Liu et al. 2012). HCT116 cells when exposed to K4 compound present a subexpression of calreticulin with a fold variation of 0.33, the lowest value presented in Table 3.7. This event may explain why Hoechst staining assays and flow cytometry assays presents low apoptosis levels. Apoptotic pathway of cells could be compromised due to subexpression of calreticulin. HSPD1 is also one of the proteins with the lowest fold variation, presenting a value of 0.52. As mitochondrial matrix protein, it is essential for protein transport from cytoplasm to mitochondria. In cancer cells, HSPD1 stimulates pro-caspase 3 activation and consequently stimulates apoptotic pathway. However, HCT116 cells exposed to K4 compound promote an HSPD1 subexpression (Rugarli & Langer 2012). As calreticulin, HSPD1 is involved in apoptotic inhibition due to its subexpression thus corroborating results from Hoechst staining and flow cytometry that showed low apoptotic levels in comparison with control groups. HSPB1 is a chaperone involved in protein folding thus protecting cells from metabolic stress such as hypoxia, radical oxygen species, and chemotherapeutic drugs among others. It is located in mitochondria, endoplasmic reticulum, nucleus, cell membrane and cytoplasm. Apoptosis inhibition is promoted when HSPB1 is activated, for example, by chemotherapeutic agents. Caspases inhibition and cytochrome c capture are some of the HSPB1 functions (Nagaraja et al. 2012). Proteasome studies reveal a fold variation of 0.63 for HSPB1, underexpression. This results suggests that exposure to compound K4 promotes apoptosis of HCT116 cells. Despite this result won't corroborate with previous assays of apoptotic evaluation, it seems that apoptosis levels are low in HCT116 cells. This may be explained by the fold variation value that although reveals underexpression, (≈0.63) it is an approximate value of the threshold (0.7). 14-3-3 protein zeta/delta exhibited a fold variation of 1.76 thus revealing that this protein is overexpressed in HCT116 cells exposed to K4. This protein regulates signal transduction pathways namely metabolism, transcription, apoptosis and cell cycle regulation. It also interacts with several pro-apoptotic proteins such as BAX, BAD and NOXA. An overexpression of this protein suggests that pro-apoptotic signals are being "captured" leading cells to the inhibition of the apoptotic pathway (Hodgkinson et al. 2012). This result corroborates previous apoptotic potential evaluation assays which revealed low apoptotic levels. TCPB is a chaperone involved in an ATP-dependent process of protein folding namely cytoskeleton proteins and cell cycle progression regulators. Therefore, low TCPB levels are associated with growth and proliferation inhibition, cell cycle arrest and apoptotic pathway (Jarkovska et al. 2014). HCT116 cells exposed to K4 compound reveal overexpression for TCPB protein. This assay corroborates cell cycle progression assays since there is no arrest but a small delay. Despite low apoptotic levels exhibited in flow cytometry assays, TCPB seems to be overexpressed thus influencing cell decision to enter into an apoptotic pathway. IFSA1 is a protein involved in translation elongation by mRNA binding, cell cycle progression, and maintenance of cell wall integrity. It is a regulator of p53/TP53 dependent apoptosis and TNF-α mediated apoptosis. It shows elevated abundancy in cancer cells and could be defined as cancer biomarkers

(Caraglia et al. 2013). It exhibits underexpression in HCT116 cells treated with K4 compound. This protein pattern could explain the cell cycle progression delay and the low levels of apoptosis obtained both, in flow cytometry and Hoechst staining assays.

Other metabolic response of HCT116 cells to K4 addition is explained by Erzin. It is a cytoplasmatic protein involved in cytoskeleton communication with cell membrane and acts as tyrosine kinase substrate in microvilli. It plays a key role in cell adhesion, migration and organization and reports show that the ERM family protein plays important roles in cell motility, invasion and metastasis (Leiphrakpam et al. 2014). HCT116 cells exposed to K4 revealed a subexpression of this protein. Despite invasion and metastasis subjects are out of the scope of this thesis, K4 compound may be inhibiting Erzin protein thus might have an active role in preventing tumor progression to other aggressive and final stages of tumorogenesis.

Overall the abundancy protein modifications are generally related to the ones which are responsible for a far more active cellular metabolism. Cu (II) compound addition to HCT116 cells triggers a metabolic stress response, namely overexpressing chaperone like proteins. Proteins involved in the inhibition of apoptotic pathways are also largely overexpressed resulting in the low levels of apoptosis in cells. These results explained the low apoptotic levels exhibited in previous assays and consequently explain a cytostatic mechanism is cells exposed to K4. It was also assessed that underexpression of Erzin could explained an inhibited tumor progression and invasion and metastatic events. A posterior Maldi-MS analysis will be performed to confirm protein nomeation.

3.7 Nanovectorization approach

3.7.1 Gold nanoparticle synthesis and characterization

Keeping in mind the improvisation of K4 Cu (II) compound, pharmacokinetic and pharmacodynamic properties, K4's incorporation into a rationally designed nanoformulation was envisaged, resorting to the use of gold nanoparticles (see section 2.9).

Gold nanoparticle (AuNP) characterization was performed resorting to techniques such as UV-Vis spectroscopy, TEM and DLS. Synthetized gold nanoparticles exhibited an absorption spectrum with a maximum peak at 519 nm, an indicative of spherical monodisperse nanoparticles with approximately 14 nm diameter. Surface Plasmon Resonance (SPR) band of colloidal gold is an important and optical feature which describes particles according to shape, dispersion and size. Additionally, through UV-Vis spectroscopy it was determined gold nanoparticle concentration using Lambert-Beer's law and assuming a molar extinction coefficient of 2.33×10^8 $M^{-1}cm^{-1}$ (Conde, Doria, et al. 2012).

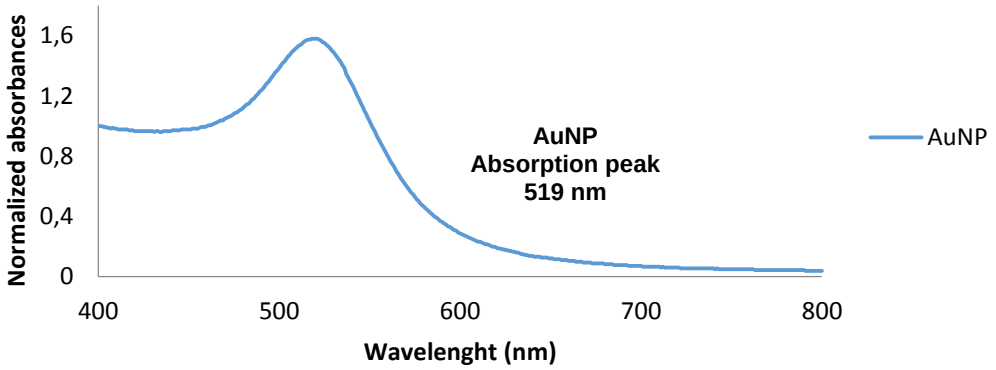

Figure 3.21 – Absorbance spectrum of naked gold nanoparticles synthetized with Turkevich method.

Previously synthetized gold nanoparticles characterization was carried out using TEM analysis which allowed a direct visualization of nanoparticles core shape, dispersion and size. In Figure 3.22, TEM results confirm UV-Vis spectroscopy indicating spherical monodisperse nanoparticles with approximately 14 nm diameter. DLS technique, in Figure 3.23, indicates a hydrodynamic diameter of the naked gold nanoparticle of approximately 16 nm, which corroborated Figure 3.21 spectrum.

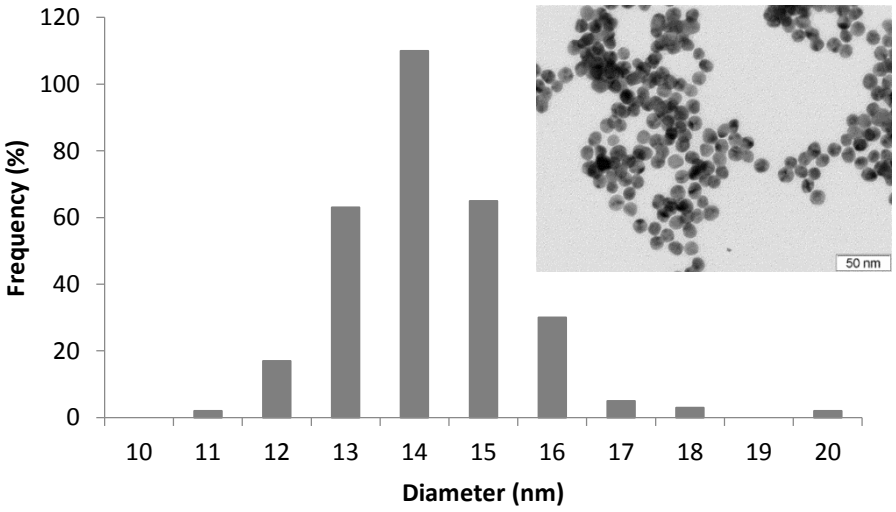

Figure 3.22 – TEM analysis of naked gold nanoparticles previous synthetized. In the upper right corner is a representative TEM image of AuNPs.

.

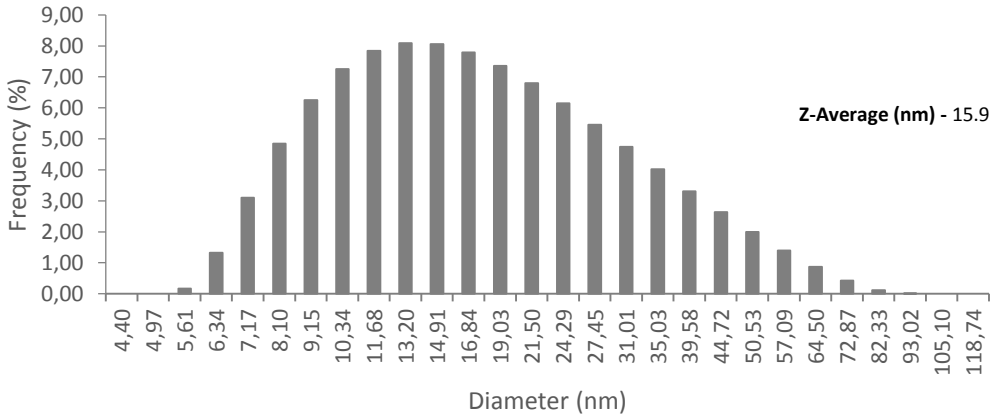

Figure 3.23 – DLS analysis of AuNP with hydrodynamic diameter (in nm) and respective frequency. In the upper right corner is represented Z-average in nm.

3.7.2 AuNP@PEG: synthesis and characterization

A subsequent PEG functionalization of gold nanoparticles was performed conducive to increase biocompatibility and stability of naked AuNP. The absorption spectrum in Figure 3.24 revealed a shift, of the maximum peak of AuNP to AuNP@PEG, from 519 to 520 nm. This variation is an indicative that the microenvironment surrounding the gold nanoparticle has changed and that the polyethylene glycol was functionalized.

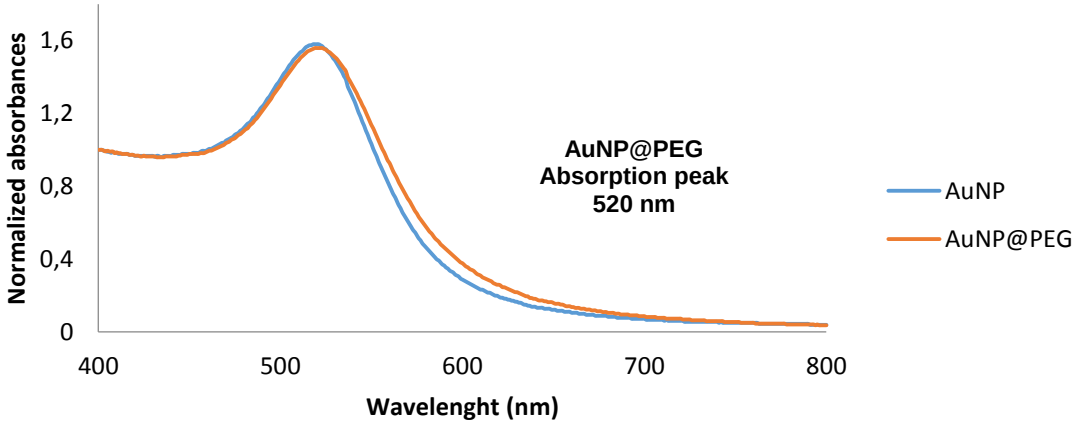

Figure 3.24 – Absorbance spectrum of naked gold nanoparticles and functionalized gold nanoparticles with PEG exhibiting a maximum peak shift of 1 nm, from 519 to 520 nm.

Functionalization efficacy determination was accomplished with an Elman's test which determines the total number of PEG molecules coated to the AuNP. Using a calibration curve (in Appendix D) it was possible to assess an 83 % success of PEG functionalization with approximately 1811 molecules per particle. Using DLS analysis it was possible to evaluate hydrodynamic diameter of PEGylated particles, obtained an average of 26.2 nm. PEG molecules have approximately 3.25 nm (http://www.iris-biotech.de/), which could be an indicative of the possibility that more than a monolayer of PEG molecules coat the gold nanoparticles. Given that PEG is a flexible molecule that can influence the Brownian movement of the AuNP@PEG, through the modification of the AuNP viscosity this effect can be responsible for the altered nanoparticle hydrodynamic diameter. An approximately 10 nm increase of hydrodynamic diameter of AuNP@PEG could indicate a bilayer of coated PEG molecules.

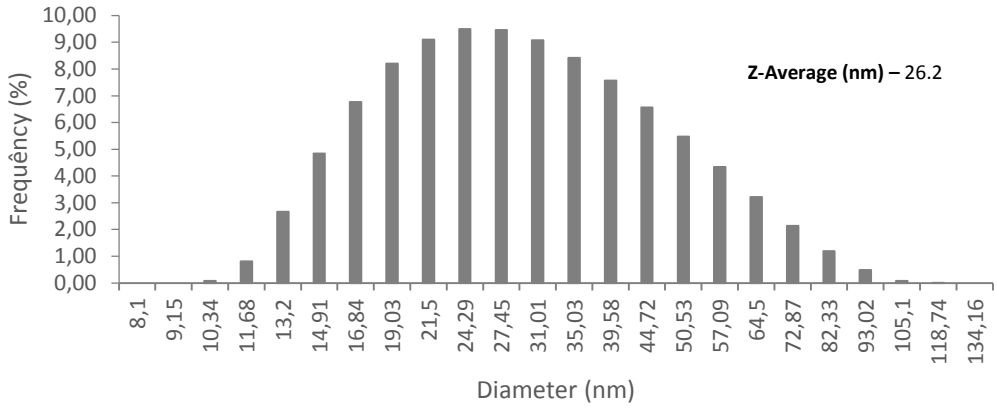

Figure 3.25 - DLS analysis of AuNP@PEG with hydrodynamic diameter (in nm) and respective frequency. In the upper right corner is represented Z-average in nm.

3.7.3 AuNP@PEG@BSA: synthesis and characterization

Serum albumin is on the most common protein in circulation and is responsible for the biodistribution of most biologically active molecules within the organism by binding to these, including most chemotherapeutic drugs thus influencing greatly drug biodistribution. The nanoformulation rational designed passed through the functionalization of the nanoparticle with BSA in order to improve the biodistribution properties and to facilitate the compound functionalization process give the fact that the compound is known to interact with these protein. BSA functionalization was performed using EDC/sulfo-NHS coupling reaction and respective spectrum is shown in Figure 3.26.

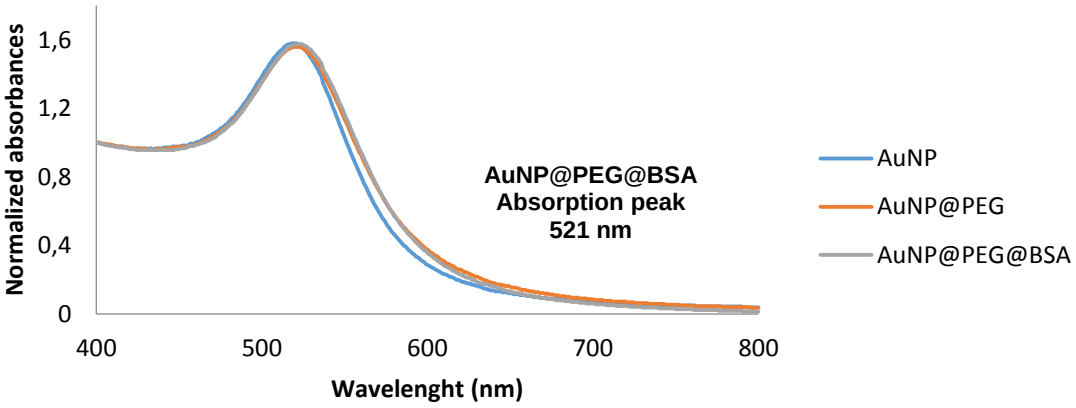

Figure 3.26 – Absorbance spectrum of AuNP@PEG@BSA exhibiting a maximum peak shift of 1 nm, from 520 to 521 nm.

Nanoparticles functionalized with PEG and BSA exhibited a maximum absorption peak at 521 nm revealing a shift when comparing to AuNP@PEG at 520 nm. As mentioned above, the surrounding nanoparticle microenvironment has slightly changed and is possible to deduce a BSA functionalization. AuNP@PEG@BSA characterization was accomplished conducive to determine the amount of BSA molecules coated to AuNP@PEG through Bradford assay (calibration curve in Appendix D). The results reveal that each particle as approximately 4 BSA molecules coated to each nanoparticle. DLS technique was performed to calculate hydrodynamic diameter of AuNP@PEG@BSA showing an average size of 35.3 nm. BSA is a protein with approximately 7 nm of hydrodynamic diameter (Yohannes et al. 2010) therefore, a monolayer of BSA molecules could be coating AuNP@PEG nanoparticles.

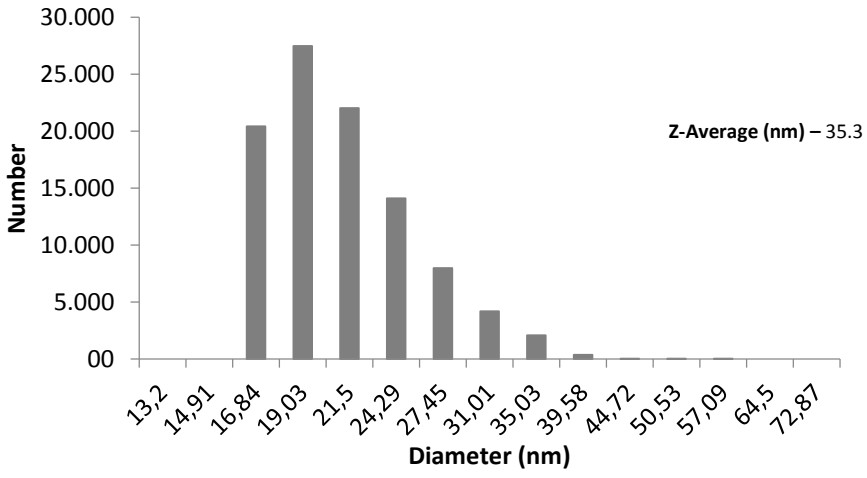

Figure 3.27 - DLS analysis of AuNP@PEG@BSA with hydrodynamic diameter (in nm) and respective frequency. In the upper right corner is represented Z-average in nm.

3.7.3 AuNP@PEG@BSA@K4: synthesis and characterization

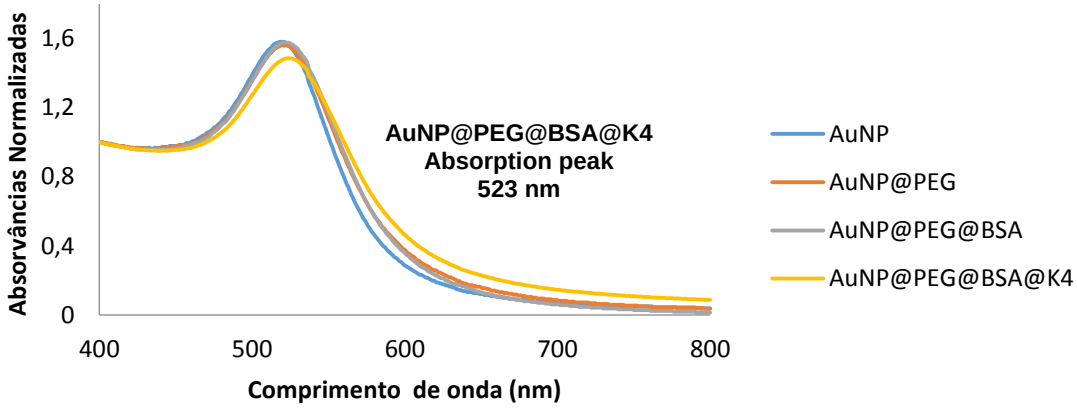

Figure 3.28 - Absorbance spectrum of AuNP@PEG@BSA@K4 exhibiting a maximum peak shift of 2 nm, from 521 to 523 nm.

A final step for the nanoformulation was to functionalize AuNP@PEG@BSA with K4 compound. Figure 3.28 exhibits a shift of the maximum absorption peak from 521 nm AuNP@PEG@BSA to 523 nm of AuNP@PEG@BSA@K4. Once more, the surrounding nanoparticle environment was changed, suggesting that K4 functionalized onto the nanoformulation's surface.

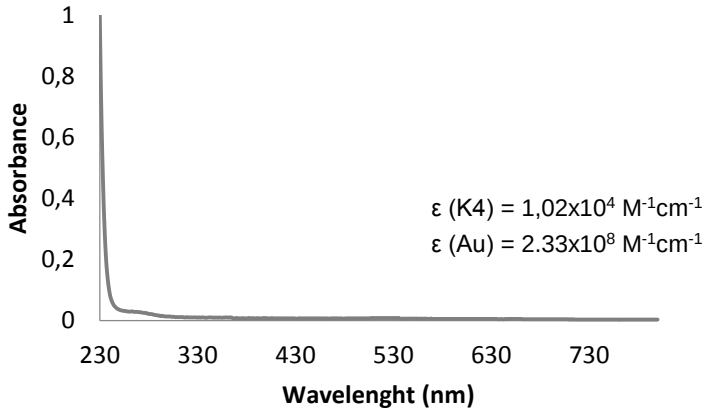

Figure 3.29 – Supernatant spectrum resulting from AuNP@PEG@BSA@K4 functionalization. In the lower down corner are represented molar extinction coefficients of K4 and Au.

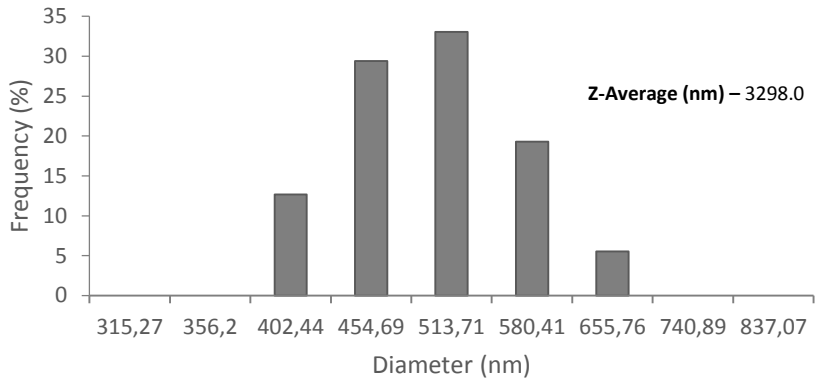

Figure 3.30 - DLS analysis of AuNP@PEG@BSA@K4 with hydrodynamic diameter (in nm) and respective frequency. In the upper right corner is represented Z-average in nm.

Supernatant spectrum, resulting from AuNP@PEG@BSA@K4 functionalization, Figure 3.29, exhibited a flat line which indicates that no K4 compound was in excess in the functionalization. However, comparing the molar extinction coefficients between Au and K4, a 4 fold difference is present thus suggesting that some K4 compound may be in supernatant but is disguised by the high molar extinction coefficient of Au. Analyzing DLS results, in Figure 3.30, it is verified a high particle diameter, approximately 3300 nm. It is possible that some particles may be agglomerated indicated by the high z-average value. However, diameters described in Figure 3.30, range from 402.44 to 655.76 nm, a lower value when comparing to Z-average (3298 nm). This particular feature could be explained by the presence of immense particle aggregates in solution contributing to the enormous z-average value. Overall results suggest a poor K4's nanovectorization which consequently leads to poor antiproliferative effects on cells or also indicate an impaired nanoparticle internalization in cells. Nanoformulation size could be preventing it to enter in cell and exhibit its antiproliferative effect.

3.7.4 Cell viability assays of vectorized compound

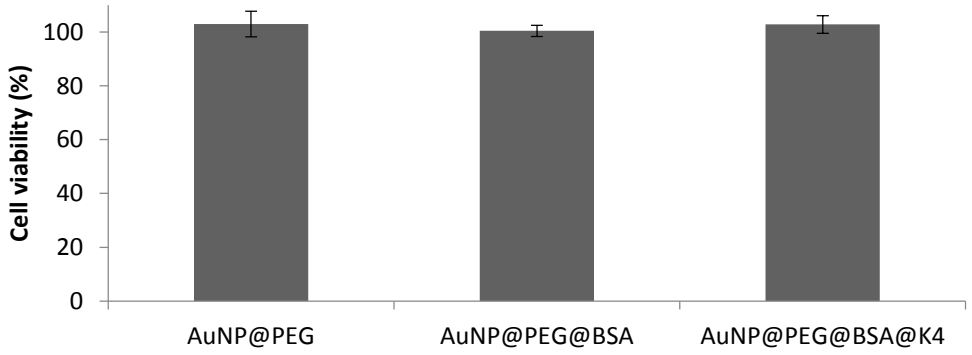

Figure 3.31 – Cell viability assays of AuNP@PEG@BSA@K4. HCT116 cells were exposed to nanoformulations for 48h. Control groups used were AuNP@PEG and AuNP@PEG@BSA.

Followed by synthesis and functionalization, nanoformulation was evaluated in *in vitro* growth inhibition assays. Control groups used were nanoparticles functionalized with PEG and BSA. AuNP@PEG and AuNP@PEG@BSA revealed 100 % cell viability reinforcing the idea that PEG and BSA are efficient biocompatible molecules. K4 compound vectorized displayed 100 % cell viability as well as control groups. According to previous results of functionalization, K4 may not be functionalized onto nanoparticles or just a small percentage could be attached, thus the effect on *in vitro* assays reveals no growth inhibition. Internalization rates could also be affecting the overall results. Concerning the nanoformulation size indicated in previous results, K4 compound could not be entering into the cell and consequently perform its mechanism of action. Regarding the compound's low solubility in aqueous buffers, it is possible to deduce that a nanovectorization based in aqueous solution was not well accomplished. A possible solution is to identify a new method were non-aqueous solvents are used conducive to improve K4s nanovectorization, such as lipossomes. The hydrophobic membrane of liposomes could prove to be a superior option in terms of the compound's vectorization, due to the poor solubility in aqueous buffers improving drug delivery efficiencies

3.8 Combined therapy strategies

3.8.1 Cytotoxic potential evaluation

Drug cocktail therapy is a chemotherapeutic approach that aims to tackle the setbacks and hindrances characteristic of single dose treatments, namely the decrease in multidrug resistance by cancer cells and to assist cancer treatment of clonal expansions by providing different mechanisms of action (Greaves & Maley, 2012). Along these lines, the approach of combining K4 with several commercial chemotherapeutic drugs was assessed in order to establish new chemotherapeutic combination strategies.

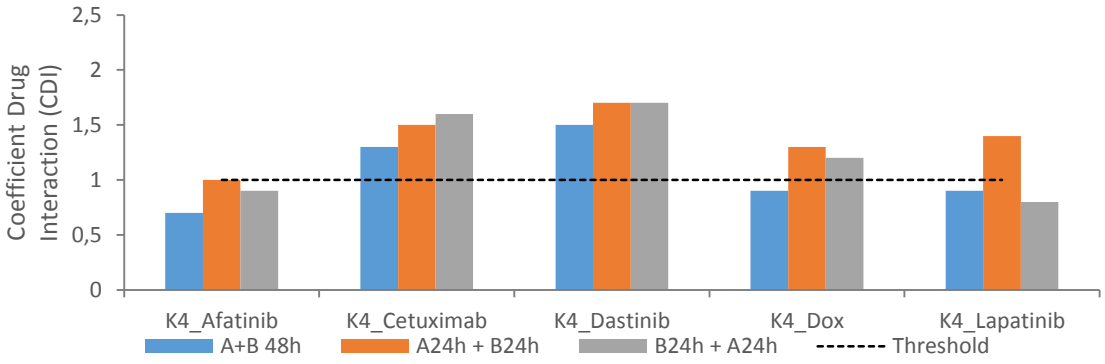

Figure 3.32 - Coefficient drug interaction (CDI) analysis of K4 with afatinib, cetuximab, dastinib, doxorubicin and lapatinib. HCT116 cells were exposed to compounds for 24h or 48h in their relative IC_{50} concentrations (see Appendix D). A-Single agent K4; B-Single agent afatinib, cetuximab, dasatinib, doxorubicin or lapatinib. Threshold- CDI value threshold (CDI=1).

Prior to combined therapy assays, relative IC_{50} of commercial chemotherapeutic drugs were calculated (See Appendix E). Cell viability assays of combinatory approaches are in Appendix F. Coefficient drug interaction was calculated to all combinatory methods as explained in section 2.10. Analyzing figure 3.32, K4 interacting with cetuximab and dasatinib exhibited antagonism for all combinatory strategies (CDI>1). Cetuximab binds to extracellular domain of EGFR inhibiting the subsequent pathway (Lenz 2007) and dasatinib is a tyrosine kinase inhibitor different from EGFR (Aguilera & Tsimberidou 2009). K4 compound may be altering the conventional chemotherapeutic drug structure thus altering their mode of action or may be interfering on their pathways resulting in the antagonistic effects. Further studies with these combinations (apoptotic potential evaluation or proteome profiling) were not pursued. Afatinib, a tyrosine kinase inhibitor namely Her-2 and EGFR, in association with K4 revealed an additive effect (for strategy A24h + B24h) and synergism for the two other strategies (see Figure 3.32). From all drug interaction assays, K4+afatinib presented the lowest CDI values for all combinatory strategies. Notwithstanding, A+B 48h strategy had the highest CDI result. Lapatinib or doxorubicin in combination with K4 exhibited both synergism and antagonism (see Figure 3.32). Lapatinib is a tyrosine kinase inhibitor and it's known to affect Her-2 and EGFR family receptors (Paul et al. 2008). In similarity with afatinib, the combination strategy with this compound revealed low CDI values. K4 mechanism of action could directly or indirectly potentiate tyrosine kinase inhibition. On the other hand, doxorubicin, a DNA intercalator (Thorn, Caroline; Oshiro, Connie; Marsh, Sharon; Hernandez-Boussard, Tina; McLeod, Howard; Klein, Teri; Altman 2012), showed a synergistic effect for A+B 48h combinatory. As seen in previous results, K4 interacts with DNA grooves, thus may be potentiating DNA damage effect and increasing cytotoxic potential for this combination strategy. The other combinatory strategies reveal antagonism that may be explain due to DNA repair mechanisms could be more efficient when drugs are applied separately.

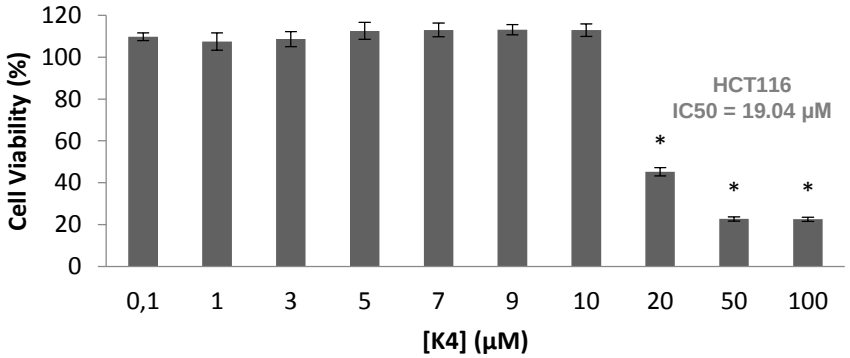

Figure 3.33 - Growth inhibition assays of HCT116 cell line using K4. Cells were exposed for 48h to compound K4 and control group was exposed to 0.1% DMSO. Results are shown as mean ± SEM from at least three independent. In the upper right corner is the reevaluated IC_{50} value, 19.04 µM *- statistical significance with $p<0.05$ compared to control group.

Due to poor storage conditions, K4's activity was thought to, after several assays, to be compromised. A re-assessment of K4 cytotoxic potential, proved the postulated hypothesis, revealing an increased IC_{50}, in an order of magnitude of 3 fold higher comparative to the initially determined IC_{50} (6.10

μM)(Figure 3.33). Due to poor storage conditions a possible deduction for the compound's loss of activity, and consequent IC_{50} increase, might be due to K4 structural modifications. K4 structure modification could be a possible deduction for altering IC_{50} value. Moreover, this evidence may suggest that K4 mode of action or molecular targets might have been altered. In this regard the following combination therapy assays were conducted with the re-established IC_{50} concentration.

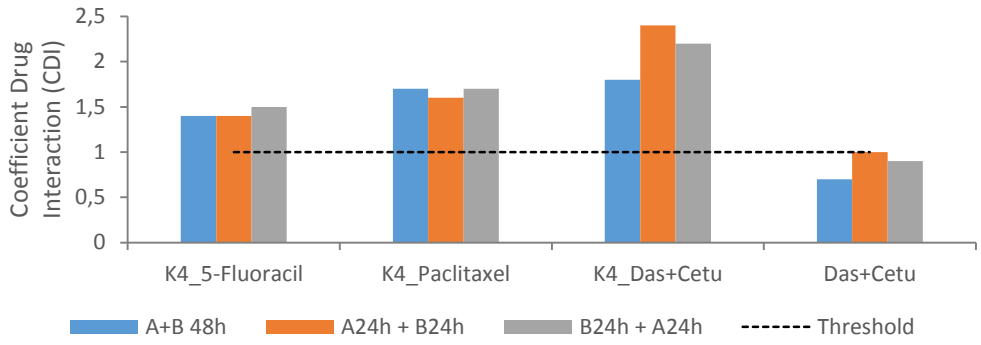

Figure 3.34 - Coefficient drug interaction (CDI) analysis of K4 with 5-fluorouracil, paclitaxel, dasatinib and cetuximab and CDI analysis of dasatinib with cetuximab. Data were obtained after K4 relative IC_{50} reevaluation. Compounds were exposed to HCT116 cell for 24h or 48h in their relative IC_{50} concentrations. A-Single agent K4; B-Single agent afatinib, cetuximab, dasatinib, doxorubicin or lapatinib. Treshold- CDI value threshold.

Figure 3.34, shows CDI values of combinatory strategies using the re-established K4 IC_{50}. Copper (II) compound interaction with 5-fluorouracil and paclitaxel exhibited antagonism for all the tested combinatory strategies (CDI>1) (see Figure 3.34). 5-Fluorouracil acts as a thymidylate synthase inhibitor (blocking DNA replication) (Longley et al. 2003) while paclitaxel interferes with the normal breakdown of microtubules during cell division (Holohan et al. 2013). A chemotherapeutic drug structure alteration due to K4 compound could be altering their mode of action or interfering on their pathways, therefore explaining the antagonistic effects. Further studies with these combinations were not pursued since these were not fruitful in terms of their pharmacodynamic properties. Combination of dasatinib with cetuximab, displayed CDI values under or equal to 1 (synergism and additive effect respectively) (see Figure 3.34). However after K4 addition to dasatinib and cetuximab, CDI values were promoted to the antagonism region (CDI values over 1). Cetuximab, an EGFR pathway inhibitor and dasatinib is a tyrosine kinase inhibitor from Bcr-Abl family and Scr family protein. In this sense, given that previous results evidenced K4's ability to bind to peptides, namely BSA, the compound could be altering Cetuximab's mode of action by binding to this monoclonal antibody. K4 compound could also modify molecular targets of dasatinib and consequently his pathway, hence the antagonistic effects. Previous combinatory strategies, (K4 with dasatinib or K4 with cetuximab) showed antagonism for both cases, suggesting that K4 with cetuximab and dasatinib interaction would also exhibit antagonism.

3.8.2 Apoptotic potential evaluation

The apoptotic potential of chemotherapeutic approaches mentioned in the previous section was evaluated. Only the synergetic and additive combinations where analyzed through Hoechst 33258 staining: i) combination of K4 with afatinib; ii) combination of K4 with doxorubicin and iii) combination of K4 with lapatinib. An important concept to keep in mind is that these assays were performed before the increase of K4 relative IC_{50}, and hence it was used the 6.10 µM of K4 as IC_{50} concentration.

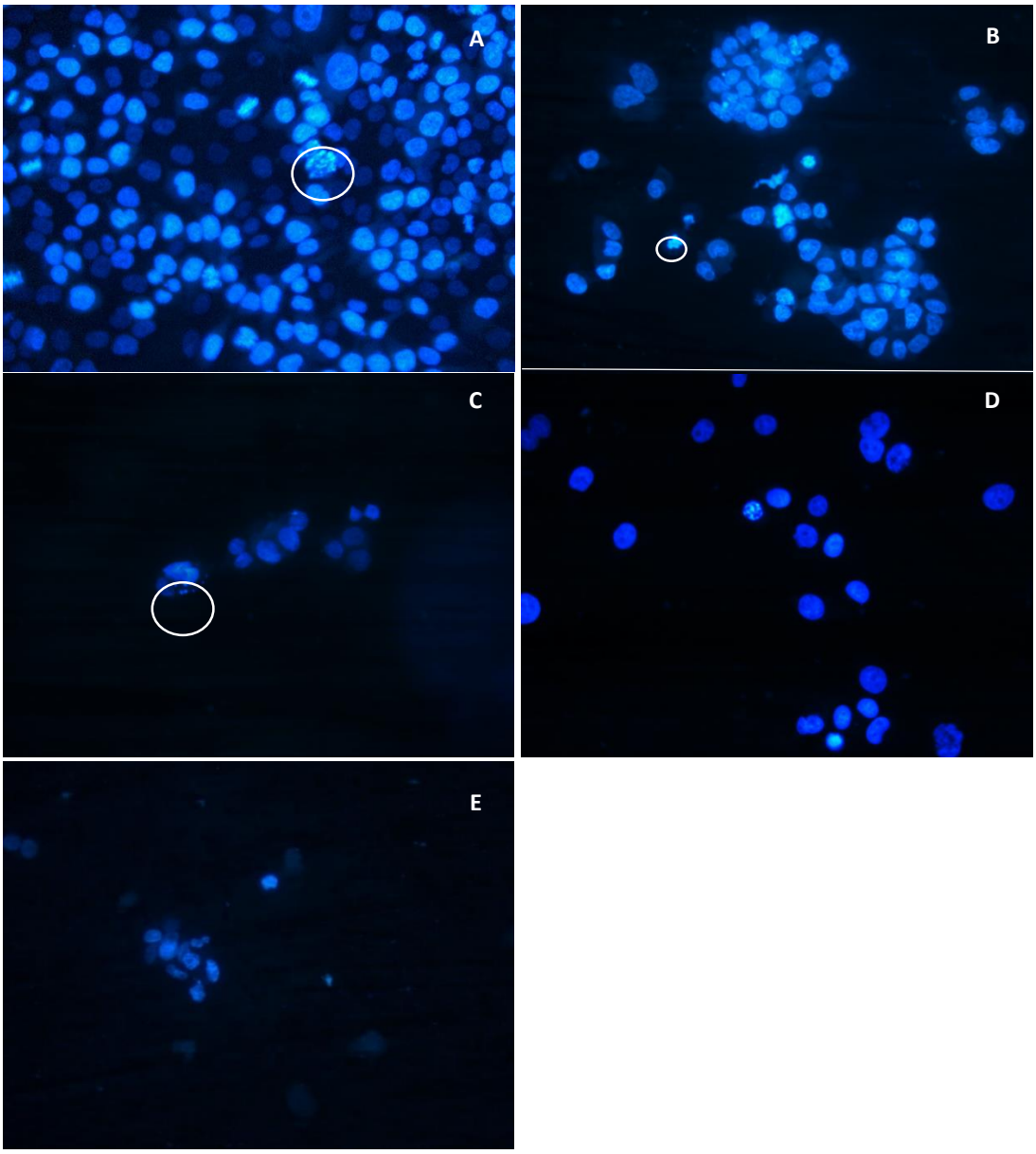

Figure 3.35 – Hoechst 33258 staining of HCT116 cell line exposed to: A – IC_{50} concentration of K4 for 48h; B – IC_{50} concentration of Afatinib for 48h; C – K4 + Afatinib for 48h at their IC_{50} concentration; D – K4 24h + Afatinib 24h at their IC_{50} concentration; E – Afatinib 24h + K4 24h at their IC_{50} concentration. Control group used were preparations A and B. White circles indicate nuclear fragmentation and apoptotic bodies' presence.

Hoechst staining results for combination of K4 compound and commercial chemotherapeutic drug afatinib are shown in Figure 3.35. As mentioned in section 3.2.1, K4 compound at their IC_{50} concentration shows low apoptotic potential in HCT116 cells (under 50 %). Figure 3.35A shows the formation of apoptotic bodies in the white circle and also exhibits a high cell density. Figure 3.35B corresponds to cells treated for 48h with afatinib at his IC_{50} concentration. It is visible apoptotic body formation similar to the preparation with K4, but a lower cell density is observed. In Figure 3.35C cells were exposed to the combinatory strategy K4+Afa during 48h, at their IC_{50} concentrations. It is visible apoptotic bodies in the preparation and a very low cell density corroborates cytotoxic assays in section 3.8.1 which showed a synergistic effect for this combinatory. Figure 3.35D shows the combinatory approach of K424h + Afa24h. Despite the lower cell density in comparison to control groups (A and B), Figure 3.35D reveals an increased cell density comparing to K4+Afa 48h. This results corroborate the cytotoxic assays where it is revealed an additive effect for this approach. Figure 3.35E relates to the combinatory approach of Afa 24h+K4 24h. It shows a low cell density and low apoptotic body presence. This results corroborate cytotoxic assays of the section 3.8.1 where a synergistic effect was obtained for this combinatory. A lower cell density when comparing to combinatory K4 24h+Afa 24h refers to a high cytotoxic effect thus corroborating previous cytotoxic results.

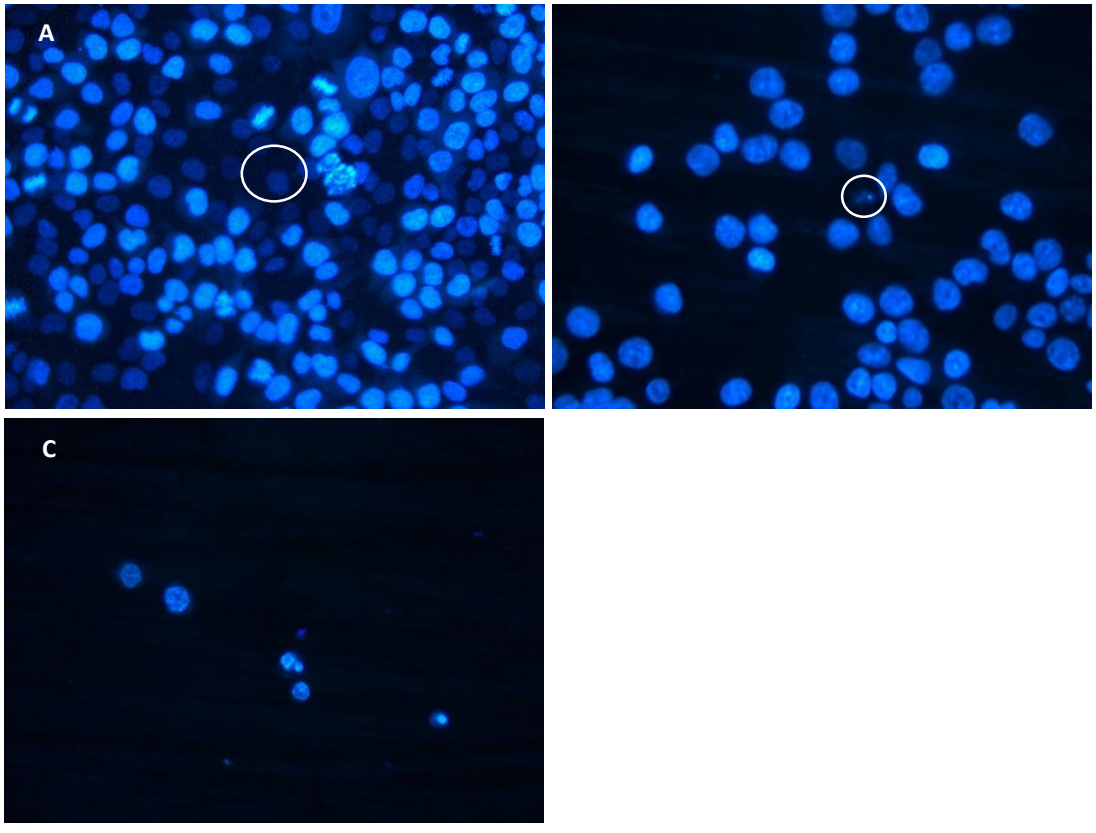

Figure 3.36 - Hoechst 33258 staining of HCT116 cell line exposed to: A – IC_{50} concentration of K4 for 48h; B – IC_{50} concentration of Doxorubicin for 48h; C – K4 + Doxorubicin for 48h at their IC_{50} concentration. Control group used were preparations A and B. White circles indicate nuclear fragmentation and apoptotic bodies' presence.

Figure 3.37 exhibits Hoechst staining results for combination of K4 compound and doxorubicin. Control groups used are in Figure 3.37A and 3.37B corresponding to cells exposed to K4 compound in his IC_{50} concentration and doxorubicin at his IC_{50} concentration, respectively. Once more, the lower cell density coincides to cells treated with K4 compound due to its cytostatic mechanism of action reported in section 3.6. Hoechst preparation of Dox 48h reveals a lower cell density than preparation of Figure 3.37A and formation of apoptotic bodies. Combinatory approach of K4 compound and doxorubicin for 48h at their IC50 concentrations reveal a substantial decrease in cell density which is explained by its synergistic effect mentioned in section 3.8.1. A higher cytotoxic effect when combining these two drugs, is verified, leading to a higher cell death and lower cell density in Hoechst preparations.

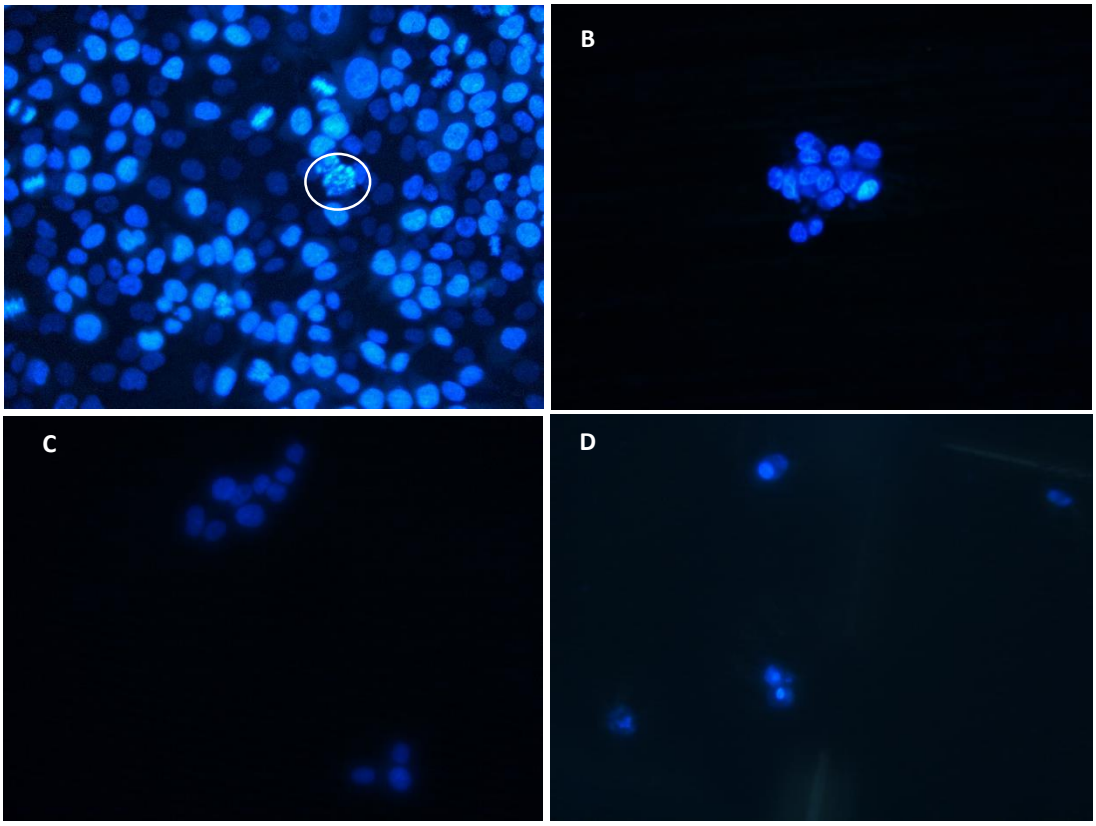

Figure 3.37 - Hoechst 33258 staining of HCT116 cell line exposed to: A – IC_{50} concentration of K4 for 48h; B – IC_{50} concentration of Lapatinib for 48h; C – K4 + Lapatinib for 48h at their IC_{50} concentration; D – Lapatinib 24h + K4 24h at their IC_{50} concentration. Control group used were preparations A and B. White circles indicate nuclear fragmentation and apoptotic bodies' presence.

Combinatory strategy of K4 compound with the commercial chemotherapeutic drug lapatinib was evaluated in terms of apoptotic potential as shown in Figure 3.37. Control groups used were in Figure 3.37A and 3.37B corresponding to K4 IC_{50} and lapatinib IC_{50} respectively. Laptinib preparation reveals a very cell density, revealing high levels of cell death. Combinatory approach of Figure 3.37C corresponds to K4+Lapainib for

a 48h incubation in their IC_{50} concentration. A low cellular density is observed revealing a high cell death mechanism. A similar effect is visible in combinatory approach of Figure 3.37D (Lapatinib 24h+K4 24h).

As an overall conclusion combinatory approaches demonstrated synergistic or additive effects presents very low cell density levels in Hoechst staining assay thus corroborating the high cytotoxic values obtained in section 3.8.1. Combinatory strategy with afatinib showed the most promising results since all combinatory approaches revealed synergism or additive effects. However, due to experimental limitations, afatinib and K4 combinatory was not possible to evaluate in further studies. In this sense, the second best combinatory, was used to a proteome profiling study – K4 and lapatinib combination.

3.8.3 Proteome Profiling: Two-Dimensional Electrophoresis

As previous assays revealed, the combinatory approach of lapatinib and K4 in HCT116 cells was chosen to study the molecular mechanism to a proteome profiling assay. Cells were exposed to lapatinib compound in his relative IC_{50} concentration (Appendix E) for 24h, followed by the addition of K4 compound in his relative IC_{50} concentration (6.10 µM). The increase relative IC50 referred in section 3.8.1, only affected cytotoxic assays. Proteome profiling assays of lapatinib and K4 were performed before the increased IC50 concentration event. As control groups were used protein extracts from HCT116 cells exposed for 48 h to K4 at his relative IC_{50} and lapatinib at his relative IC_{50}. Obtained gels were analyzed through Melanie 7.0 software and spots with fold variation under 0.7 were considered as underexpression or over 1.5 were consider as overexpression. A total of 13 proteins were identified and compared with reference gel (Appendix C) to determine under- and overexpressed proteins. An important concept to grasp when considering proteome profiling of lapatinb and K4 combination is that fold variation calculous of Lapatinib+K4 was made with control group of K4. Considering the focus of this thesis, K4+lapatinib proteome profiling was compared to K4 proteome profiling.

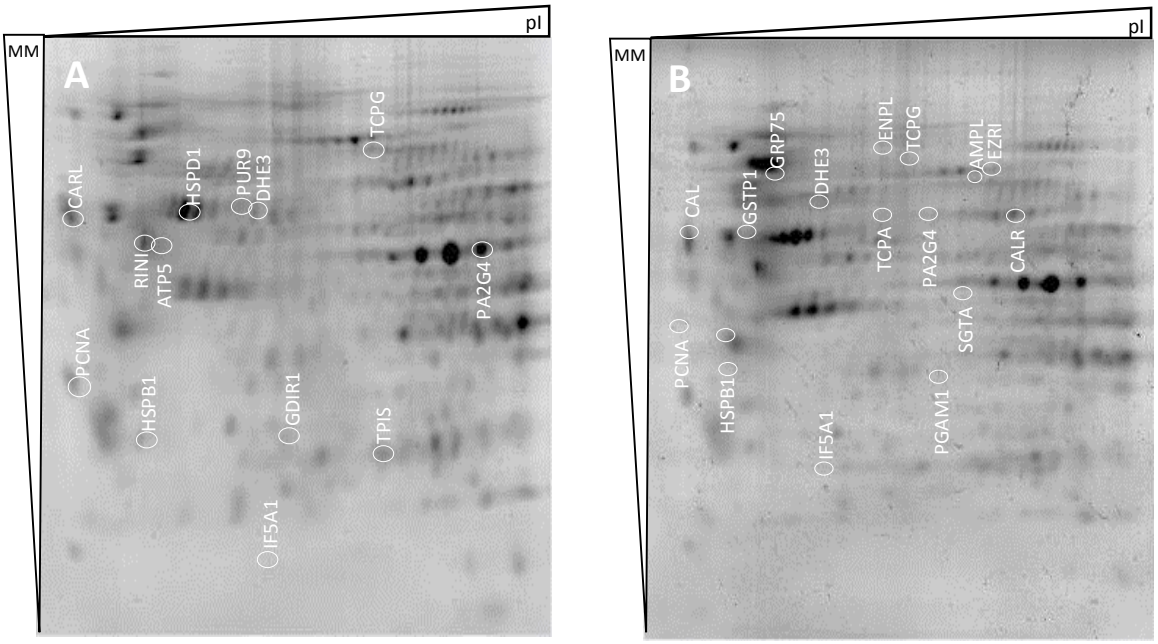

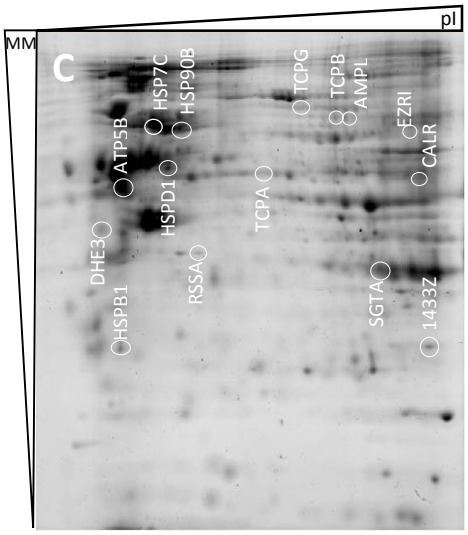

Figure 3.38 - 2D-Electrophoressis gel of HCT116 cells exposed to (A) 19.60 µM of Lapatinib incubated for 24 h followed by incubation of 6.10 µM of K4 compound for 24h and (B) 19.60 µM Lapatinib for 48h (C) 6.10 µM K4 for 48h. 200 µg of protein extract were loaded and obtained gels were stained with Comassie Blue. Spots with a significant variance of abundancy (fold variation under 0.7 or over 1.5) were marked in circles and tagged with abbreviation name.

Table 3.8 – Proteome analysis of cells exposed to 24 h lapatinib followed by 24 h K4 at their IC_{50} concentrations. Proteins are presented as their abbreviation, name, molecular weight in Da, isoelectric point and fold variation (obtained from comparison to control group). It also presented fold variation of samples exposed to K4 compound and to lapatinib for 48 h at their IC_{50} concentrations. Data represented is from two independent assays. Fold variation under 0.7 was consider as underexpression (green) and fold variation over 1.5 was considered as overexpression (red).

Abrev.	Protein	MW (Da)	pI	Fold Variation			Protein function
				K4+Lapa	K4	Lapa	
ATP5B_Human	ATP synthase subunit beta, mitochondrial	56560.0	5.10	0.49	1.56	2.74	Metabolic activity
CALR_Human	Calreticulin	48111,8	4.29	1.60	0.33	0.27	Chaperone/ Stress response
DHE3_Human	Glutamate dehydrogenase 1, mytochondrial	61359.2	7.66	2.17	2.20	3.83	Metabolic activity
GDIR1_Human	Rho GDP-dissociation inhibitor 1	23192.7	5.02	0.39	-	-	Protein binding/ folding
HSPB1_Human	Heat shock protein beta-1	22768.5	5.98	0.54	0.63	0.42	Chaperone/ Stress response
HSPD1_Human	Heat shock 60kDa protein 1	61016.4	5.70	1.67	0.52	-	Cytoskeleton mobility
IF5A1_Human	Eukaryotic translation initiation factor 5A-1	17060.4	4.90	0.57	0.49	0.08	Transcriptional/ translational machinery
PA2G4_Human	Proliferation-associated protein 2G4	44129.1	6.11	2.71	-	-	Signal transduction

PCNA_human	Proliferating cell nuclear antigen	29111.0	4.38	**1.52**	-	**2.03**	Transcriptional/ translational mechinery
PUR9_Human	Bifunctional purine biosynthesis protein PURH	65129.2	6.26	**1.54**	-	-	Transcriptional/ translational mechinery
RINI_Human	Ribonuclease inhibitor	35953.7	8.14	**0.52**	-	-	Transcriptional/ translational mechinery
TCPG_Human	T-complex protein 1 subunit gamma	61104.3	6.06	**1.51**	-	-	Chaperone/ Stress response
TPIS_Human	Triosephosphate isomerase	31076.2	5.55	**2.15**	-	-	Metabolic activity

A range of extrinsic cellular stresses, such chemotherapeutic drugs or metallic complexes, could trigger a response of increasing metabolic activity in cells, which includes protein synthesis, ATP synthesis and signaling cascade activation (O'Brien et al., 2013). Table 3.8, indicates several identified proteins that could explain the increased metabolic activity due to K4 and lapatinib presence in HCT116 cells. Glutamate dehydrogenase 1 mitochondrial, DHE3 is an enzyme involved in metabolic activity regulation namely in α-ketoglutarate catalysis in citric acid cycle (Singh & Costello, 2012). Cancer cells preferably obtain ATP from glycolysis instead of oxidative phosphorylation which mainly occurs in healthy cells. The altered mechanism enables cancer cells to obtain ATP in a faster process (Jiang et al., 2012). This protein seems to be overexpressed in combinatory approach but also in control groups, as shown in Table 3.8. These results suggest that cells increase their metabolism activities as a response to the presence of compounds such as K4 and lapatinib. PA2G4 is the most overexpressed protein of those identified. It plays a role in ERBB3-regulated signal transduction pathway and in promoting cell growth. Moreover it inhibits transcription of some E2F1-regulated promoters. It also binds to RNA and is involved in ribosome assembly. It has two isoforms in which isoform 1 suppresses apoptosis and isoform 2 promotes cell differentiation (Keene et al., 2011). As seen in Hoechst staining assays, samples of Lapatinib in combination with K4 have a low cell density and consequently high apoptotic potential, thus suggesting that PA2G4 identified is not isoform 1. Overexpression of isoform 2 of PA2G4 protein could indicate an increase of cell metabolism due to the extrinsic stress caused by Lapatinib and K4 compounds. In, Table 3.8, it is visible that this protein is only overexpressed in the combinatory strategy and not in the single agent exposure, thus suggesting that the overexpression is due to the combination of these two drugs in the cell. T-complex protein 1 subunit gamma, TCPG, is a molecular chaperone, involved in protein folding upon ATP hydrolysis (Brunelli et al., 2012). It exhibits an overexpression pattern in cells exposed to lapatinib and K4. This result suggests that HCT116 cells increase their metabolism and their protein folding as a response of extrinsic stress such as lapatinib and K4 compound's presence. Mitochondrial ATP synthase subunit beta, ATP5B, is a protein involved in

ATP synthesis catalysis from mitochondria (Singh & Costello, 2012). HCT116 cells exposed to lapatinib and K4 compounds exhibit an underexpression pattern. It is important to consider that (K4+Lapatinib) fold variation is compared to K4 compound thus suggesting that the underexpression is compared to K4 compound proteome profiling assays. Despite the data presented these results do not have a direct correlation with an increase of the metabolic activity. Nonetheless the majority of the identified proteins point towards an increase of metabolic activity. As mentioned befor, cancer cells tend to obtain ATP from glycolysis instead of oxidative phosphorylation when comparing to healthy cells, since it is a faster method of acquiring ATP. TPIS is a protein involved in glycolysis mechanism and is responsible to synthetize D-glyceraldehyde 3-phophate from glycerone phosphate (Ramão et al., 2012). It exhibits overexpression in HCT116 cells treated with lapatinib and K4. Like DHE3 protein, this result suggests that cell metabolism increases in response to two extrinsic stress such as lapatinib and K4 compound.

As shown in section 3.8.2, apoptotic evaluation of combined therapies suggested a high apoptosis percentage due to the low cell density observed in Hoechst preparations. Some of the identified proteins in Table 3.8 could explain these evidences. Rho GDP-dissociation inhibitor 1, GDIR1 controls Rho proteins homeostasis, namely RAC1. Upon binding to RAC1, it prevents its cleavage by caspase 3. GDIR1 is overexpressed in colorectal cancer thus promoting apoptosis inhibition in response to chemotherapeutic agents (Yamashita et al., 2012). Combination of lapatinib and K4 promotes underexpression of this protein in HCT116 cells, leading to RAC1 cleavage by caspase 3 and apoptosis induction. These results corroborate apoptotic potential assays of section 3.8.2 where high levels of apoptosis were detected. Calreticulin, is a calcium-binding chaperone present in endoplasmic reticulum. It also regulates protein folding in cells. Upon translocation to the cell surface, promoted by Ca^{2+} accumulation, it acts as an apoptosis marker, recruiting macrophages to opsonize cells (Liu et al., 2012). The overexpression pattern of this apoptotic marker in the combinatory strategy could explain high apoptosis percentage referred in the previous section. Heat shock protein beta-1, HSPB1 is a chaperone involved in protein folding thus protecting cells from metabolic stress namely hypoxia, radical oxygen species, and chemotherapeutic drugs among others. It inhibits caspases action and recruits cytochrome c. Apoptosis inhibition is promoted when HSPB1 is activated, for example, by chemotherapeutic agents (Nagaraja et al., 2012). Underexpression pattern is similar to lapatinib proteome profiling assays (see Table 3.8). It indicates progression into the apoptotic pathway which corroborates Hoechst staining assays of the section 3.8.2. HSPD1 is a mitochondrial matrix protein, essential to protein transport from cytoplasm to mitochondria. In cancer cells, HSPD1 stimulates pro-caspase 3 activation and consequently stimulates apoptotic pathway (Rugarli & Langer, 2012). It exhibits overexpression in cells exposed to K4 and lapatinib indicating a progression into the apoptotic pathway. These results corroborate Hoechst staining assays. Additionally, cells exposed to the combinatory strategy lapatinib 24h + K4 24h express different results when exposed to K4 or lapatinib as single agents. As shown in section 3.2.1, K4 has low apoptotic levels and also underexpression pattern in proteome profiling.

Cu (II) compound showed in previous assays the ability to bind to DNA molecule and delaying S-phase progression with possible involvement in DNA replication. Lapatinib, an EGFR pathway inhibitor also prevents DNA replication and cell growth signaling (Paul et al., 2008). In response to DNA damage or DNA replication pathways' deficiency, cells increase their DNA damage repair mechanisms (Curtin, 2012)(Beli et al., 2012). Some identified proteins in Table 3.8 could explain this mechanism. PCNA is a protein involved in the control of eukaryotic DNA replication and in DNA damage response. Lapatinib mechanism of action is intrinsically connected with PCNA protein abundancy. EGFR phosphorylates PCNA protecting it from polyubiquitylation and consequent degradation. Lapatinib inhibits EGFR, preventing PCNA phosphorylation and consequently degrades this protein (Lo, Ho, & Wang, 2012). A compensatory mechanism could be occurring when lapatinib is exposed to cells. As shown in Table 3.8, PCNA is overexpressed in cells exposed to lapatinib and also in cells exposed to lapatinib and K4. Results shown in Table 3.8 suggests that the overexpression of PCNA in lapatinib samples is also occurring in cells exposed to lapatinib and K4. Ribonuclease inhibitor, RINI, is a protein involved in RNASE1, RNASE2 and ANG inhibition thus inhibiting RNA cleavage (Yao et al., 2013). Underexpression pattern of this protein suggests that protein synthesis is not interrupted. PUR9 is a bifunctional enzyme that catalyzes 2 steps of purine biosynthesis. Overexpression of this protein and subsequently, increased purine synthesis, in cells exposed to lapatinib and K4 suggests that DNA replication is being promoted. RINI and PUR9 proteins suggests the progression of processes related to DNA replication, which could be explained as compensatory mechanisms, of DNA regulation, that already has been described for PCNA protein. Redundant pathways of DNA replication could be activated concerning the inhibitory effects of lapatinib in EGFR and K4 DNA binding effects. Eukaryotic translation initiation factor 5A-1, IFSA1 is a protein involved in translation elongation by mRNA binding. It is a regulator of p53/TP53 dependent apoptosis and TNF-α mediated apoptosis. It shows elevated abundancy in cancer cells and is frequently defined as cancer biomarkers (Caraglia et al., 2013). This protein exhibits underexpression in combinatory strategy (lapatinib 24 h + K4 24 h) and in single agent exposure. It should be noted that for lapatinib analysis it exhibits the lowest fold variation value determined, approximately 0.08. These results could also evidence a compensatory mechanism of cells in response to high apoptotic signaling of cells exposed to K4 or lapatinib and K4 in combination.

Overall protein abundance modification suggests the overexpression of proteins involved in increased metabolic activity, apoptosis progression and compensatory mechanisms of DNA repair. As a response of an extrinsic stress such as lapatinib or K4, cells increase their metabolic activity to overcome energetic cell needs, in regards to the activity of drug efflux pumps (to counteract the compounds activity), as well as in order to provide energy into the cell's biosynthetic machinery to "repair" the damages promoted by the therapeutic effects of K4. High apoptosis levels presented in section 3.8.2 were corroborated by proteome profiling assays which indicated apoptotic pathway progression. Lapatinib and K4 compounds are involved in DNA replication inhibition mechanisms which also triggered compensatory mechanisms in HCT116 cells, as suggested by proteome profiling assays.

4. Conclusion and Future Perspectives

The anticancer potential of several metallic compounds was assessed in preliminary assays. Cu (II) compound (K4) exhibited the highest cytotoxic potential with a relative IC_{50} of 19.09 μM for A549 cell line and 6.10 μM for HCT116 cell line. Cu (II) compound revealed a lower IC_{50} for both cell lines when compared to cisplatin, a well-known chemotherapeutic agent with a metallic core. Following assays were performed concerning an evaluation of cytotoxic potential in a non-tumoural cell line, fibroblasts, as means to determine the damage extent in healthy cells, and eventually the extent of side effects upon a future and potential clinical translation. The relative IC_{50} obtained was 9.18 μM thus revealing a higher cytotoxicity in HCT116 cell line and a lesser cytotoxicity in A549 cell line. In this sense, further assays were pursued in HCT116 cell line with the K4.

Apoptotic potential evaluation exhibited apoptosis levels under 50 % suggesting that the metallic compound has a cytostatic mechanism of action. In Hoechst staining assays, high cell density was observed as well as the formation of apoptotic bodies. Nonetheless, double staining procedure followed by flow cytometer analysis, revealed a 5 % increase of late apoptosis for cells exposed to K4 IC_{50} concentration and a 15 % increase of late apoptosis for cells exposed to K4 1.5 fold IC_{50} concentration, when comparison with the control group.

Cell cycle progression assays revealed a delay in S-phase after K4 exposure. HCT116 cells incubated with K4 for 6 h period, revealed to be mainly in S-phase, whereas the control group cell population appeared to be in G2/M phase, suggesting the cell cycle progression for the control group and a significant delay in cells exposed to K4. Similarly at 9 h exposure, HCT116 cells are mainly in S-phase but progressing into G2/M phase whereas control group cells appear to be progressing into G1/G0 phase. Cell cycle delay could be involved in intra S-phase checkpoint which regulates complete and correct DNA replication, or could be involved in the regulation of CDK2-cyclin A, the prime protein regulator for cell cycle S-phase.

Previous assays were performed in order to evaluate chemical stability of K4 compound in 0.2 M Tris-HCl pH 7.0 with 50 mM NaCl buffer. Results revealed that, over time, K4's characteristic peak absorbance values decreased. Thus a 30 minute incubation period was selected conducive to maintain approximately 80 % of compound's peak in UV-Vis spectroscopy assays. DNA interactions assays, through UV-Vis spectroscopy revealed that K4 compound binds to this macromolecule in a binding groove fashion. Binding constant affinity value for K4 compound, $2.17 \pm 1{,}42 \times 10^5\ M^{-1}$, revealed to be in the same order of magnitude of doxorubicin's, thus suggesting a strong interaction with DNA. pDNA cleavage assays also revealed an electrophoretic mobility delay for increasing K4 concentrations which suggested that K4 induce single breaks in the DNA molecule and binds to it. These results suggested that K4 mechanism of action is intrinsically correlated with DNA binding and with consequent DNA repair mechanisms recruitment which triggers an S-phase delay. Upon activation inability of the DNA's repair mechanisms, cells would enter into

an apoptotic or senescence state, thus corroborating low levels of apoptosis in apoptotic potential evaluation assays.

Previous assays were performed in order to evaluate chemical stability of K4 compound in 10 mM phosphate buffer pH 7.0 /0.15 M NaCl buffer. Results revealed that over time, K4's characteristic peak absorbance values decreased, to a minimum percentage of about 70 % of its original peak (for a 360 min incubation period). Nonetheless in order to mimic the previous assay's conditions, a 30 min incubation period was selected. BSA interaction assays exhibited that K4 binds to BSA (quenching effect) not altering the conformational structure, due to the absence of red or blue shift in UV-Vis absorption spectra or steady-state fluorescence spectra. BSA in the presence of quencher exhibited higher fluorescence intensities than in the absence of the quencher (except for K4 concentrations equal or superior to 80 μM). However, K4 revealed no significant increase of fluorescence. The results evidence that K4 addition to BSA could lead to an increase of fluorescence, but were inconclusive as to deducing any mechanism of interaction with the macromolecule. Furthermore it was not possible to determine number of binding sites of K4 to BSA due to the same circumstances.

Proteome profiling assays of K4 compound revealed that the majority of proteins with increased or decreased abundance ratios were the ones involved in metabolic activity increase and in the suppression of apoptotic pathways. The most overexpressed protein was found to be DHE3_Human, which is involved in metabolic stress response. In response to different extrinsic stresses such as Cu (II) compound addition, cells increase their metabolic activities in order to compensate and overcome cell machinery damages. On the other hand, CALR_Human, was the protein with lowest fold variation value indicative of an underexpression, which consequently suggests that apoptotic pathway is not being accomplished thus corroborating apoptotic potential evaluation assays.

Nanovectorization approach assays revealed that none or only a small percentage of K4 effectively functionalized to the nanoparticles surface leading to the absence of cytotoxic effect upon the nanoformulation exposure to HCT116 cells. As described above, K4 compound revealed a low stability in aqueous solvents which could be related to unsuccessful nanoparticle nanovectorization in mili-Q water. In this sense, a future assay could include the encapsulation of K4 compound into liposomes, to overcome solubility problems.

In combination therapy assays, K4 compound was combined with 5-fluorouracil, afatinib, cetuximab, dasatinib, doxorubicin, lapatinib and paclitaxel. Cytotoxic potential evaluation assays revealed that the synergistic and additive effects were observed in K4 combination with afatinib, doxorubicin and lapatinib. The other combinatory approaches revealed antagonism effects and were discarded from further investigation. For apoptotic potential evaluation, combinatory approaches of K4 with doxorubicin, afatinib and lapatinib revealed very low cell density suggesting high cytotoxic mechanisms for these combinatory strategies. The most promising combinatory approach revealed to be, lapatinib incubation for 24 h followed

by K4 incubation for 24 h in HCT116 cells. A proteome profiling assay was performed conducive to identify molecular targets and possible mechanism of action of this combinatory strategy. In similarity with K4's results assays revealed that proteins involved in increased metabolic activity were significantly altered, such as DHE3_Human, an enzyme involved in citric acid cycle. Results also reported the overexpression of proteins involved in the progression of the apoptotic pathway such as CALR_Human, which corroborates apoptotic potential assays of lapatinib and K4. Proteins involved in transcriptional and translational machinery were also modified when exposed to lapatinib and K4. In these sense a compensatory mechanism of activation of redundant proteins could be activated in order to overcome DNA damage prompt by lapatinib or K4 compounds, however significantly more assays have to be performed in order to obtain a full comprehension of the mechanisms of action of these compound.

5. Bibliography

Agarwal, S., Jangir, D.K. & Mehrotra, R., 2013. Spectroscopic studies of the effects of anticancer drug mitoxantrone interaction with calf-thymus DNA. *Journal of Photochemistry and Photobiology B: Biology*, 120, pp.177–182.

Aguilera, D.G. & Tsimberidou, A.M., 2009. Dasatinib in chronic myeloid leukemia: A review. *Therapeutics and Clinical Risk Management*, 5(1), pp.281–289.

Aitken, R.J. et al., 2011. Apoptosis in the germ line. *Reproduction*, 141(2), pp.139–150.

Alderton, G.K. & Bordon, Y., 2012. Tumour immunotherapy — leukocytes take up the fight. *Nature Reviews Immunology*, 12(4), pp.237–237.

Alessio, E. ed., 2011. *Bioinorganic Medicinal Chemistry*, Weinheim, Germany: Wiley-VCH Verlag GmbH & Co. KGaA. Available at: http://doi.wiley.com/10.1002/9783527633104

Bagnoli, M., Canevari, S. & Mezzanzanica, D., 2010. Cellular FLICE-inhibitory protein (c-FLIP) signalling: A key regulator of receptor-mediated apoptosis in physiologic context and in cancer. *International Journal of Biochemistry and Cell Biology*, 42(2), pp.210–213.

Bao, C. et al., 2014. A promising road with challenges : where are gold nanoparticles in translational. *Nanomedicine (London, England)*, 9(15), pp.2353–2370.

Bardelli, A. & Siena, S., 2010. Molecular mechanisms of resistance to cetuximab and panitumumab in colorectal cancer. *Journal of Clinical Oncology*, 28(7), pp.1254–1261.

Barenholz, Y., 2012. Doxil?? - The first FDA-approved nano-drug: Lessons learned. *Journal of Controlled Release*, 160(2), pp.117–134.

Beli, P. et al., 2012. Proteomic Investigations Reveal a Role for RNA Processing Factor THRAP3 in the DNA Damage Response. *Molecular Cell*, 46(2), pp.212–225.

Bensinger, S.J. & Christofk, H.R., 2012. New aspects of the Warburg effect in cancer cell biology. *Seminars in cell & developmental biology*, 23(4), pp.352–61.

Vanden Berghe, T. et al., 2014. Regulated necrosis: the expanding network of non-apoptotic cell death pathways. *Nature reviews. Molecular cell biology*, 15(2), pp.135–47.

Bertoli, C., Skotheim, J.M. & de Bruin, R.A.M., 2013. Control of cell cycle transcription during G1 and S phases. *Nature reviews. Molecular cell biology*, 14(8), pp.518–28.

Bolze, A. et al., 2013. Ribosomal Protein SA Haploinsufficiency in Humans with Isolated Congenital Asplenia. *Science*, 340(6135), pp.976–978.

Bostock, C.J., Prescott, D.M. & Kirkpatrick, J.B., 1971. An evaluation of the double thymidine block for synchronizing mammalian cells at the G1-S border. *Experimental cell research*, 68(1), pp.163–168.

Bouwman, P. & Jonkers, J., 2012. The effects of deregulated DNA damage signalling on cancer chemotherapy response and resistance. *Nature reviews. Cancer*, 12(9), pp.587–98.

Brannon-Peppas, L. & Blanchette, J.O., 2012. Nanoparticle and targeted systems for cancer therapy. *Advanced Drug Delivery Reviews*, 64, pp.206–212.

Brenner, S., 1974. Caenorhabdztzs elegans. *Methods*, 77(1), pp.71–94.

Brooks, S. a. et al., 2010. Molecular interactions in cancer cell metastasis. *Acta Histochemica*, 112(1), pp.3–25.

Brunelli, L. et al., 2012. Exploratory investigation on nitro- and phospho-proteome cerebellum changes in hyperammonemia and hepatic encephalopathy rat models. *Metabolic brain disease*, 27(1), pp.37–49.

Cabral, R.M. & Baptista, P. V, 2014. Anti-cancer precision theranostics: a focus on multifunctional gold nanoparticles. *Expert review of molecular diagnostics*, 14(8), pp.1041–52.

Caraglia, M. et al., 2013. EIF5A isoforms and cancer: Two brothers for two functions? *Amino Acids*, 44(1), pp.103–109.

Chakraborty, B. & Basu, S., 2009. Interaction of BSA with proflavin: A spectroscopic approach. *Journal of Luminescence*, 129, pp.34–39.

Coimbra, J. et al., 2015. Inorganic Compounds Going NANO. , 1, pp.1–5.

Colditz, G.A., Wolin, K.Y. & Gehlert, S., 2012. Applying what we know to accelerate cancer prevention. *Science translational medicine*, 4(127), p.127rv4.

Conde, J., Baptista, P. V, et al., 2012. Modification of plasmid DNA topology by “histone-mimetic” gold nanoparticles. *Nanomedicine*, pp.1–10.

Conde, J., Doria, G., et al., 2012. RNA quantification using noble metal nanoprobes: simultaneous identification of several different mRNA targets using color multiplexing and application to cancer diagnostics. *Methods in molecular biology (Clifton, N.J.)*, 906, pp.71–87.

Coronado, D. et al., 2013. A short G1 phase is an intrinsic determinant of na??ve embryonic stem cell pluripotency. *Stem Cell Research*, 10(1), pp.118–131.

Curtin, N.J., 2012. DNA repair dysregulation from cancer driver to therapeutic target. *Nature reviews. Cancer*, 12(12), pp.801–17.

Denny, W.A., 1989. DNA-intercalating ligands as anti-cancer drugs: prospects for future design. *Anti-cancer drug design*, 4(4), pp.241–63.

Drexler, H.G. & Uphoff, C.C., 2002. Mycoplasma contamination of cell cultures: Incidence, sources, effects, detection, elimination, prevention. *Cytotechnology*, 39(2), pp.75–90.

DrugBanK, 2015. DrugBank: Cetuximab (DB00002). Available at: http://www.drugbank.ca/drugs/DB00002 [Accessed August 19, 2015].

Ellis, H.M. & Horvitz, H.R., 1986. Genetic control of programmed cell death in the nematode C. elegans. *Cell*, 44(6), pp.817–829.

Elmore, S., 2007a. Apoptosis: a review of programmed cell death. *Toxicologic pathology*, 35(4), pp.495–516.

Elmore, S., 2007b. NIH Public Access. *Changes*, 29(6), pp.997–1003.

Ferlay, J. et al., 2012. Cancer incidence and mortality worldwide : sources , methods and major patterns in GLOBOCAN 2012.

Finka, A. & Goloubinoff, P., 2013. Proteomic data from human cell cultures refine mechanisms of chaperone-mediated protein homeostasis. *Cell Stress and Chaperones*, 18(5), pp.591–605.

Galluzzi, L. et al., 2014. Essential versus accessory aspects of cell death: recommendations of the NCCD 2015. *Cell Death and Differentiation*, 22(1), pp.58–73.

Galluzzi, L., Vitale, I., et al., 2012. Molecular definitions of cell death subroutines: recommendations of the Nomenclature Committee on Cell Death 2012. *Cell Death and Differentiation*, 19(1), pp.107–120.

Galluzzi, L., Senovilla, L., et al., 2012. Molecular mechanisms of cisplatin resistance. *Oncogene*, 31(15), pp.1869–1883. Available at: http://dx.doi.org/10.1038/onc.2011.384.

Galluzzi, L., Blomgren, K. & Kroemer, G., 2009. Mitochondrial membrane permeabilization in neuronal injury. *Nature reviews. Neuroscience*, 10(7), pp.481–494.

Galluzzi, L., Kepp, O. & Kroemer, G., 2012. Mitochondria: master regulators of danger signalling. *Nature reviews. Molecular cell biology*, 13(12), pp.780–8.

Gelamo, E.L. et al., 2002. Interaction of bovine (BSA) and human (HSA) serum albumins with ionic surfactants: Spectroscopy and modelling. *Biochimica et Biophysica Acta - Protein Structure and Molecular Enzymology*, 1594(1), pp.84–99.

Ghosh, S., Jana, S. & Guchhait, N., 2012. Domain specific association of small fluorescent probe trans -3-(4-monomethylaminophenyl)-acrylonitrile (MMAPA) with bovine serum albumin (BSA) and its dissociation from protein binding sites by Ag nanoparticles: Spectroscopic and molecular docking study. *Journal of Physical Chemistry B*, 116(3), pp.1155–1163.

Gloghini, A. et al., 2014. Primary effusion lymphoma: Secretome analysis reveals novel candidate biomarkers with potential pathogenetic significance. *American Journal of Pathology*, 184(3), pp.618–630.

Greaves, M. & Maley, C.C., 2012. Clonal evolution in cancer. *Nature*, 481(7381), pp.306–313.

Guirgis, B.S.S. et al., 2012. Gold nanoparticle-based fluorescence immunoassay for malaria antigen detection. *Analytical and Bioanalytical Chemistry*, 402(3), pp.1019–1027.

Haggar, F. a, Boushey, R.P. & Ph, D., 2009. Colorectal Cancer Epidemiology : Incidence , Mortality , Survival , and Risk Factors. *Clinics in colon and rectal surgery*, 6(212), pp.191–197.

Hanahan, D. & Weinberg, R. a., 2011. Hallmarks of cancer: The next generation. *Cell*, 144(5), pp.646–674. Available at: http://dx.doi.org/10.1016/j.cell.2011.02.013.

Hanahan, D. & Weinberg, R. a., 2000. The hallmarks of cancer. *Cell*, 100, pp.57–70.

Healthcare, 2009. 2-D Clean-Up Kit. , pp.2–5.

Healthcare, 2006. Ettan IPGphor 3 - Intrument user manual.

Hodgkinson, V.C. et al., 2012. Proteomic identification of predictive biomarkers of resistance to neoadjuvant chemotherapy in luminal breast cancer: A possible role for 14-3-3 theta/tau and tBID? *Journal of Proteomics*, 75(4), pp.1276–1283.

Holohan, C. et al., 2013. Cancer drug resistance: an evolving paradigm. *Nature reviews. Cancer*, 13(10), pp.714–26.

Http://www.cancerrxgene.org/translation/Drug/1005, 2015. http://www.cancerrxgene.org/translation/Drug/1005. [Accessed September 11, 2015].

Hu, J. et al., 2012. The intra-S phase checkpoint targets Dna2 to prevent stalled replication forks from reversing. *Cell*, 149(6), pp.1221–1232.

Huang, F. et al., 2007. Identification of candidate molecular markers predicting sensitivity in solid tumors to dasatinib: Rationale for patient selection. *Cancer Research*, 67(5), pp.2226–2238.

Huang, J.T. et al., 2013. DNA binding and nuclease activity of a water-soluble sulfonated manganese(III) corrole. *Transition Metal Chemistry*, 38(3), pp.283–289.

Huang, S., 2013. Genetic and non-genetic instability in tumor progression: link between the fitness landscape and the epigenetic landscape of cancer cells. *Cancer metastasis reviews*, 32(3-4), pp.423–48.

Hurley, L.H., 2002. DNA and its associated processes as targets for cancer therapy. *Nature reviews. Cancer*, 2(3), pp.188–200.

Iakovidis, I., Delimaris, I. & Piperakis, S.M., 2011. Copper and its complexes in medicine: a biochemical approach. *Molecular biology international*, 2011, p.594529.

Invitrogen, 2010. FITC Annexin V / Dead Cell Apoptosis Kit with FITC annexin V and PI , for Flow Cytometry. , pp.1–5.

Invitrogen, 2005. Hoechst Stains. *Journal of Histochemistry and Cytochemistry*, (3), pp.9–12.

Jaividhya, P. et al., 2012. Efficient DNA cleavage mediated by mononuclear mixed ligand copper(II) phenolate complexes: The role of co-ligand planarity on DNA binding and cleavage and anticancer activity. *Journal of Inorganic Biochemistry*, 114, pp.94–105.

Janjigian, Y.Y. et al., 2014. Dual inhibition of EGFR with afatinib and cetuximab in kinase inhibitor-resistant EGFR-mutant lung cancer with and without T790M mutations. *Cancer discovery*, 4(9), pp.1036–45.

Jarkovska, K. et al., 2014. Revelation of fibroblast protein commonalities and differences and their possible roles in wound healing and tumourigenesis using co-culture models of cells. *Biology of the Cell*, 106(7), pp.203–218.

Jego, G. et al., 2013. Targeting heat shock proteins in cancer. *Cancer Letters*, 332(2), pp.275–285.

Jiang, S. et al., 2012. A novel miR-155/miR-143 cascade controls glycolysis by regulating hexokinase 2 in breast cancer cells. *The EMBO Journal*, 31(8), pp.1985–1998.

Kang, M.H. & Reynolds, C.P., 2009. Bcl-2 inhibitors: targeting mitochondrial apoptotic pathways in cancer therapy. *Clinical cancer research : an official journal of the American Association for Cancer Research*, 15(4), pp.1126–1132.

Kar, S. et al., 2009. Exploring the roles of noise in the eukaryotic cell cycle. *Proceedings of the National Academy of Sciences of the United States of America*, 106(16), pp.6471–6476.

Keene, K.L. et al., 2011. Evidence for two independent associations with type 1 diabetes at the 12q13 locus. *Genes and Immunity*, 13(1), pp.66–70.

Khare, S. & Verma, M., 2012. Epigenetics of colon cancer. *Methods in molecular biology (Clifton, N.J.)*, 863, pp.177–85.

Konecny, G.E. et al., 2006. Activity of the dual kinase inhibitor lapatinib (GW572016) against HER-2-overexpressing and trastuzumab-treated breast cancer cells. *Cancer Research*, 66(3), pp.1630–1639.

Kopylovich, M.N., Lasri, J. & Pombeiro, A.J.L., 2010. Electronic Supplementary Information (ESI). , (c), pp.1–7.

Krishan, 1975. Rapid Flow Cytofluorometric Mammalian Analysis of. *The Journal of cell biology*, 66, pp.188–193.

Kroemer, G. et al., 2009. Classification of Cell Death 2009. *Cell death and differentiation*, 16(1), pp.3–11.

Kushi, L.H. et al., 2012. American Cancer Society Guidelines on nutrition and physical activity for cancer prevention: reducing the risk of cancer with healthy food choices and physical activity. *CA: a cancer journal for clinicians*, 62(1), pp.30–67.

Kustermann, S. et al., 2013. A label-free, impedance-based real time assay to identify drug-induced toxicities and differentiate cytostatic from cytotoxic effects. *Toxicology in Vitro*, 27(5), pp.1589–1595.

Larguinho, M. & Baptista, P. V., 2012. Gold and silver nanoparticles for clinical diagnostics - From genomics to proteomics. *Journal of Proteomics*, 75(10), pp.2811–2823.

Lavrik, I.N. & Krammer, P.H., 2012. Regulation of CD95/Fas signaling at the DISC. *Cell Death and Differentiation*, 19(1), pp.36–41.

Leiphrakpam, P.D. et al., 2014. Ezrin expression and cell survival regulation in colorectal cancer. *Cellular Signalling*, 26(5), pp.868–879.

Lenz, H.-J., 2007. Cetuximab in the management of colorectal cancer. *Biologics : targets & therapy*, 1(2), pp.77–91.

Lever, J.R., 2012. Medicinal chemistry Opioid Receptors and Ligands : Targets for Cancer Imaging and Therapy. , 2(7), pp.142–146.

Lim, S. & Kaldis, P., 2013. Cdks, cyclins and CKIs: roles beyond cell cycle regulation. *Development (Cambridge, England)*, 140(15), pp.3079–93.

Liu, R. et al., 2012. Calreticulin as a potential diagnostic biomarker for lung cancer. *Cancer Immunology, Immunotherapy*, 61(6), pp.855–864.

Lo, Y.H., Ho, P.C. & Wang, S.C., 2012. Epidermal growth factor receptor protects proliferating cell nuclear antigen from cullin 4A protein-mediated proteolysis. *Journal of Biological Chemistry*, 287(32), pp.27148–27157.

Longley, D.B., Harkin, D.P. & Johnston, P.G., 2003. 5-Fluorouracil: Mechanisms of Action and Clinical Strategies. *Nature reviews. Cancer*, 3(5), pp.330–338.

Luís, D. V, 2011. *Caracterização do efeito anti-tumoral de complexos*.

Luo, H. et al., 2012. Selenium nanoparticles inhibit the growth of HeLa and MDA-MB-231 cells through induction of S phase arrest. *Colloids and Surfaces B: Biointerfaces*, 94, pp.304–308.

Marchina, E. et al., 2010. BRCA1 and BRCA2 genetic test in high risk patients and families: counselling and management. *Oncology reports*, 24(6), pp.1661–7.

Martins, P. et al., 2014. Organometallic Compounds in Cancer Therapy_ Past Lessons and Future Directions. *Anticancer Agents Med Chem.*, 14(9), pp.1199–1212.

Mendo, A.S. et al., 2015. Characterization of antiproliferative potential and biological targets of a copper compound containing 4'-phenyl terpyridine. *Journal of biological inorganic chemistry : JBIC : a publication of the Society of Biological Inorganic Chemistry*, 20(6), pp.935–48.

Nagaraja, G.M., Kaur, P. & Asea, A., 2012. Role of Human and Mouse HspB1 in Metastasis. *Current Molecular Medicine*, 12(9), pp.1142–1150.

Neubig, R.R. et al., 2003. International Union of Pharmacology Committee on Receptor Nomenclature and Drug Classification. XXXVIII. Update on terms and symbols in quantitative pharmacology. *Pharmacological reviews*, 55(4), pp.597–606.

Niida, H. & Nakanishi, M., 2006. DNA damage checkpoints in mammals. *Mutagenesis*, 21(1), pp.3–9.

Novák, Sible & Tyson, 2009. Encyclopedia of life sciences. , (August).

O'Brien, P.J. et al., 2013. Monitoring metabolic responses to chemotherapy in single cells and tumors using nanostructure-initiator mass spectrometry (NIMS) imaging. *Cancer & metabolism*, 1(1), p.4.

O'Connor, M. et al., 2012. Copper(II) complexes of salicylic acid combining superoxide dismutase mimetic properties with DNA binding and cleaving capabilities display promising chemotherapeutic potential with fast acting in vitro cytotoxicity against cisplatin sensitive and resista. *Journal of medicinal chemistry*, 55(5), pp.1957–68.

Ouyang, L. et al., 2012. Programmed cell death pathways in cancer: a review of apoptosis, autophagy and programmed necrosis. In *Cell proliferation*. pp. 487–98.

Paul, B., Trovato, J. a. & Thompson, J., 2008. Lapatinib: A dual tyrosine kinase inhibitor for metastatic breast cancer. *American Journal of Health-System Pharmacy*, 65(18), pp.1703–1710.

Perez, E. a et al., 2012. new Frontiers and treatment Paradigms for Metastatic Breast cancer. , 9(8).

Perez, I. et al., 2015. Altered Activity and Expression of Cytosolic Peptidases in Colorectal Cancer. *International Journal of Medical Sciences*, 12(6), pp.458–467.

Philp, L.K. et al., 2013. SGTA: A New Player in the Molecular Co-Chaperone Game. *Hormones and Cancer*, 4(6), pp.343–357.

Pinto, A.C., Moreira, J.N. & Simões, S., 2010. Combination Chemotherapy in Cancer : Principles , Evaluation and Drug Delivery Strategies. *Current Cancer Treatment*, pp.695–714.

Promega, 2012. Non-Radioactive Cell Proliferation Assay.

Ramão, A. et al., 2012. Changes in the expression of proteins associated with aerobic glycolysis and cell migration are involved in tumorigenic ability of two glioma cell lines. *Proteome Science*, 10(1), p.53.

Rugarli, E.I. & Langer, T., 2012. Mitochondrial quality control: a matter of life and death for neurons. *The EMBO Journal*, 31(6), pp.1336–1349.

Saha, S. et al., 2010. Enhanced photodynamic effect of cobalt(III) dipyridophenazine complex on thyrotropin receptor expressing HEK293 cells. *Metallomics : integrated biometal science*, 2(11), pp.754–765.

Sanatkar, T.H. et al., 2014. Characterization, photocleavage, molecular modeling, and DNA- and BSA-binding studies of Cu(II) and Ni(II) complexes with the non-steroidal anti-inflammatory drug meloxicam. *Inorganica Chimica Acta*, 423, pp.256–272.

Sanchez-Barcelo, E.J. & Mediavilla, M.D., 2014. Recent patents on light based therapies: photodynamic therapy, photothermal therapy and photoimmunotherapy. *Recent patents on endocrine, metabolic & immune drug discovery*, 8(1), pp.1–8.

Scientific, T., 2012. Coomassie (Bradford) Protein Assay Kit. , 0747(815).

Seddon, B.M. & Workman, P., 2003. The role of functional and molecular imaging in cancer drug discovery and development. *The British journal of radiology*, 76 Spec No, pp.S128–38.

Sigma-Aldrich, 2014. Ellman's Reagent. *Sigma-Adrich Product Note*, pp.7–8.

Silva, J., 2012. *Caracterização do Potencial Citotóxico e Mecanismos de Acção de um Complexo de Platina de Configuração trans em Células Animais*.

Singh, K.K. & Costello, L.C., 2012. Mitochondria and cancer. *Mitochondria and Cancer*, pp.1–289.

Sinha, K. et al., 2013. Oxidative stress: the mitochondria-dependent and mitochondria-independent pathways of apoptosis. *Archives of toxicology*, 87(7), pp.1157–80.

Sirajuddin, M., Ali, S. & Badshah, A., 2013. Drug-DNA interactions and their study by UV-Visible, fluorescence spectroscopies and cyclic voltametry. *Journal of Photochemistry and Photobiology B: Biology*, 124, pp.1–19.

Snigdha, S. et al., 2012. Caspase-3 activation as a bifurcation point between plasticity and cell death. *Neuroscience bulletin*, 28(1), pp.14–24.

Soares, P.I.P. et al., 2012. Application of hyperthermia for cancer treatment: recent patents review. *Recent patents on anti-cancer drug discovery*, 7(1), pp.64–73.

Solca, F. et al., 2012. Target binding properties and cellular activity of afatinib (BIBW 2992), an irreversible ErbB family blocker. *The Journal of pharmacology and experimental therapeutics*, 343(2), pp.342–50.

Stumpf, C.R. et al., 2013. The translational landscape of the mammalian cell cycle. *Molecular cell*, 52(4), pp.574–82.

Subhan, M. a., Islam, M.M. & Chowdhury, M.R.U., 2012. Binding Studies and Effect of Light on the Conductance of Intercalated Curcumin into DNA. *Journal of Scientific Research*, 4(2).

Thermo, 2000. Pierce ™ 660nm Protein Assay. , 0747(22660).

Thorn, Caroline; Oshiro, Connie; Marsh, Sharon; Hernandez-Boussard, Tina; McLeod, Howard; Klein, Teri; Altman, R., 2012. Doxorubicin pathways:pharmacodynamics and adverse effects. *Pharmacogenet Genomics*, 21(7), pp.440–446.

Tukenova, M. et al., 2010. Role of cancer treatment in long-term overall and cardiovascular mortality after childhood cancer. *Journal of clinical oncology : official journal of the American Society of Clinical Oncology*, 28(8), pp.1308–1315.

Turkevich, J., Stevenson, P.C. & Hillier, J., 1951. A study of the nucleation and growth processes in the synthesis of Colloidal Gold. *Discuss. Faraday Soc.*, 11(c), pp.55–75.

Vermeulen, K., Bockstaele, D.R. Van & Berneman, Z.N., 2003. The cell cycle : a review of regulation , deregulation and therapeutic targets in cancer. , pp.131–149.

Wang, A.Z., Langer, R. & Farokhzad, O.C., 2012. Nanoparticle Delivery of Cancer Drugs. *Annual Review of Medicine*, 63(1), pp.185–198.

Watanabe, T. et al., 2012. Japanese Society for Cancer of the Colon and Rectum (JSCCR) guidelines 2010 for the treatment of colorectal cancer. *International journal of clinical oncology*, 17(1), pp.1–29.

Weinberg, R., 2013. *The Biology of Cancer, Second Edition*

WHO, 2015a. Fact Sheets by Cancer. Available at: http://globocan.iarc.fr/Pages/fact_sheets_cancer.aspx?cancer=colorectal [Accessed August 26, 2015].

WHO, 2014. Portugal Mortality and Incidence Ratios. Available at: http://www.who.int/cancer/country-profiles/prt_en.pdf?ua=1 [Accessed August 2, 2015].

WHO, 2015b. WHO | Cancer. Available at: http://www.who.int/mediacentre/factsheets/fs297/en/ [Accessed August 21, 2015].

Wickman, G.R. et al., 2013. Blebs produced by actin–myosin contraction during apoptosis release damage-associated molecular pattern proteins before secondary necrosis occurs. *Cell Death and Differentiation*, 20(10), pp.1293–1305.

Wu, Q. et al., 2013. Microwave-assisted synthesis of arene ruthenium(II) complexes that induce S-phase arrest in cancer cells by DNA damage-mediated p53 phosphorylation. *European Journal of Medicinal Chemistry*, 63, pp.57–63.

Yamashita, T. et al., 2012. Rho GDP-dissociation inhibitor alpha is associated with cancer metastasis in colon and prostate cancer. *Pharmazie*, 67(3), pp.253–255.

Yao, X. et al., 2013. A novel role of ribonuclease inhibitor in regulation of epithelial-to-mesenchymal transition and ILK signaling pathway in bladder cancer cells. *Cell and Tissue Research*, 353(3), pp.409–423.

Yohannes, G. et al., 2010. Thermal aggregation of bovine serum albumin studied by asymmetrical flow field-flow fractionation. *Analytica chimica acta*, 675(2), pp.191–8.

Zhou, X. et al., 2012. Azithromycin synergistically enhances anti-proliferative activity of vincristine in cervical and gastric cancer cells. *Cancers*, 4(4), pp.1318–1332.

Appendix A

Mycoplasma detection protocol

Cells were initially trypsinized and centrifuged as mentioned in section 2.2. Deoxyribonucleic acid (DNA) extraction of the cell samples was accomplished using High Pure PCR Template Preparation Kit (Roche Diagnostic, Indianapolis, USA), following manufacturer's procedure. Using Nanodrop2000 (Thermo Scientific, Waltham, MA, USA), absorbance ratios 280/260nm and 230/260nm (used as purity parameters) along with total DNA concentration were registered and a master mix was prepared conducive to start polymerase chain reaction. With a final volume of 20 µL, each reaction contained 75 mU/µL of Taq Red DNA Polymerase, PCR Buffer 10x, High Specific, 1 mM from each dNTP, 2 mM of magnesium chloride, forward and reverse primers (Table 3); all reagents from Bioline, London, UK) and 20 ng/µL of DNA sample. Selected primers were specifically design to detect 16S rRNA coding region of mycoplasma genome allowing detection of contamination in DNA samples and hence in the cell cultures. Following table summarizes forward and reverse primers sequences as well as the average amplicon size.

Gene	Forward Primer (5'-3')	Reverse Primer (5'-3')	Amplicon size (bp)
16S rRNA	*GAGGGCAAGTACGAGTGGCAA*	*CTGCGCATTGCTCCGCTAACC*	≈ 700 bp

Appendix B

Cell viability assays of K0, K1, K2 and K3 compounds on A549 and HCT116 cell lines.

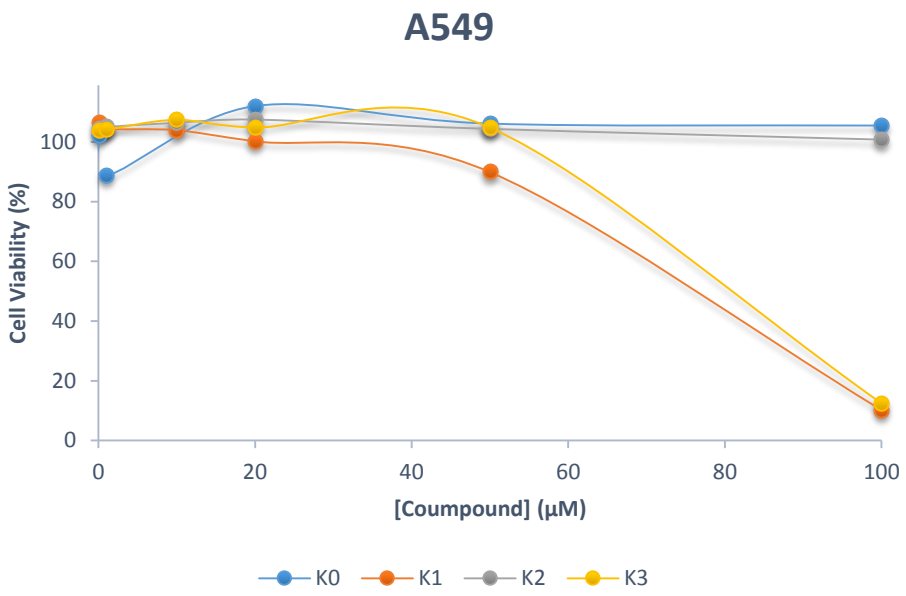

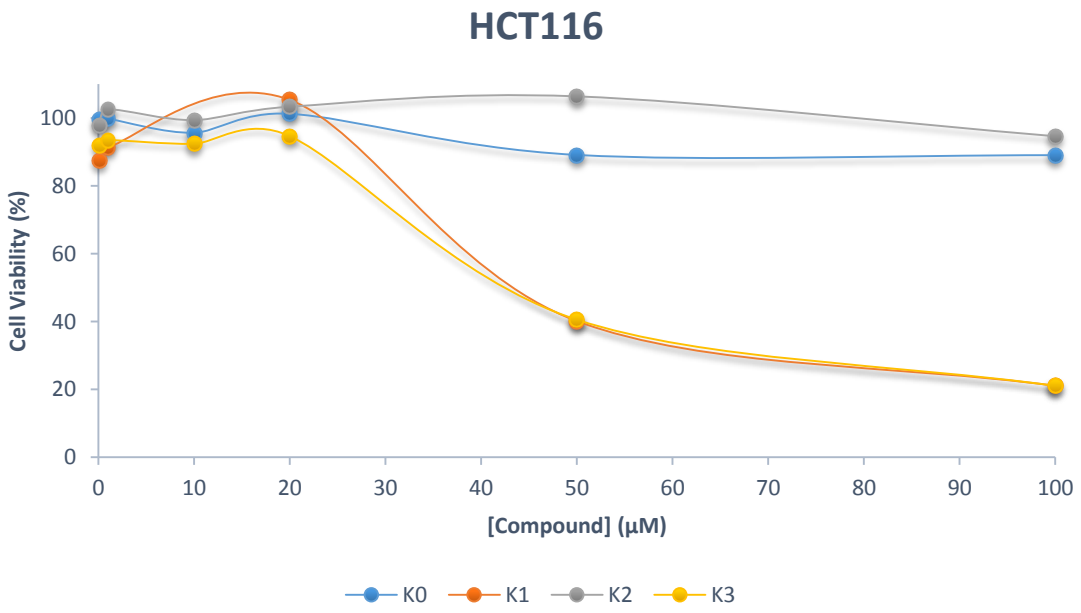

b

Appendix C

Reference gel of HCT116 cell line

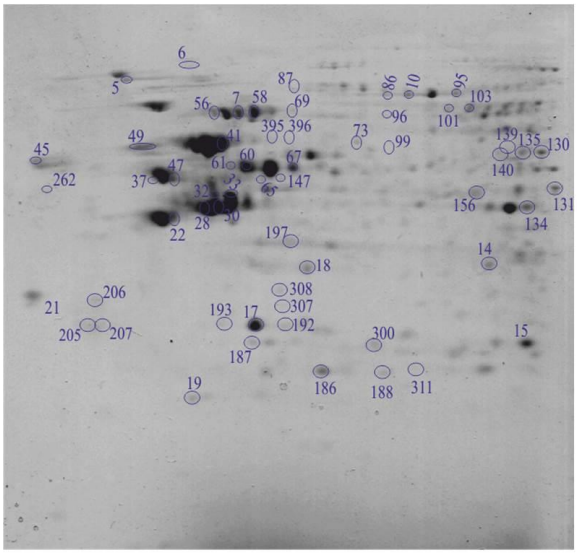

5 – TCPQ_Human - T-complex protein 1 subunit theta (molecular chaperone)
6 – HSP90B_Human - Heat shock protein HSP 90-beta
7 – HSP90B_Human - Heat shock protein HSP 90-beta
10 – ENPL_Human - Endoplasmin
14 – SGTA_Human - Small glutamine-rich tetratricopeptide repeat-containing protein alpha
15 – 1433Z_Human - 14-3-3 protein zeta/delta (implicated in the regulation of signaling pathways)
17 – GSTP1_Human - Glutathione S-transferase P
18 – PSME1_Human - Proteasome activator complex subunit 1
19 – IF5A1_Human - Eukaryotic translation initiation factor 5A-1 (involved in actin dynamics)
21 – PCNA_Human - Proliferating cell nuclear antigen (involved in the control of DNA replication)
22 – DHE3_Human - Glutamate dehydrogenase 1, mitochondrial
28 – ACTG_Human - Actin, cytoplasmic 2
32 – ACTG_Human - Actin, cytoplasmic 2
33 – IF4AI_Human - Eukaryotic initiation factor 4A-I
37 – RINI_Human - Ribonuclease inhibitor (redox homeostasis)
41 – HSPD1_Human - Heat shock 60kDa protein 1
45 – CALR_Human - Calreticulin
47 – ATP5B_Human - ATP synthase subunit beta, mitochondrial
49 – P4HB_Human - Protein disulfide-isomerase (beta subunit of prolyl 4-hydroxylase)
56 – HSP7C_Human - Heat shock cognate 71 kDa protein
58 – GRP75_Human - Stress-70 protein, mitochondrial
60 – PDIA3_Human - Protein disulfide-isomerase A3
61 – RSSA_Human - 40S ribosomal protein SA
65 – RuvB2_Human - RuvB-like 2 (helicase)
69 – GRP75_Human - Stress-70 protein, mitochondrial
73 – TCPA_Human - T-complex protein 1 subunit alpha
86 – HSP71_Human - Heat shock 70 kDa protein 1A/1B
87 – EZRI_Human - Ezrin (involved in connections of cytoskelet to the plasma membrane)
95 – EZRI_Human - Ezrin
96 – TCPG_Human - T-complex protein 1 subunit gamma
99 – STIP1_Human - Stress-induced-phosphoprotein 1
101 – TCPG_Human - T-complex protein 1 subunit gamma
103 – XRCC6_Human - X-ray repair cross-complementing protein 6
130 – EZRI_Human - Ezrin
131 – CALR_Human - Calreticulin
134 – PA2G4_Human - Proliferation-associated protein 2G4
135 – AMPL_Human - Cytosol aminopeptidase
139 – TCPB_Human - T-complex protein 1 subunit beta
140 – TBA1B_Human - Tubulin alpha-1B chain
147 – QCRI_Human - Cytochrome b-c1 complex subunit 1, mitochondrial (2
156 – PA2G4_Human - Proliferation-associated protein 2G4
182 – PRDX2_Human - Peroxiredoxin-2
186 – SODC_Human - Superoxide dismutase [Cu-Zn]
187 – PRDX2_Human - Peroxiredoxin-2
188 – TPIS_Human - Triosephosphate isomerase
192 – GDIR1_Human - Rho GDP-dissociation inhibitor 1
193 – GDIR1_Human - Rho GDP-dissociation inhibitor 1
197 – RSSA_Human - 40S ribosomal protein SA
205 – 1433Z_Human - 14-3-3 protein zeta/delta
206 – RANG_Human - Ran-specific GTPase-activating protein
207 – HSPB1_Human - Heat shock protein beta-1
235 – PHB_Human - Prohibitin
262 – CALU_Human - Calumenin
300 – PGAM1_Human - Phosphoglycerate mutase 1
307 – HSPB1_Human - Heat shock protein beta-1
395 – PUR9_Human - Bifunctional purine biosynthesis protein PURH
396 – DHE3_Human - Glutamate dehydrogenase 1, mitochondrial

Appendix D

Ellman's and Bradford calibration curves

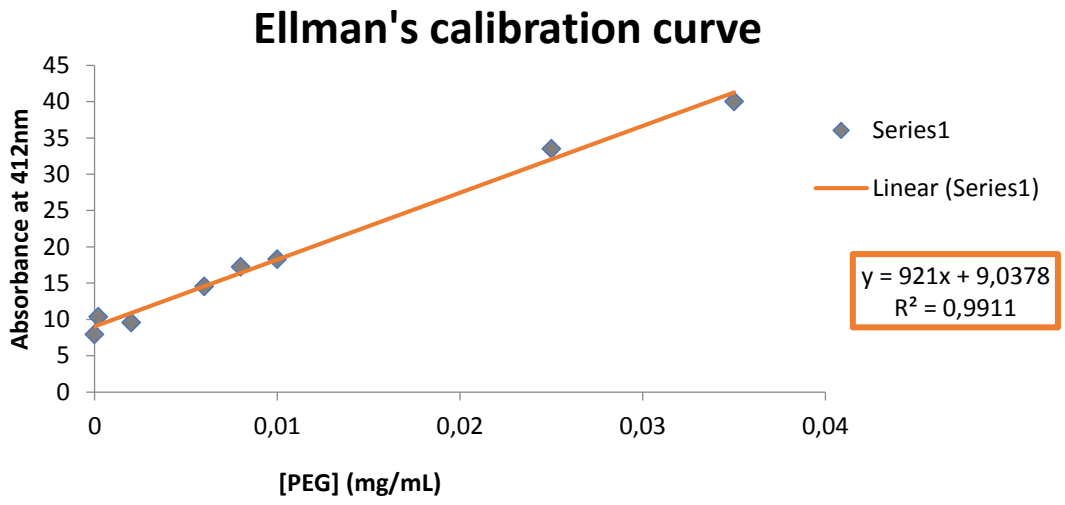

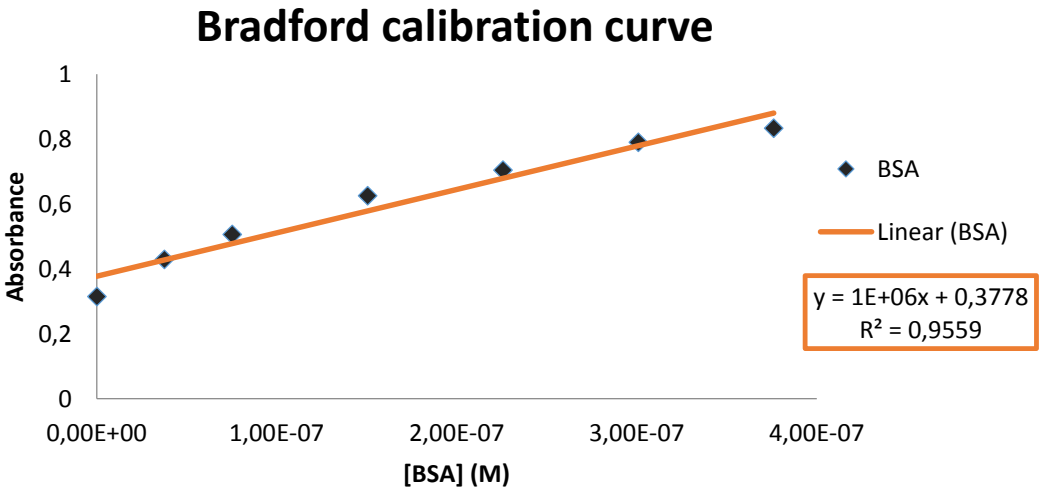

d

Appendix E

Cell viability assays of 5-fluororuracil, afatinib, cetuximab, dasatinib, doxorubicin, lapatinib and paclitaxel.

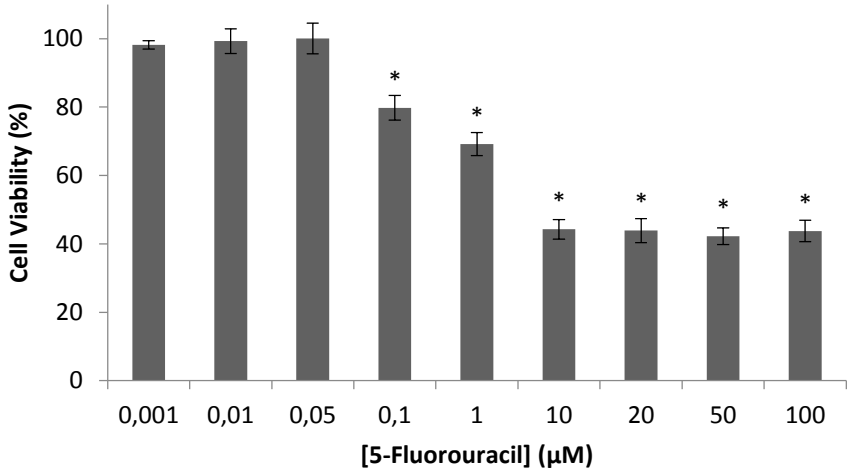

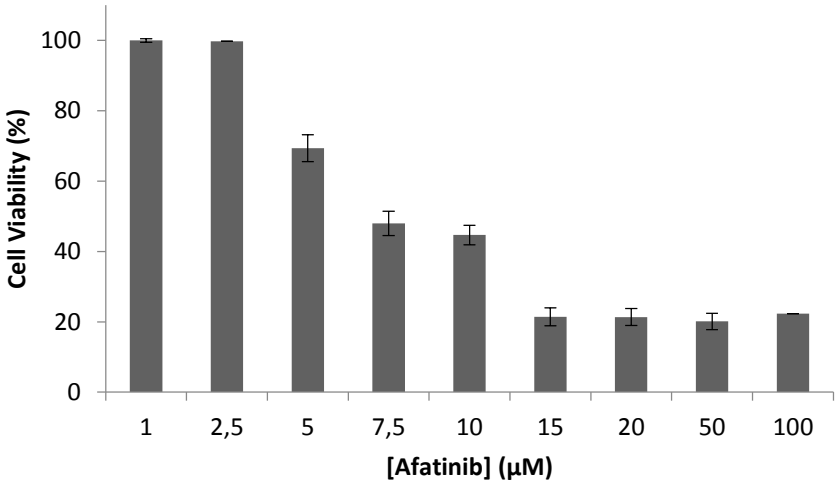

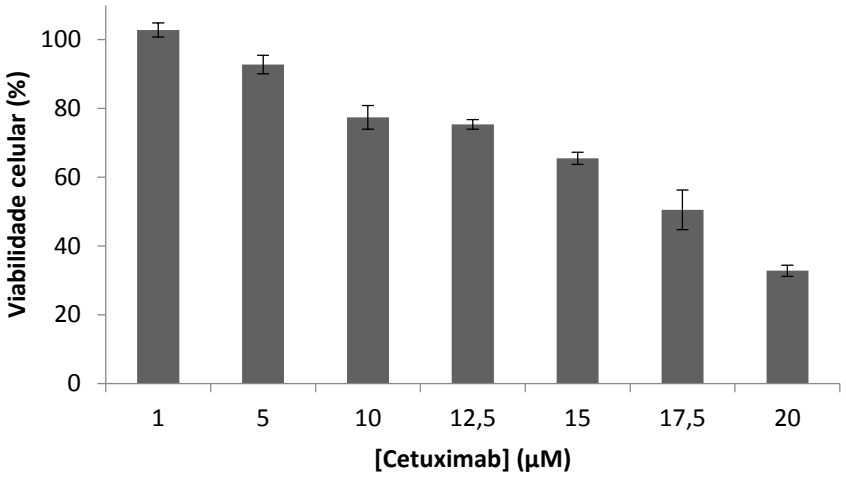
Viabilidade celular (%)
100
80
60
40
20
0
1
5
10
12,5
15
17,5
20
[Cetuximab] (µM)

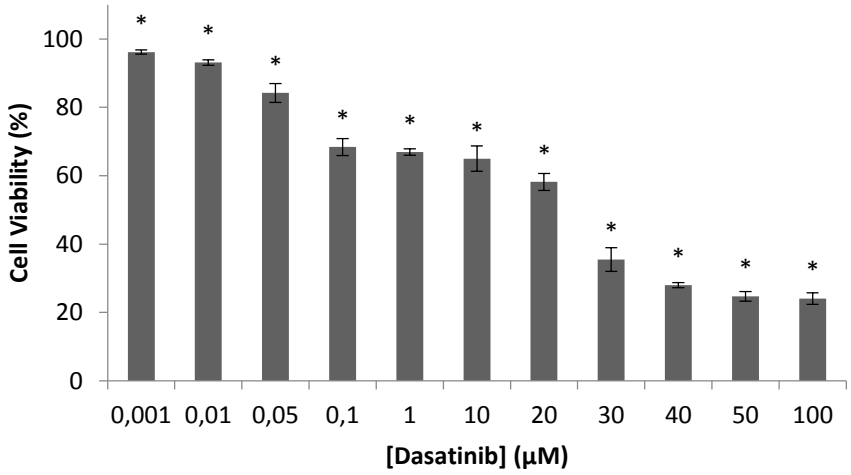
Cell Viability (%)
100
80
60
40
20
0
0,001
0,01
0,05
0,1
1
10
20
30
40
50
100
[Dasatinib] (µM)

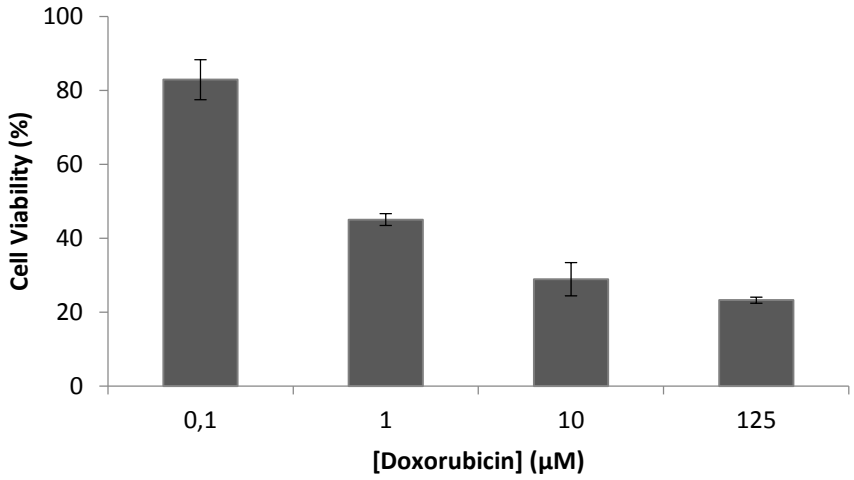
Cell Viability (%)
100
80
60
40
20
0
0,1
1
10
125
[Doxorubicin] (µM)

f

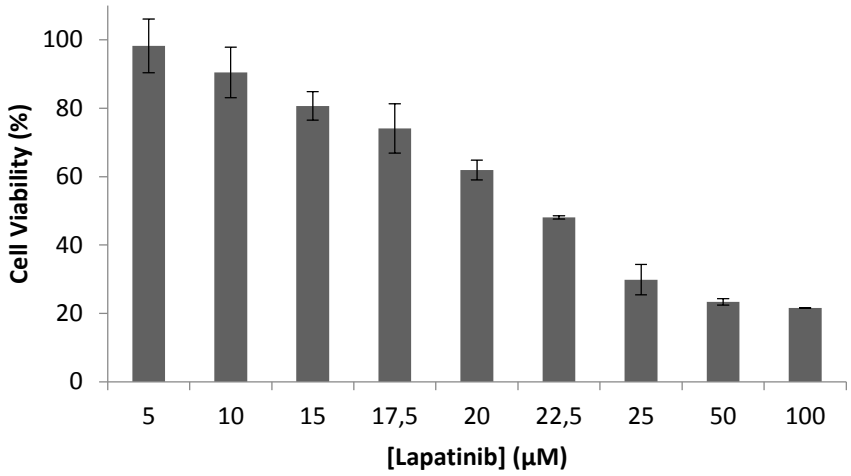

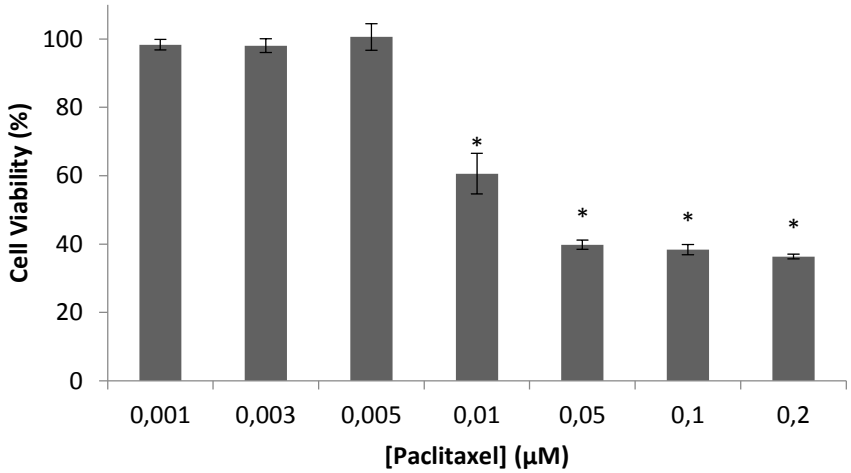

Compound	Relative IC_{50} (µM)
5-Fluorouracil	1.27
Afatinib	6.25
Cetuximab	14.65
Dasatinib	21.30
Doxorubicn	0.42
Lapatinib	19.60
Paclitaxel	9.91 nM

g

Appendix F

Cell viability assays of combined therapies. Data are represented as means ± SEM. *- one way ANOVA test with $p<0.05$. Results were normalized in relation to control group of cells treated with 0.1%DMSO.

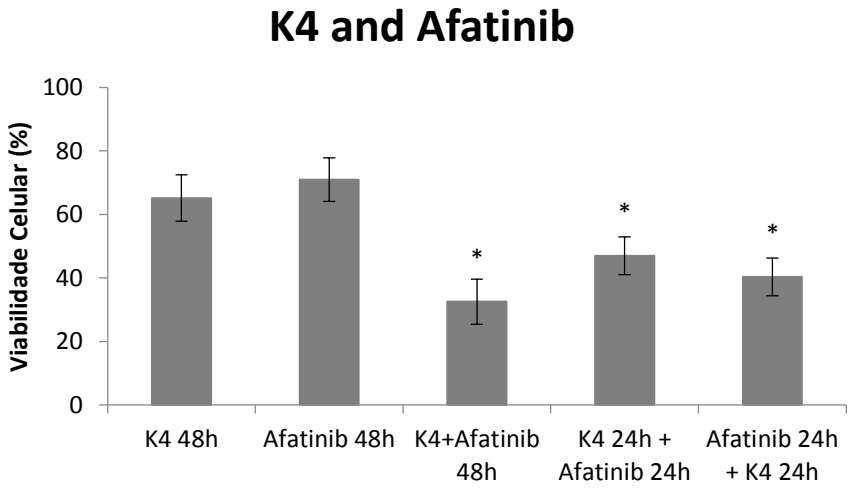

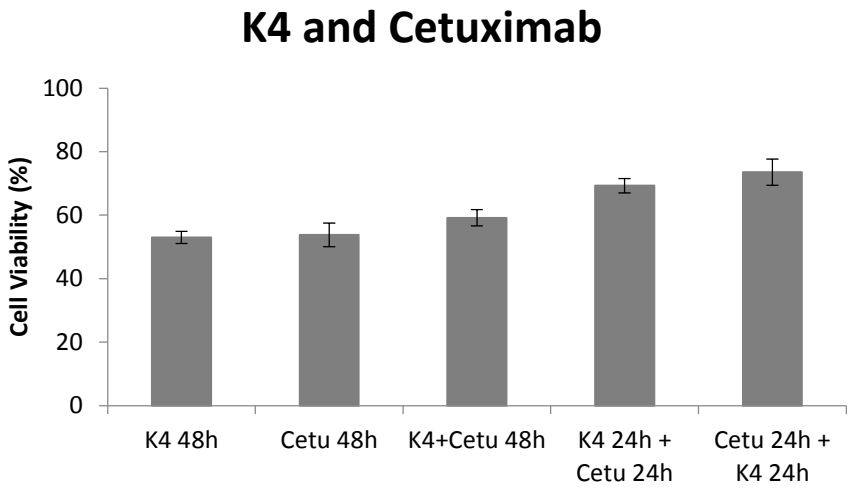

h

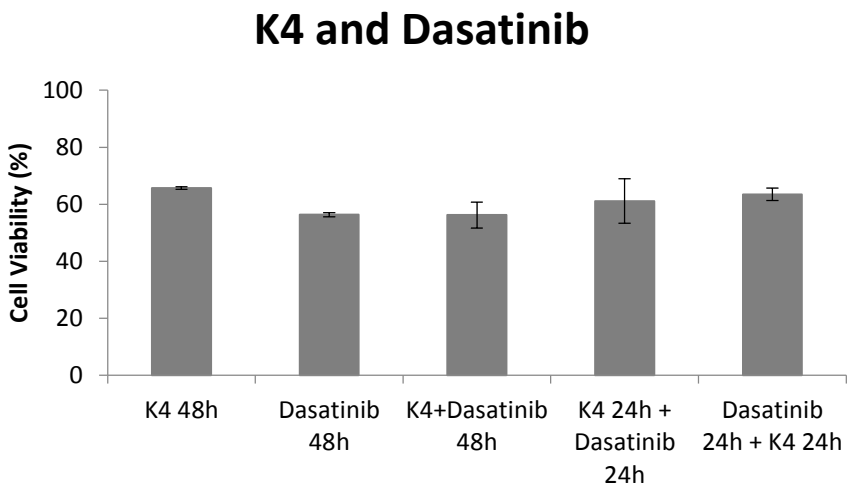
K4 and Dasatinib
Cell Viability (%)
100
80
60
40
20
0
K4 48h
Dasatinib 48h
K4+Dasatinib 48h
K4 24h + Dasatinib 24h
Dasatinib 24h + K4 24h

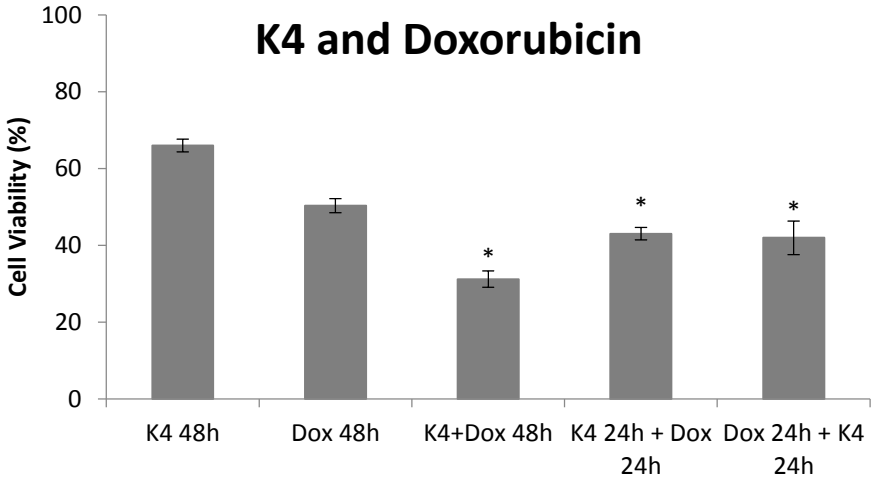
K4 and Doxorubicin
Cell Viability (%)
100
80
60
40
20
0
*
*
*
K4 48h
Dox 48h
K4+Dox 48h
K4 24h + Dox 24h
Dox 24h + K4 24h

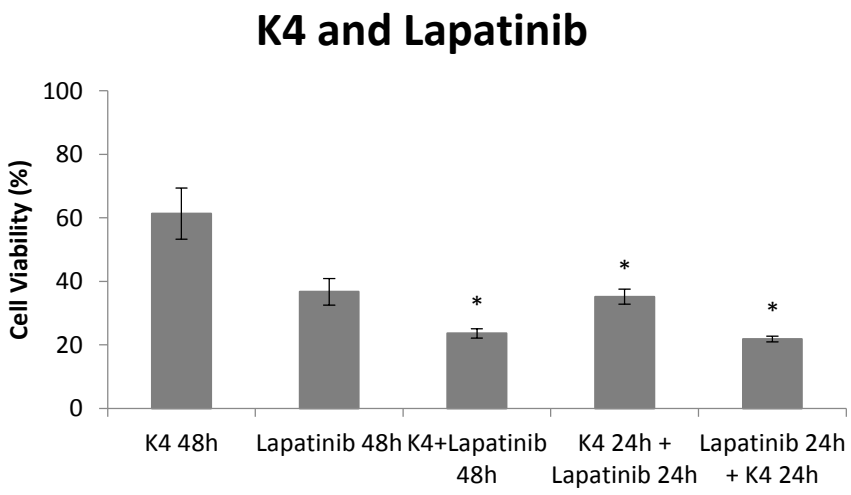
K4 and Lapatinib
Cell Viability (%)
100
80
60
40
20
0
*
*
*
K4 48h
Lapatinib 48h
K4+Lapatinib 48h
K4 24h + Lapatinib 24h
Lapatinib 24h + K4 24h

Dasatinib and Cetuximab

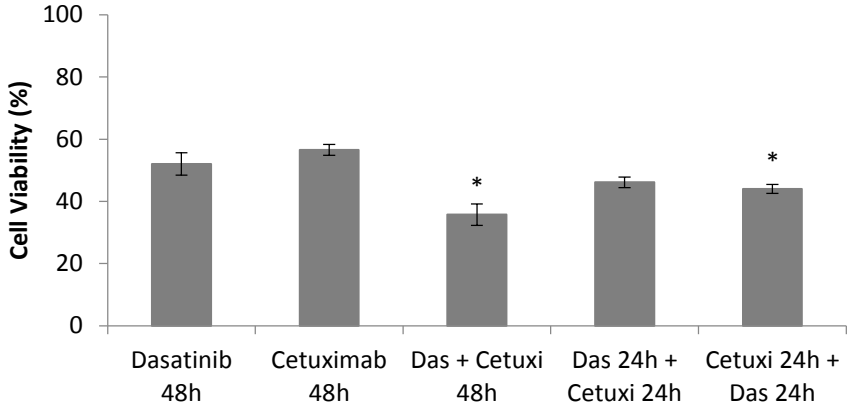

K4, Dasatinib and Cetuximab

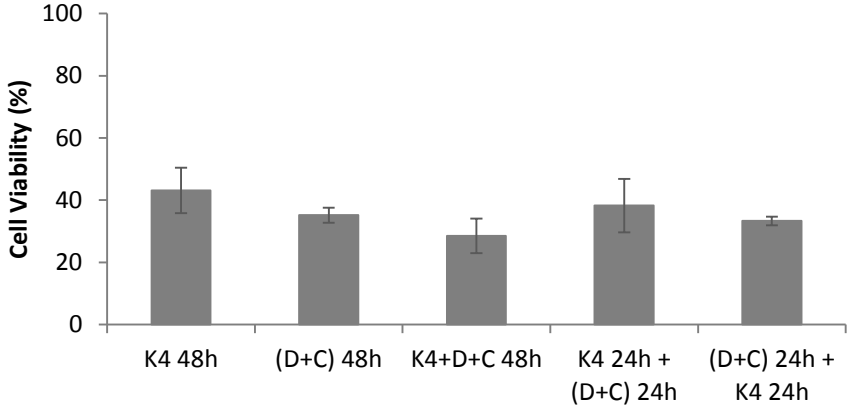

K4 and 5-fluorouracil

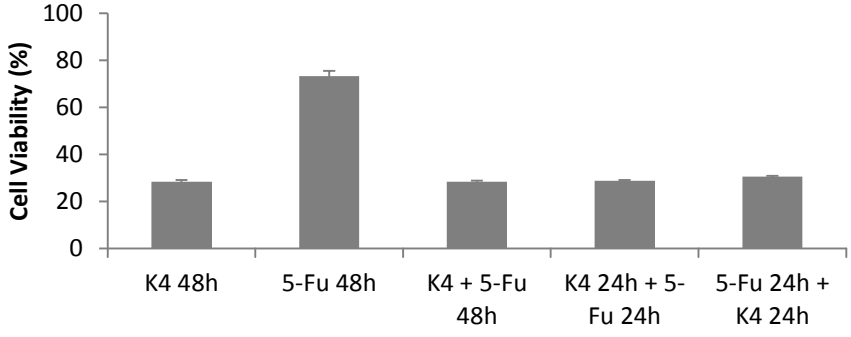

j

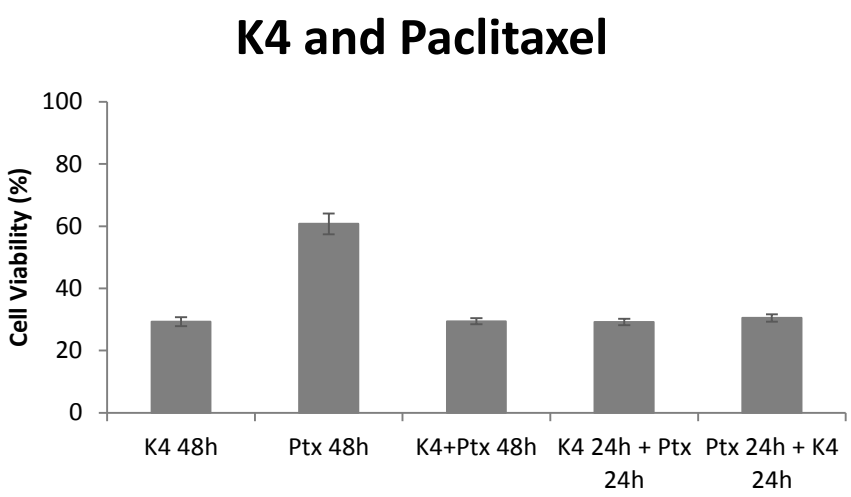
K4 and Paclitaxel
Cell Viability (%)
100
80
60
40
20
0
K4 48h
Ptx 48h
K4+Ptx 48h
K4 24h + Ptx 24h
Ptx 24h + K4 24h

k